NASA Contractor Report 174686

Crack Tip Field and Fatigue Crack Growth in General Yielding and Low Cycle Fatigue

Zheng Minzhong and H. W. Liu

Syracuse University
Syracuse, New York

September 1984

Prepared for

NATIONAL AERONAUTICS AND SPACE ADMINISTRATION
Lewis Research Center
Under Grant NAG 3-348

Low cycle fatigue has been a subject of extensive study [1,2]. Fatigue damage consists of crack nucleation and crack propagation. A small crack can be nucleated under a cyclic load by repeated cyclic slip, creep void nucleation and void coalescence at elevated temperatures, oxidation or other environmental attacks on grain boundary, fracture of oxides, intermetallic compounds or other inclusions, and debonding at the particle-matrix interface. Once a micro-crack is nucleated, and the crack is large enough, it will propagate to failure under a continued cyclic load. Therefore, the total fatigue life, N_f, consists of two parts: N_o and N_p for crack nucleation and propagation albeit the dividing line between nucleation and propagation is not definitive.

It is generally agreed, at the higher applied load range, that the relative portion of the nucleation life to the total life, N_o/N_f, is lower. Therefore, in the low cycle fatigue range, fatigue life is consumed mainly for crack propagation, especially where environmental attack is severe.

It is necessary to extend fatigue crack growth analysis into the region of general yielding in order to study low cycle fatigue life. This paper analyzes the crack tip field in general yielding, relates the crack tip field to far field parameters, analyzes Solomon's fatigue crack growth rate measurement [3] in terms of characteristic crack tip field, i.e. in terms of J, develops a general expression for fatigue crack growth, derives a correlation for low cycle fatigue life and compares the derived correlation with experimental data.

I. CRACK TIP FIELD IN GENERAL YIELDING AND FAR FIELD PARAMETERS

Hutchinson [4] and Rice and Rosengren [5] studied the characteristic crack tip field in an elastic-plastic solid. According to their analyses, the crack tip field can be characterized by a single parameter, K_σ, or K_ε, or J, as defined by Hutchinson, and Rice and Rosengren. The crack tip paramters, J, K_σ and K_ε are related to the far field parameters, and the detailed relation depends on specimen geometry as well as on the stress-strain relation. J is defined as a contour integral, and it can be determined experimentally for elastic-plastic solids by the deformation work difference ΔW_D as shown in Fig. 1.1.

Under a cyclic loading, the stress-strain relation in the plastic region often exhibits a power relation. Three different power hardening relations have been used to simulate the real behaviors of materials:

1. Pure power hardening, pure PH

$$\frac{\varepsilon}{\varepsilon_o} = \alpha\left(\frac{\sigma}{\sigma_o}\right)^N \tag{1.1}$$

where, σ_o, ε_o , are reference stress and strain, and α and N are constants.

2. Ramberg-Osgood power hardening - Ramberg-Osgood PH

$$\frac{\varepsilon}{\varepsilon_o} = \frac{\sigma}{\sigma_o} + \alpha\left(\frac{\sigma}{\sigma_o}\right)^N \tag{1.2}$$

with $\sigma_o = E\varepsilon_o$.

3. Piecewise power hardening - piecewise PH

$$\sigma = E\varepsilon \qquad \sigma \leq \sigma_Y \tag{1.3a}$$

$$\frac{\sigma}{\sigma_Y} = \left(\frac{\varepsilon}{\varepsilon_Y}\right)^n \qquad \sigma > \sigma_Y \tag{1.3b}$$

The stress-strain relations of piecewise power hardening materials can also be simulated by

$$\frac{\varepsilon}{\varepsilon_Y} = \frac{\sigma}{\sigma_Y} + \left(\frac{\sigma - \sigma_Y}{\sigma_Y}\right)^N \qquad \sigma > \sigma_Y \tag{1.3c}$$

$$\sigma = E\varepsilon \qquad \sigma \leq \sigma_Y \tag{1.3d}$$

The second term of the right hand side of Eqn. (1.3c) is the plastic strain. It is applicable only when $\sigma > \sigma_Y$.

In this section, the earlier development of the characteristic crack tip field in large scale yielding and general yielding will be reviewed. The detailed characteristic crack tip field was derived by Hutchinson and Rice and Rosengren for pure PH materials. The relations between J and far field parameters for pure PH materials have been studied by Goldman and Hutchinson [6] and Shih and Hutchinson[7] for plane strain and plane stress cracked panels in tension. Amazigo [8] analyzed the pure PH solid in anti-plane shear. Rice [9] related J to the applied deformation work density W_D for a piecewise PH semi-infinite-cracked infinite-strip under antiplane shear. Shih [10] obtained the antiplane shear results for both piecewise PH and Ramberg-Osgood PH materials for a finite specimen. Shih and Hutchinson [7] have also studied the plane stress center-cracked panel in tension for Ramberg-Osgood PH solid.

In this section, the relation between J and the far field parameters, the applied stress, σ_∞, the applied strain, ε_∞, and the deformation work density, W_D are studied for piecewise PH materials by FEM. The pure PH relation neglects the elastic part of the stress-strain relation entirely. For Ramberg-Osgood PH relation, J is related to two terms of far field parameters [7,10]. For piecewise PH relation, J is related to only one term of far field parameter, which is simpler in analyzing low cycle fatigue behavior.

I.1 Characteristic Crack Tip Field - Elastic-Plastic Solids

Goldman and Hutchinson [6] formulated the fully plastic crack problems to deduce the crack tip field characteristics. With the assumptions of (1) small strain deformation theory, (2) incompressible solids, (3) proportional loading and (4) pure power hardening stress-strain relation, Ilyushin concluded that if the boundary traction P_i increases linearly in proportion to a single load parameter t, the stresses at each point in the solid also vary linearly with t [11,6,12]. With the pure power hardening relation,

$$\frac{\varepsilon}{\varepsilon_o} = \alpha\left(\frac{\sigma}{\sigma_o}\right)^N \tag{1.4}$$

or

$$\frac{\varepsilon_{ij}}{\varepsilon_o} = \frac{3}{2}\alpha\left(\frac{\sigma_e}{\sigma_o}\right)^{N-1}\frac{S_{ij}}{\sigma_o} \tag{1.5}$$

where

$$S_{ij} = \sigma_{ij} - \frac{1}{3}\sigma_{pp}\delta_{ij} \quad \text{and} \quad \sigma_e^2 = \frac{3}{2}S_{ij}S_{ij}$$

the stresses, strains, and displacements of the characteristic crack tip field have the form [13]:

$$[\sigma_{ij},\sigma_e] = \sigma_o K_\sigma r^{-\frac{1}{1+N}}[\tilde{\sigma}_{ij}(\theta,N),\tilde{\sigma}_e(\theta,N)]$$

$$\varepsilon_{ij} = \alpha\varepsilon_o K_\varepsilon r^{-\frac{N}{1+N}}\tilde{\varepsilon}_{ij}(\theta,N) \tag{1.6}$$

$$u_i = \alpha\varepsilon_o K_\varepsilon r^{\frac{1}{1+N}}\tilde{u}_i(\theta,N)$$

where r and θ are the polar coordinates with the origin at the crack tip and the crack line lies along the line $\theta = \pi$. K_σ and K_ε are stress and strain intensity factors, and they are related by $(K_\sigma)^N = K_\varepsilon$. $\tilde{\sigma}_{ij}(\theta,N)$, $\tilde{\sigma}_e(\theta,N)$, $\tilde{\varepsilon}_{ij}(\theta,N)$, and $\tilde{u}_i(\theta,N)$ are the dimensionless functions of θ and N. They define the θ-distributions of their corresponding stress, strain or displacement components. σ_o and ε_o are reference stress and strain. α and N are the dimensionless constants.

The strain energy of a non-linear elastic Ilyushin solid is defined as

$$W = \int_0^{\sigma_{ij}} \sigma_{kl}\, d\varepsilon_{kl} = \alpha\, \sigma_o\, \varepsilon_o \left(\frac{N}{1+N}\right)\left(\frac{\sigma_e}{\sigma_o}\right)^{1+N} \tag{1.7}$$

Rice [9] defined J-integral as

$$J = \int_\Gamma \left(W n_1 - \sigma_{ij}\, n_j\, u_{i,1}\right) ds \tag{1.8}$$

and J is related to K_σ and K_ε

$$J = \alpha\, \sigma_o \varepsilon_o\, K_\sigma\, K_\varepsilon I_n = \alpha\, \sigma_o\, \varepsilon_o (K_\sigma)^{1+N} I_n = \alpha\, \sigma_o\, \varepsilon_o (K_\varepsilon)^{\frac{1+N}{N}} I_n \tag{1.9}$$

where I_n is a numerical constant dependent on N, and the values are given in Ref. [13].

Equations (1.6) define the crack tip field, and they are asymptotic solutions valid only when r approaches the crack tip. These equations give the characteristic crack tip field for non-linear elastic Ilyushin solids. It has been accepted that these equations also approximate the crack tip field in power hardening elastic-plastic solids; and Equations (1.6) have been widely used in elastic-plastic fracture mechanics. Indeed, if there exists a unique crack tip field invariant to in-plane geometric variations and the types of loading, these equations together with the relations for J, K_σ and K_ε will be able to form a basis for a generalized elastic-plastic fracture mechanics theory. However, McMeeking and Parks [14] and Shih and German [15] have shown that the plane strain crack tip field is dependent on sample geometry and the types of loading. Therefore, the characteristics of the crack tip field in general yielding have to be examined carefully before the use of a mechanical parameter such as J, K_σ, K_ε, and r_p to characterize a specific crack tip field.

To begin with, a reference characteristic crack tip field has to be chosen. The elastic-plastic crack tip field in the condition of small scale yielding seems to be the best choice as the reference field. Hu [16] and Hu and Liu [17] have suggested the use of direct correspondence between the crack tip field in a large sample in small scale yielding and the crack tip field in a small sample in general yielding as the basis of elastic-plastic fracture mechanics.

I.2 J and Far Field Parameters

For Ilyushin solids, the crack tip stresses and strains are linearly proportional to the boundary traction, σ_∞. Therefore, the crack tip field can be expressed in the form [6]

$$\frac{\sigma_{ij}}{\sigma_o} = \left(\frac{\sigma_\infty}{\sigma_o}\right) \tilde{\sigma}_{ij}\left(\frac{x}{a}, \frac{y}{a}, \frac{a}{w}, N\right)$$

$$\frac{\varepsilon_{ij}}{\varepsilon_o} = \alpha\left(\frac{\varepsilon_\infty}{\varepsilon_o}\right)^N \tilde{\varepsilon}_{ij}\left(\frac{x}{a}, \frac{y}{a}, \frac{a}{w}, N\right) \tag{1.10}$$

and

$$J = \alpha\, \sigma_o\, \varepsilon_o\, a\left(\frac{\sigma_\infty}{\sigma_o}\right)^{1+N} \tilde{J}\left(\frac{a}{w}, N\right) \tag{1.11}$$

where a and w are crack length and panel width, and the dimensionless functions topped by "$\sim$" are independent of the boundary stress σ_∞.

Plane stress and plane strain crack tip fields in pure PH materials have been calculated by Goldman and Hutchinson [6] and Shih and Hutchinson [7] for center cracked panels in tension. J is related to the applied stresses, and the relations are given in the following form:

$$\frac{J}{\alpha\sigma_o\varepsilon_o a} = g\left(\frac{a}{w}, N\right)\left(\frac{w}{w-a}\right)^N\left(\frac{\sigma_\infty}{\sigma_o}\right)^{1+N}, \quad \text{for plane stress} \tag{1.12}$$

$$\frac{J}{\alpha\sigma_o\varepsilon_o a} = f\left(\frac{a}{w}, N\right)\left(\frac{w}{w-a}\right)^N\left(\frac{\sqrt{3}}{2}\right)^{\frac{1+N}{N}}\left(\frac{\sqrt{3}}{2}\frac{\sigma_\infty}{\sigma_o}\right)^{1+N}, \quad \text{for plane strain} \tag{1.13}$$

The values of g and f for pure PH materials are tabulated over the ranges $\frac{1}{8} \le \frac{a}{w} \le \frac{3}{4}$ and $1 \le N \le 20$ [6,7].

For both Ramberg-Osgood PH and piecewise PH materials, the stress-strain relations do not fulfill the requirements of an Ilyushin solid. Therefore Eqn. (1.11) has to be modified.

Rice [9] has shown that the J-integral of a semi-infinite crack in an infinite slab with clamped boundaries at a constant shearing displacement is

$$J = 2hW_\infty$$

where 2h is the height of the slab. In an elastic solid, W_∞ is the constant strain energy at $x = +\infty$ as shown in Fig. 1.2 . For piecewise PH materials,

$$\frac{\tau}{\tau_Y} = \frac{\gamma}{\gamma_Y} \qquad \tau \leq \tau_Y \tag{1.14}$$

$$\frac{\tau}{\tau_Y} = \left(\frac{\gamma}{\gamma_Y}\right)^n \qquad \tau > \tau_Y$$

J is given by [9]

$$\begin{aligned} \frac{J}{2h\tau_Y\gamma_Y} &= \frac{1}{2}\left(\frac{\tau_\infty}{\tau_Y}\right)^2 && \tau_\infty \leq \tau_Y \\ &= \frac{1}{2} + \left(\frac{1}{1+n}\right)\left[\left(\frac{\tau_\infty}{\tau_Y}\right)^{1+\frac{1}{n}} - 1\right] && \tau_\infty > \tau_Y \end{aligned} \tag{1.15}$$

Shih and Hutchinson [7] have obtained the numerical results for plane-stress center-cracked panel in tension for Ramberg-Osgood PH materials. This section deals with the numerical calculations of plane stress and plane strain single-edge cracked panels in tension using piecewise PH relation following the procedure of Shih and Hutchinson [7].

For piecewise PH materials in tension

$$\frac{\sigma}{\sigma_Y} = \frac{\varepsilon}{\varepsilon_Y} \qquad \sigma \leq \sigma_Y$$

$$\frac{\sigma}{\sigma_Y} = \left(\frac{\varepsilon}{\varepsilon_Y}\right)^n \qquad \sigma > \sigma_Y \tag{1.16}$$

where σ_Y and ε_Y are yield stress and strain respectively.

Based on Eqns. (1.12), (1.13) and (1.15), the expression for J-integral can be generalized to the following form:

$$\begin{aligned} \frac{J}{\sigma_Y\varepsilon_Y a\beta\left(\frac{w}{w-a}\right)^{\frac{1}{n}}} &= g\left(\frac{a}{w},\ n\ \right)\left(\frac{\sigma_\infty}{\sigma_Y}\right)^{1+\frac{1}{n}} \\ &= g\left(\frac{a}{w}, n=1\right)\frac{\sigma_\infty\varepsilon_\infty}{\sigma_Y\varepsilon_Y} \quad ; \qquad \text{for } \sigma_\infty \leq \sigma_Y \end{aligned} \tag{1.17a}$$

$$\frac{J}{\sigma_Y \varepsilon_Y a \beta \left(\frac{w}{w-a}\right)^{\frac{1}{n}}} = g\left(\frac{a}{w}, n=1\right) + \left[\frac{\sigma_\infty \varepsilon_\infty}{\sigma_Y \varepsilon_Y} - 1\right] g\left(\frac{a}{w}, n\right); \quad \text{for } \sigma_\infty > \sigma_Y \tag{1.17b}$$

where $\beta = 1$ for plane stress case, and $\beta = \left(\frac{\sqrt{3}}{2}\right)^{1+n}$ for plane strain case. g is a function of $\left(\frac{a}{w}\right)$ and n. The values of g for plane stress and plane strain cases are different, and they are tabulated in References [6,7]. As indicated by Goldman and Hutchinson [6], for plane strain case, when x_2 approaches ∞, we have $\sigma_{11} \to 0$, $\sigma_{22} \to \sigma_\infty$, $\sigma_{33} \to \frac{1}{2}\sigma_\infty$, $\sigma_e \to \frac{\sqrt{3}}{2}\sigma_\infty$, $\varepsilon_{33} = 0$, $\varepsilon_{22} = -\varepsilon_{11} \to \varepsilon_\infty$. From Eqn. (1.5), we also have the following for the pure PH materials in the plane strain case:

$$\frac{\varepsilon_\infty}{\varepsilon_Y} = \frac{\sqrt{3}}{2}\left(\frac{\sqrt{3}}{2}\frac{\sigma_\infty}{\sigma_Y}\right)^{\frac{1}{n}} \tag{1.18}$$

and

$$\frac{\sigma_\infty \varepsilon_\infty}{\sigma_Y \varepsilon_Y} = \left(\frac{\sqrt{3}}{2}\frac{\sigma_\infty}{\sigma_Y}\right)^{1+\frac{1}{n}} \tag{1.19}$$

In Eqn. (1.17b), the first term is the elastic contribution, and the second terms are the plastic part.

The expressions for the stress intensity factors in the linear elastic fracture mechanics are modified by using a_{eff} in order to take account of the plastic effects [18]. To account for this effect, following the practice by Shih and Hutchinson for the Ramberg-Osgood PH materials[7], Eqns. (1.17a and b) are modified to the following forms for piecewise PH materials.

$$\frac{J}{\sigma_Y \varepsilon_Y a \beta \left(\frac{w}{w-a}\right)^{\frac{1}{n}}} = \psi g\left(\frac{a_{eff}}{w}, n=1\right)\left(\frac{\sigma_\infty \varepsilon_\infty}{\sigma_Y \varepsilon_Y}\right); \ \sigma_\infty \leq \sigma_Y \tag{1.20a}$$

$$\frac{J}{\sigma_Y \varepsilon_Y a \beta \left(\frac{w}{w-a}\right)^{\frac{1}{n}}} = \psi g\left(\frac{a_{eff}}{w}, n=1\right) + \left[\left(\frac{\sigma_\infty \varepsilon_\infty}{\sigma_Y \varepsilon_Y}\right) - 1\right] g\left(\frac{a}{w}, n\right); \ \sigma_\infty > \sigma_Y \tag{1.20b}$$

where

$$a_{eff} = a + r_p \qquad \text{for } \sigma_\infty \leq \sigma_Y$$
$$a_{eff} = (a_{eff})_{\sigma_\infty = \sigma_Y} \qquad \text{for } \sigma_\infty > \sigma_Y \tag{1.21}$$

$$r_p = \begin{cases} \frac{1}{2\pi}\left(\frac{1-n}{1+n}\right)\left(\frac{K_I}{\sigma_Y}\right)^2 ; & \text{for plane stress} \\ \frac{1}{6\pi}\left(\frac{1-n}{1+n}\right)\left(\frac{K_I}{\sigma_Y}\right)^2 ; & \text{for plane strain} \end{cases} \tag{1.22}$$

$$\psi = \frac{a_{eff}}{a}\left(\frac{w-a}{w-a_{eff}}\right) \tag{1.23}$$

For the study of fatigue lives of smooth specimens, the relevant fatigue crack is often very small relative to the other dimensions of a specimen. Therefore, the case $\frac{a}{w} \to 0$ is of particular importance. In this case:

$$\psi = \frac{a_{eff}}{a}\left(\frac{w-a}{w-a_{eff}}\right) \simeq \frac{a_{eff}}{a} = \left[1 + \frac{1}{2}\left(\frac{1-n}{1+n}\right)\left(\frac{\sigma_\infty}{\sigma_Y}\right)^2\right] ; \quad \text{for } \sigma \leq \sigma_Y$$
$$= \left[1 + \frac{1}{2}\left(\frac{1-n}{1+n}\right)\right] ; \quad \text{for } \sigma > \sigma_Y$$

$$g\left(\frac{a_{eff}}{w}, n=1\right) \simeq g(0,1)$$

$$\frac{w}{w-a} \simeq 1 ; \qquad 1 - \frac{a}{w} \simeq 1$$

$$K_I = \sigma_\infty \sqrt{\pi a}$$

Equations (1.20a and 1.20b) become

$$\frac{J}{\sigma_Y \varepsilon_Y a_{eff}} = g(0,1)\left(\frac{\sigma_\infty \varepsilon_\infty}{\sigma_Y \varepsilon_Y}\right) ; \qquad \sigma_\infty \leq \sigma_Y \tag{1.24a}$$

$$\frac{J}{\sigma_Y \varepsilon_Y a} = g(0,1)\left[1 + \frac{1}{2}\left(\frac{1-n}{1+n}\right)\right] + \left[\left(\frac{\sigma_\infty \varepsilon_\infty}{\sigma_Y \varepsilon_Y}\right) - 1\right] g(0,n); \quad \sigma_\infty > \sigma_Y \tag{1.24b}$$

where $g(0,n)$ is given by

$$g(0,n) \simeq \left[3.85\sqrt{\frac{1}{n}}(1-n) + \pi n\right]$$

for a center cracked panel in the plane stress case [7]. A similar formula can be written for the plane strain case.

Equation (1.24) can also be written as

$$\frac{J}{\sigma_Y \varepsilon_Y a_{eff}} = g(0,1)\left(\frac{\sigma_\infty \varepsilon_\infty}{\sigma_Y \varepsilon_Y}\right) = 2g(0,1)\left(W_D/\sigma_Y \varepsilon_Y\right); \quad \sigma_\infty \leq \sigma_Y \tag{1.25a}$$

$$\frac{J}{\sigma_Y \varepsilon_Y a} = g(0,1)\left(1 + \frac{1}{2}\frac{1-n}{1+n}\right) + \left[\frac{1}{1+n}\left(\frac{\sigma_\infty \varepsilon_\infty}{\sigma_Y \varepsilon_Y}\right) - \frac{1}{1+n}\left(\frac{\sigma_Y \varepsilon_Y}{\sigma_Y \varepsilon_Y}\right)\right](1+n)g(0,n)$$

$$+ (1+n)g(0,n)\,\frac{1}{2}\,\frac{\sigma_Y \varepsilon_Y}{\sigma_Y \varepsilon_Y} - \frac{1}{2}(1+n)g(0,n)\,\frac{\sigma_Y \varepsilon_Y}{\sigma_Y \varepsilon_Y}$$

$$= \left[\frac{1}{1+n}\left(\frac{\sigma_\infty \varepsilon_\infty}{\sigma_Y \varepsilon_Y}\right) - \frac{1}{1+n}\left(\frac{\sigma_Y \varepsilon_Y}{\sigma_Y \varepsilon_Y}\right) + \frac{1}{2}\left(\frac{\sigma_Y \varepsilon_Y}{\sigma_Y \varepsilon_Y}\right)\right](1+n)g(0,n)$$

$$+ \left[g(0,1)\left(1 + \frac{1}{2}\frac{1-n}{1+n}\right) - \frac{1}{2}(1+n)g(0,n)\right]$$

$$= (1+n)g(0,n) \cdot W_D/\sigma_Y \varepsilon_Y + \eta_2''; \quad \sigma_\infty > \sigma_Y \tag{1.25b}$$

where

$$\frac{W_D}{\sigma_Y \varepsilon_Y} = \left[\frac{1}{1+n}\left(\frac{\sigma_\infty \varepsilon_\infty}{\sigma_Y \varepsilon_Y}\right) - \frac{1}{1+n}\left(\frac{\sigma_Y \varepsilon_Y}{\sigma_Y \varepsilon_Y}\right) + \frac{1}{2}\left(\frac{\sigma_Y \varepsilon_Y}{\sigma_Y \varepsilon_Y}\right)\right] = \left[\frac{1}{1+n}\,\frac{\sigma_\infty \varepsilon_\infty}{\sigma_Y \varepsilon_Y} - \frac{1}{1+n} + \frac{1}{2}\right] \tag{1.26a}$$

and

$$\eta_2'' = \left[g(0,1)\left(1 + \frac{1}{2}\frac{1-n}{1+n}\right) - \frac{1}{2}(1+n)g(0,n)\right] \tag{1.26b}$$

W_D is far field deformation work density as illustrated in Fig. 1.3, and it is given by $W_D = \int_0^{\varepsilon_\infty} \sigma_\infty d\varepsilon_\infty$. The size of a critical fatigue crack at failure is usually rather small. Therefore, for a very small crack, σ_∞ and ε_∞ approach σ and ε of a smooth specimen.

The deformation work done to a non-linear elastic solid is stored as potential energy , i.e. strain energy. But for an elastic-plastic solid, a large part of the deformation work is dissipated in the form of heat; only a small part is stored as potential energy.

Equations (1.24) and (1.25) can be written in the simpler form:

$$\begin{aligned} J &= g(0,1)(\sigma_\infty \varepsilon_\infty) a_{eff} && \sigma_\infty \leq \sigma_Y \\ &= [\eta_1' \sigma_\infty \varepsilon_\infty + \eta_2' \sigma_Y \varepsilon_Y] a , && \sigma_\infty > \sigma_Y \end{aligned} \qquad (1.27a)$$

and

$$\begin{aligned} J &= 2g(0,1) W_D \, a_{eff} && \sigma_\infty \leq \sigma_Y \\ &= [\eta_1'' W_D + \eta_2'' \sigma_Y \varepsilon_Y] a , && \sigma_\infty > \sigma_Y \end{aligned} \qquad (1.27b)$$

where η_1', η_2', η_1'' and η_2'' are functions of n. For plane strain case, the relation between J and the far field parameters can be expressed in the same form. Equations (1.27a and 1.27b) will be used as the basic forms of the expressions of J for a small crack in a wide plate of a piecewise PH material. These two relations will be checked with the finite element calculations and the values of η_1', η_2', η_1'', and η_2'' will be determined.

I.3 The Finite Element Method Analysis

In order to assess the validity of the above analysis, an elastic-plastic finite element study was undertaken. The ABAQUS FEM program was used. The finite element idealization of a single edge cracked panel in tension is shown in Fig. 1.4. The crack length to width ration, a/w = 0.1. The material obeyed the Von Mises criterion and the piecewise power hardening relation,

$$\sigma = E\varepsilon \; ; \qquad \sigma \leq \sigma_Y$$

$$\frac{\sigma}{\sigma_Y} = \left(\frac{\varepsilon}{\varepsilon_Y}\right)^n \; ; \qquad \sigma > \sigma_Y \tag{1.28}$$

The exponent of the stress-strain relation, n, was taken 0.2 and 0.3. $E = 7.0 \times 10^4$ MPa and $\sigma_Y = 350$ MPa were assumed.

The plane eight noded quadratic isoparametic element was used. The crack tip triangular quadratic isoparametric elements were formed by collapsing one side of the quadratic element and placing the mid-side node closer to the crack tip at the quarter point [19]. Crack-tip blunting is modelled by separating the condensed crack tip nodes as shown in Fig. 1.5. Displacement control was used. Both plane stress and plane strain analysis were made.

J-integral are evaluated from the field values obtained by the finite element analysis. Both rectangular path and circular path are chosen. The paths are shown as dashed lines in Fig. 1.4. The detail procedures of the calculation were reported by Zhuang [20].

Path dependency are less than 3% for all the plane stress cases and less than 7% for all the plane strain cases.

Figures 1.6 to 1.13 show the plots of σ_{yy}/σ_Y, $\varepsilon_{yy}/\varepsilon_Y$, $\varepsilon_e^p/\varepsilon_Y$, and σ_e/σ_Y along the crack line versus $r/(J/\sigma_Y)$. J/σ_Y is a measure of crack opening displacement. In Figs. 1.6 to 1.9, the different symbols represent the data at different boundary displacement levels. The solid symbols indicate that the applied nominal strain is beyond the yield strain, ε_Y. The open symbols indicate that the nominal strains are below ε_Y. The nominal strain is the quotient of loading displacement divided by height of the specimen. In each dimensionless plot, all the data near crack tip for small scale yielding, large scale yielding and general yielding fall on the same curve. The fact that, at various load levels, the data of σ_{yy}, ε_{yy}, σ_e, and ε_e^p, in the crack tip region fall on the same curves suggest that there exists a characteristic crack tip field and that a single parameter J, K_σ or K_ε can characterize the crack tip field.

Close to the crack tip, the strain, ε_{yy}, stress, σ_{yy}, effective stress, σ_e, and effective plastic strain ε_e^p, can be expressed as

$$\varepsilon_{yy} = \varepsilon_Y \beta_1 \left[r/\left(\frac{J}{\sigma_Y}\right)\right]^{-m_1}; \quad \beta_1 = \left(\varepsilon_{yy}/\varepsilon_Y\right)_{r=\left(\frac{J}{\sigma_Y}\right)} \tag{1.29a}$$

$$\sigma_{yy} = \sigma_Y \beta_2 [r/(\frac{J}{\sigma_Y})]^{-m_2} \; ; \; \beta_2 = (\sigma_{yy}/\sigma_Y)_{r=(\frac{J}{\sigma_Y})} \tag{1.29b}$$

$$\varepsilon_e^p = \varepsilon_Y \beta_3 [r/(\frac{J}{\sigma_Y})]^{-m_3} \; ; \; \beta_3 = (\varepsilon_e^p/\varepsilon_Y)_{r=(\frac{J}{\sigma_Y})} \tag{1.30a}$$

$$\sigma_e = \sigma_Y \beta_4 [r/(\frac{J}{\sigma_Y})]^{-m_4} \; ; \; \beta_4 = (\sigma_e/\sigma_Y)_{r=(\frac{J}{\sigma_Y})} \tag{1.30b}$$

The values of the slopes of the line segments close to the crack tip in Figs. 1.6 to 1.9, m_1, m_2, m_3, and m_4, are tabulated in Table 1.1. These values are very close to those given by Hutchinson [4], and Rice and Rosengren [5], except the plane strain, m_1 and m_2, which are slightly different. The sums of the calculated values of $(m_1 + m_2)$ and$(m_3 + m_4)$ vary from 0.94 to 1.04. These are close to unity as predicted by the HRR theory.

Figures 1.6 - 1.9 are for n = 0.3. Similar plots for n = 0.2 are shown in Figs. 1.10 - 1.13. In these figures the individual points have been deleted, and the far field data are shown.

TABLE 1.1

COMPARISON OF THE FEM AND HRR THEORY FOR THE VALUES OF m_1, m_2, m_3, and m_4

Stress-Strain State	n	m_1		m_2		m_3		m_4	
		FEM	HRR	FEM	HRR	FEM	HRR	FEM	HRR
Plane Stress	0.2	0.77	0.83	0.167	0.167	0.83	0.83	0.167	0.167
Plane Stress	0.3	0.71	0.77	0.23	0.23	0.81	0.77	0.23	0.23
Plane Strain	0.2	0.78	0.83	0.225	0.167	0.83	0.83	0.167	0.167
Plane Strain	0.3	0.75	0.77	0.29	0.23	0.79	0.77	0.23	0.23

Figures 1.14 to 1.16 plot the product of $(\frac{\sigma_{yy}}{\sigma_\gamma} \cdot \frac{\varepsilon_{yy}}{\varepsilon_\gamma})$ at various distances from the crack tip, r, as a function of the product of the far field parameters, $(\frac{\sigma_\infty}{\sigma_\gamma} \cdot \frac{\varepsilon_\infty}{\varepsilon_\gamma})$. In Figs. 1.17 to 1.19, the normalized J-integral values are plotted against $(\sigma_\infty\varepsilon_\infty/\sigma_\gamma\varepsilon_\gamma)$ and deformation work density W_D respectively for all the cases analyzed. It is demonstrated in these figures that both in the small scale yielding region $(\sigma_\infty\varepsilon_\infty/\sigma_\gamma\varepsilon_\gamma \leq 0.5)$ and in the general yielding region $(\sigma_\infty\varepsilon_\infty/\sigma_\gamma\varepsilon_\gamma \geq 1.4)$ the relations between $(\sigma_{yy}\varepsilon_{yy}/\sigma_\gamma\varepsilon_\gamma)$ and $(\sigma_\infty\varepsilon_\infty/\sigma_\gamma\varepsilon_\gamma)$, $(J/\sigma_\gamma\varepsilon_\gamma a)$ and $(\sigma_\infty\varepsilon_\infty/\sigma_\gamma\varepsilon_\gamma)$, and $(J/\sigma_\gamma\varepsilon_\gamma a)$ and $(W_D/\sigma_\gamma\varepsilon_\gamma)$ appear linear. There is a nonlinear region in between (e.g. $0.5<(\sigma_\infty\varepsilon_\infty/\sigma_\gamma\varepsilon_\gamma)<1.4$). Several correlations between J and far field parameters in this region have been suggested in the recent years [21-24]

Guided by Eqns. (1.20a) and (1.20b), an obvious modification to approximate the relation between J and $(\sigma_\infty\varepsilon_\infty)$ for the single edge cracked specimen in tension, both plane stress and plane strain is [7]

$$\frac{J}{\sigma_\gamma\varepsilon_\gamma a(\frac{W}{W-a})^{1/n}} = \psi F(\frac{a_{eff}}{W}, 1)\ (\frac{\sigma_\infty\varepsilon_\infty}{\sigma_\gamma\varepsilon_\gamma});\ \sigma_\infty \leq \sigma_\gamma \qquad (1.31a)$$

$$\frac{J}{\sigma_\gamma\varepsilon_\gamma a(\frac{W}{W-a})^{1/n}} = \psi F(\frac{a_{eff}}{W}, 1) + [(\frac{\sigma_\infty\varepsilon_\infty}{\sigma_\gamma\varepsilon_\gamma})-1]F(\frac{a}{W}, n);\ \sigma_\infty > \sigma_\gamma \qquad (1.31b)$$

where $F(\frac{a}{W},n)$ is the factor similar to $g(\frac{a}{W},n)$ and $f(\frac{a}{W},n)$ in Eqns. (1.12) and (1.13) for pure power hardening materials. We assume that F is related to g and f in Eqns. (1.12) and (1.13)

$$F(\frac{a}{W},n) = k(\frac{\sqrt{3}}{2})^{1+n} f(\frac{a}{W},n) \qquad \text{for plane strain} \qquad (1.32a),$$

$$F(\frac{a}{W},n) = kg(\frac{a}{W},n) \qquad \text{for plane stress} \qquad (1.32b).$$

The values of f and g are tabulated as f_5 and g_1 in the References [6] and [7] for pure hardening materials with center cracked strip. These values are used for the correlation for this study. The value of k = 1.12 was used to fit the data.

According to the results of Kumar et al. [25] for Ramberg-Osgood power hardening materials, the value of k varies with a/w and n. The value of F, at a given applied stress, must be the asymptotic value as a/w approaches zero, and J will be linearly proportional to a.

Figure 1.17 shows the comparison of the results from FEM calculation and the results based on the simple estimates of Eqn. (1.31) for n = 0.2, a/w = 0.1. The results of the FEM calculations and the estimates by Eqn. (1.31) are listed in Tables 1.2 and 1.3 for comparison. The maximum error is less than 9% for both the plane stress and plane strain cases at the point of $\sigma_\infty\varepsilon_\infty/\sigma_Y\varepsilon_Y = 1$.

Figures 1.17, 1.18, and 1.19 show the correlation between J and $\sigma_\infty\varepsilon_\infty$ and W_D. These results substantiate that J can be linearly related to these two far field parameters in the general yield region, i.e. $\sigma_\infty > \sigma_Y$

$$J = [\eta_1'\sigma_\infty\varepsilon_\infty + \eta_2'\sigma_Y\varepsilon_Y]a \tag{1.33}$$

$$J = [\eta_1''W_D + \eta_2''\sigma_Y\varepsilon_Y]a \tag{1.34}$$

η_2' and η_2'' are the intercepts of the lines when $\sigma_\infty\varepsilon_\infty$ and W_D are zero. η_2'' is nearly equal to zero, if the strain hardening exponent n is not too small. Both $\sigma_\infty\varepsilon_\infty$ and W_D are related to deformation work done to a solid, DW. Therefore Eqns. (1.33 and 1.34) can be written in the form

$$J = [\eta_1\ DW + \eta_2\ \sigma_Y\ \varepsilon_Y]a \tag{1.35}$$

where

$$DW = \sigma_\infty\varepsilon_\infty$$

or

$$= W_D,$$

and it is the primary driving force for crack extension.

Table 1.2

$\frac{\sigma_\infty \varepsilon_\infty}{\sigma_Y \varepsilon_Y}$	$\frac{J}{\sigma_Y \varepsilon_Y a}$	$\frac{J}{\sigma_Y \varepsilon_Y a}$
	Full numerical calculation	Simple estimates
0.60	2.11	2.19
0.80	2.98	3.10
1.00	4.10	4.50
1.10	4.71	5.08
1.20	5.69	5.66
1.38	6.92	6.71
1.66	8.80	8.34
2.06	11.06	10.67
2.41	13.02	12.71
2.68	14.58	14.28
3.18	17.50	17.20
3.45	19.07	18.77
3.73	20.70	20.40
4.20	23.34	23.14

Table 1.2
Comparison of the simple estimates based on Eqns. (1.31) and full numerical calculations for single edge cracked panel in tension with n=0.2 and $\frac{a}{w}$=0.1 for plane strain case.

Table 1.3

$\frac{\sigma_\infty \varepsilon_\infty}{\sigma_Y \varepsilon_Y}$	$\frac{J}{\sigma_Y \varepsilon_Y a}$	$\frac{J}{\sigma_Y \varepsilon_Y a}$
	Full numerical calculation	Simple estimates
0.60	2.40	2.42
0.80	3.44	3.66
1.00	5.11	5.45
1.18	7.52	7.16
1.34	8.78	8.44
1.46	9.81	9.50
1.72	11.95	11.64
1.99	14.14	13.84
2.24	16.28	15.98
2.77	20.64	20.34
3.49	26.62	26.32
4.26	32.99	32.69
5.02	39.27	38.97

Table 1.3
Comparison of the simple estimates based on Eqns. (1.31) and full numerical calculations for single edge cracked panel in tension with n=0.2 and $\frac{a}{w}$=0.1 for plane stress case.

II. J-INTEGRAL AND FATIGUE CRACK GROWTH

In strain controlled fatigue or low cycle fatigue, cracks are initiated and the cracks propagate in cyclic general-yielding loading. Therefore, the LEFM can no longer be used to analyze fatigue crack growth rate.

Dowling and Begley [26] and Dowling [22] suggested to use ΔJ to correlate with fatigue crack growth rate, Figure 2.1. The value of J was evaluated as the "deformation work difference" for through cracks in plates. Dowling [22] has developed an equation for surface crack by combining the FEM calculations of center-cracked and edge-cracked panels by Shih and Hutchinson [7]. Haddad and Mukerjee [27] and Tanaka, Hoshide, and Nakata [28] followed the same procedure to evaluate J and correlated J with da/dN. Kaisand and Mowbray [21] correlated fatigue crack growth in general yielding with ΔJ. ΔJ was divided into two parts: elastic and plastic.

$$\Delta J = \Delta J_e + \Delta J_p \tag{2.1}$$

Using Shih and Hutchinson's calculation and following a procedure similar to Dowling's, ΔJ_p for a surface crack is approximated by

$$\Delta J_p = 1.96\sqrt{1/n'}\ \Delta W_p^{\infty} a \tag{2.2}$$

where n' = cyclic strain hardening exponent. ΔW_p^{∞} = plastic deformation work density at infinity.

Tomkins [29] and Tomkins, Summer and Wareing [30] correlated crack growth rate with crack tip opening displacement, CTOD, and J. J consists of two parts

$$J = \frac{\pi\sigma^2 a}{E} + \frac{\alpha\pi\sigma\varepsilon_p a}{1+n} \tag{2.3}$$

where n is monotonic strain hardening exponent.

Solomon [3] measured fatigue crack growth in specimens in general yielding. In this section, the crack tip field of Solomon's specimens will be calculated with FEM. The J values will be evaluated, and the measured crack growth rate will be correlated with the calculated J values. The crack growth data of a number of steels and aluminum alloys were examined and used to develop a general expression for the characteristic fatigue crack growth behavior in terms of ΔJ.

2.1 *The Analysis of Solomon's Experiment*

The test section of the Solomon's specimen is shown in Fig. 2.2. The test section of the cylindrical specimen was reduced by two semi-circular notches. The gross cross-section of the specimen was 1.24 x 12.6 mm^2. A sharp notch was used to initiate the fatigue crack. A specimen was rigidly attached to the loading frame of the test machine. Fatigue crack growth rates at six cyclic plastic strain ranges were measured. The applied strain range was controlled by an extensometer located at 7.62 mm from the edge of the specimen as shown in Fig. 2.2. The specimens were made of 1018 steel. The chemical composition is given in Table 2.1. The cyclic stress-strain relation of this steel is

$$\frac{\Delta\sigma}{2} = 1360\left(\frac{\Delta\varepsilon_p}{2}\right)^{0.26} \tag{2.4}$$

where $\frac{\Delta\sigma}{2}$ and $\frac{\Delta\varepsilon_p}{2}$ are cyclic stress amplitude and cyclic plastis strain amplitude. $\frac{\Delta\sigma}{2}$ is in MPa. This cyclic stress-strain relation was used in the FEM calculations.

The total strain consists of two parts

$$\Delta\varepsilon = \Delta\varepsilon_e + \Delta\varepsilon_p \tag{2.5a}$$

and

$$\Delta\varepsilon_e = \frac{\Delta\sigma}{E} \tag{2.5b}$$

The cyclic yield stress (170 MPa) is obtained as the intersection of two straight line segments in the log $\Delta\sigma/2$ versus log $\Delta\varepsilon/2$ plot, one in the elastic region and one in the plastic region (see Fig. 2.3).

Solomon [3] plotted his crack growth data in terms of a pseudo stress intensity factor defined as

$$\Delta(PK) = E(\Delta\varepsilon)\sqrt{a} \tag{2.6}$$

where $\Delta\varepsilon = \Delta\varepsilon_e + \Delta\varepsilon_p$

Subsequently, the data was analyzed by Haigh and Skelton [31] in terms of strain intensity factor defined as

$$\Delta K_\varepsilon = \left(\frac{1}{2}\Delta\varepsilon_e + \Delta\varepsilon_p\right)\sqrt{\pi a} \tag{2.7}$$

In order to compare with Eqn. (2.7), Eqn. (2.6) can be written in the form

$$\frac{\sqrt{\pi}\ \Delta(PK)}{E} = (\Delta\varepsilon_e + \Delta\varepsilon_p)\sqrt{\pi a} \tag{2.8}$$

Solomon correlated his data with the total strain range $\Delta\varepsilon$. In Haigh and Skelton's analysis, the elastic strain amplitude was used instead of the elastic strain range because of the consideration of crack closure. The data and the correlations proposed by Solomon [3] and Haigh and Skelton [31] are shown in Fig. 2.4. The scatter band of Solomon's correlation is a factor of slightly more than 3, and the scatter band is reduced to a factor of 2.5 by Haigh and Skelton correlation.

Brown et al. [32] calculated the plane stress crack tip field of Solomon's specimen with the FEM. In their calculation, a constant stress boundary condition was used. The crack growth rate was correlated with the size of severe strain zone, r_s.

A plane stress finite element method calculation was made for the Solomon's specimen in the present work. The mesh is shown in Fig. 2.5a with an enlarged view of the detailed mesh near the crack tip in Fig. 2.5c. The lateral curvature of the specimen was simulated by layers of varying thicknesses as illustrated in Fig. 2.5b.

The solid lines in Fig. 2.5c delineate the meshes, and the dashed curves are the paths for J-integral evaluation. The details of the calculation procedure have been discussed earlier in Section I. All the elements in the layer closest to the crack line are of the same thickness, and the values of J-integral are evaluated along the paths within this layer.

Solomon's specimens were tested in the strain controlled fatigue test fixture. Both ends of the specimen were firmly attached to a rigid test frame. Therefore, a constant displacement boundary condition simulates the test condition closely, and a constant displacement boundary condition was used in the FEM calculation.

Crack tip stresses and strains for three crack lengths, a = 1.27, 2.54, and 5.08 mm, were calculated. The data on effective stress, effective plastic strain, stress σ_{yy}, strain ε_{yy} are plotted in Figs. 2.6 and 2.7. Figure 2.8 shows the normalized strain distribution near the crack tip for three different crack lengths. It is interesting to note that the normalized strain data near the crack tip are on the same straight line for all three crack lengths. The

results in Figs. 2.6, 2.7 and 2.8 suggest that J Integral characterizes the crack tip field for Solomon's specimens, and J can be used to analyze his crack growth data.

The J-values were calculated following the dashed contours in Fig. 2.5c. The J-values of three specimens with three different crack lengths are plotted in Fig. 2.9 as a function of the plastic strain at the location of the extensometer, i.e. at x = 7.62 mm from the left hand side edge of the specimen. J is also plotted as a function of the total strain, ε_{yy} at the location of the extensometer.

For a strain controlled fatigue test, the stabilized hysteresis loop is symmetrical as shown in Fig. 2.10. During the lower half of the cycle when the applied stress is negative, a crack will close and will lose its effectiveness, and the whole specimen will deform uniformly [31]. This deformation does not contribute to the characteristic crack tip field. Therefore, the applied ΔJ, which causes a crack to open, induces the characteristic crack tip field, and propagates the crack, corresponds to the positive part of the loading cycle, ABC in Fig. 2.10.

During the positive part of the loading cycle, the stress-strain follows the curve ABC. This segment of the stress-strain curve consists of the elastic and plastic parts. The plastic part is $\Delta\varepsilon_p$ and the elastic part is $(\Delta\varepsilon-\Delta\varepsilon_p)/2$. The ΔJ-value for Solomon's specimen was evaluated at the plastic strain range $\Delta\varepsilon_p$, and it corresponds to the ΔJ along the loading curve ABC in Fig. 2.10.

The stress-strain relation along ABC differs from the cyclic stress-strain curve. However, the cyclic stress-strain curve was used to calculate the crack tip field for Solomon's test. From the figure, the ΔJ-values of the 18 combinations of three crack lengths and six cyclic plastic strain ranges can be obtained.

The crack growth rates at these 18 combinations of crack lengths and $\Delta\varepsilon_p$ are obtained from Solomon's data with $\Delta(PK) = E\Delta\varepsilon_{yy}\sqrt{a}$. The correlation of ΔJ with da/dN for Solomon's test is shown in Fig. 2.11. The scatter band in Fig. 2.11 is much narrower than the plot in terms of either $\Delta(PK)$ or ΔK_ε in Fig. 2.4. The data in Fig. 2.11 gives the empirical relation

$$\frac{da}{dN} = 0.25 \times 10^{-6}\Delta J^{1.6} \text{ (mm/cycle)} \qquad (2.9)$$

for Solomon's 1018 steel. Equation (2.9) is also plotted in Fig. 2.1 as the dashed line. The data of 1018 steel is very close to the data band of A533B steel.

2.2 Fatigue Crack Growth in the Near Threshold Region

An abundance of information on fatigue crack growth is available in the literature. The overwhelming majority of the data in the near threshold region is correlated with the stress intensity factor range, ΔK. Since K and J are related, the same data can be converted to correlation with ΔJ.

Crack growth rate decreases with ΔK and ΔJ. da/dN starts to decrease rapidly at the transition point at $da/dN = \ell_t$ and $\Delta K = \Delta K_t$ or $\Delta J = \Delta J_t$. Liu and Liu [33] have shown that, in the near threshold region, fatigue crack growth rate can be expressed as

$$\frac{da}{dN} = D\left[\frac{\Delta K}{\Delta K_{th}}\right] - \beta]^m = F\ell_t\left[\frac{\Delta K}{\Delta K_{th}} - \beta\right]^m \tag{2.10a}$$

Yoder et al. [34] suggested that for steels, the transition point is related to the mean free path for dislocation movement, $\bar{\ell}$, Young's modulus E, and cyclic yield strength σ_{YC}, and we have

$$\frac{da}{dN} = C\bar{\ell}\,\frac{\sigma_{YC}}{E}\left[\frac{\Delta K}{\Delta K_{th}} - \beta\right]^m \tag{2.10b}$$

where D, F, C, β, m, ℓ_t and ΔK_{th} are empirical constants.

Since K and J are related, therefore these equations can be written as

$$\frac{da}{dN} = D'\left[\frac{\Delta J}{\Delta J_{th}} - \beta'\right]^{m'} = F'\ell_t\left[\frac{\Delta J}{\Delta J_{th}} - \beta'\right]^{m'} \tag{2.11a}$$

and

$$\frac{da}{dN} = C'\bar{\ell}\,\frac{\sigma_{YC}}{E}\left[\frac{\Delta J}{\Delta J_{th}} - \beta'\right]^{m'} \tag{2.11b}$$

Equation (2.11b) is used to make the regression analysis of the fatigue crack growth data of a number of steels, which were analyzed earlier by both Yoder et al. [34] and Liu and Liu [33]. In the regression analysis, the values of C', β', and

m' are allowed to vary. The values of C_1', β_1', and m_1' of each data set are determined at the point of minimum error. These values are tabulated in Table 2.2. Both of the average values of β' and m' are close to one. Once the value of β' is accepted as equal to one, a second regression analysis was made to determine the values of C' and m', C_2' and m_2'. These values of C_2' and m_2', and $\beta = 1$ are used to plot the curves in Fig. 2.12 . With the average values of β_1' and m_1', the data of all the steels in Fig. 2.12, give the empirical equation, which is shown as the dashed line in the same figure.

$$\frac{da}{dN} = 0.1\ \bar{\ell}\ \frac{\sigma_{YC}}{E}\left(\frac{\Delta J}{\Delta J_{th}} - 1\right) \tag{2.12a}$$

With $\bar{\ell} = \Delta K_t^2/8\pi\sigma_{YC}^2 = \Delta J_t\ E/8\pi\sigma_{YC}^2$ and $(\Delta K_t/\Delta K_{th})^2 \simeq \Delta J_t/\Delta J_{th} = 2$, Eqn. (2.12a) can be written in the form

$$\frac{da}{dN} = A\ \frac{\Delta J_{th}}{\sigma_{YC}}\left(\frac{\Delta J}{\Delta J_{th}} - 1\right)^m \tag{2.12b}$$

The data in Fig. 12 give an average value of A equal to $1/40\pi$.

The data of nine additional steels are plotted in Fig. 2.13 according to Eqn. (2.11a). Table 2.3 shows the regression results of these nine steels. Figures 2.15 to 2.24 show individual regression curve for each fatigue crack growth curve. The original data and the references of the data sources are shown in Fig. 2.13.

The data of several aluminum alloys are shown in Fig. 2.14. The data starts to deviate from Eqn. (2.11a) when da/dN exceeds 2×10^{-2} mm/cycle. Even for low cycle fatigue tests, da/dN does not often exceed this growth rate. Therefore, one may conclude that fatigue crack growth data in the near threshold region correlates well with Eqns. (2.11a and 2.11b).

If the second term of Eqn. (2.12) is neglected for the FCG rate in the higher ΔJ region, and if the relation $\bar{\ell} = \Delta K_t^2/8\pi\sigma_{YC}^2 = \Delta J_t\ E/8\pi\sigma_{YC}^2$, $(\Delta K_t/\Delta K_{th})^2 = \Delta J_t/\Delta J_{th} = 2$, and C' = 0.1 are used, Eqn. (2.12) becomes

$$\frac{da}{dN} = 0.01\ \frac{\Delta J}{\sigma_{YC}} \tag{2.13}$$

Eqn. (2.13) agrees reasonably well with the unzipping FCG calculation obtained by Kuo and Liu [35,36]

$$\frac{da}{dN} = 0.02\ \frac{\Delta J}{\sigma_{YC}} \tag{2.14}$$

In conclusion, a general expression of the following form will fit well with each individual fatigue crack growth curve

$$\frac{da}{dN} = A[\Delta J - \Delta J_{th}]^m \tag{2.15}$$

In the higher ΔJ region, the second term can be neglected and

$$\frac{da}{dN} = A\Delta J^m \tag{2.16}$$

TABLE 2.1

COMPOSITION OF THE 1018 STEEL AND A533B PRESSURE VESSEL STEEL

	C	Mn	P	S	N	O	H	Ni	Mo	Si
1018 Steel	0.18	0.89	0.013	0.022	0.0047	0.0019	<0.002	0	0	0
A533B Steel	0.25	1.15∿1.50	0.035	0.40	0	0	0	0.4∿0.7	0.45∿0.60	0.15∿0.30

TABLE 2.2

THE REGRESSION RESULTS OF YODER'S DATA BY USING da/dN VERSUS ΔJ

Steel	$\bar{\ell}$(mm)	σ_Y (MPa)	ΔK_{th} (MPa$\sqrt{M}$)	ΔJ_{th} MPa M	$E\frac{da}{dN}/\sigma_Y\bar{\ell} = C_1'(\frac{\Delta J}{\Delta J_{th}} - \beta_1')^{m_1'}$			$E\frac{da}{dN}/\sigma_Y\bar{\ell} = C_2'(\frac{\Delta J}{\Delta J_{th}} - 1)^{m_2'}$	
	Grain Size	Yield Stress		$\frac{\Delta K_{th}^2}{E^*}$	C_1'	β_1'	m_1'	C_2'	m_2'
1005	24×10^{-3}	411	8.8	3.688×10^{-4}	2.22×10^{-6}	1.1	1.013	1.83×10^{-7}	1.07
1055	27×10^{-3}	399	12.0	6.857×10^{-4}	1.53×10^{-5}	1.1	1.183	1.13×10^{-6}	1.12
2¼Cr-1Mo	36×10^{-3}	290	9.0	3.857×10^{-4}	3.92×10^{-6}	0.98	0.987	3.77×10^{-7}	1.169
1018	36×10^{-3}	293	7.8	2.897×10^{-4}	3.72×10^{-6}	1.1	1.046	2.60×10^{-7}	1.144
1020	7.8×10^{-3}	366	5.3	1.338×10^{-4}	9.56×10^{-7}	1.0	1.15	3.35×10^{-7}	1.15
1020	20.5×10^{-3}	275	5.7	1.547×10^{-4}	1.94×10^{-6}	1.05	1.06	2.37×10^{-7}	1.17
1020	55×10^{-3}	194	6.8	2.202×10^{-4}	4.03×10^{-6}	1.1	1.125	1.56×10^{-7}	1.00
4Cr-0.35C	0.83×10^{-3}	1324	4.4	0.922×10^{-4}	1.21×10^{-6}	1.0	1.04	8.77×10^{-7}	1.092
4Cr-0.35C	0.47×10^{-3}	1324	3.4	0.5505×10^{-4}	1.23×10^{-6}	0.9	0.927	1.68×10^{-6}	0.991
4Cr-0.35C	0.41×10^{-3}	1303	3.3	0.5186×10^{-4}	1.15×10^{-6}	0.9	0.93	1.61×10^{-6}	0.993
4Cr-0.35C	0.38×10^{-3}	1324	3.0	0.4285×10^{-4}	8.71×10^{-7}	0.9	0.962	9.15×10^{-7}	1.155
304 S.S.	76×10^{-3}	715*	16.0	1.22×10^{-3}	4.53×10^{-5}	0.93	0.92	8.95×10^{-7}	1.232
Average Value						1.005	1.0203	4.76×10^{-7}	

E* = 210 GPa

TABLE 2.3

REGRESSION ANALYSES OF FATIGUE CRACK GROWTH DATA

Steel	Heat Treat Condition or Environment Condition	R Stress Ratio	C_2'	m_2'
0.55%C-2.23%Mn		0.36	0.68	1.24
		0.05	1.41	1.38
		0.72	0.71	0.97
2¼Cr-1Mo	Air		0.76	1.17
	Dry He		2.29	1.24
	Dry H_2	0.05	1.23	1.18
	Dry H_2	0.3-0.8	1.12	1.12
300M	Moist Air		0.46	0.8
	Dry H_2	0.05	0.31	1.11
	Dry H_2	0.3	0.48	1.20
0.55%C-0.66%Mn		0.36	1.05	1.12
		0.08	1.32	1.15
300M	Quenching 470°	0.7	2.40	0.99
	Plus 300°	0.7	1.74	1.04
	Tempering 100°	0.7	1.70	1.06
	650°	0.7	1.18	1.33
	100°	0.05	0.83	1.19
	300°	0.05	1.35	1.04
	470°	0.05	1.35	1.17
	650°	0.05	0.83	1.27

$$\frac{da}{dN}/\ell_t = C_2'\left(\frac{\Delta J}{\Delta J_{th}} - 1\right)^{m_2'}$$

$$\frac{\sum m_2'}{N} = 1.1$$

$$\frac{\sum C_2'}{N} = 1.05$$

$$\frac{da}{dN}/\ell_t = 1.05\ \left(\frac{\Delta J}{\Delta J_{th}} - 1\right)^{1.1}$$

Table 2.3 (continued)

Steel			R	C_2'	m_2'
Fe-4% Cr-0.35%	Austenitizing Temperature	870°C		0.65	1.19
		1000°C		1.23	0.91
		1100°C		0.98	0.95
		1200°C		0.74	1.0
AF1410				0.89	0.87
HP9-4-20				0.91	0.99
HP9-4-20				1.26	1.01
SA387			0.3	1.51	1.28
0.12%C-2.48%Cr			0.8	0.50	1.03
0.14%Ni-1.06%Mo			0.05	0.81	1.20
			0.5	0.81	1.10
0.88%C - 0.27%Mn			0.12	0.80	1.57
			0.35	0.54	1.22
			0.72	0.98	0.65

III. FATIGUE CRACK GROWTH IN GENERAL YIELDING AND LOW CYCLE FATIGUE LIFE

Fatigue damage includes the processes of crack initiation and propagation. Owing to the defects and damage during material processing and fabrication, and owing to environmental attacks such as oxidation and hydrogen embrittlement, the crack initiation period might be shortened, and fatigue lives of such engineering components or structures are mainly fatigue crack propagation periods.

Elastic-plastic fracture mechanics can be used to study the life of a low cycle fatigue specimen based on crack propagation. Kaisand and Mowbray [21] derived the expression relating the life of strain controlled fatigue specimen to the far field deformation work density, ΔW^{∞}. The J-integral relation developed by Shih and Hutchinson [7] for the Ramberg-Osgood hardening materials was used.

According to Kaisand and Mowbray [21] the relation between ΔW^{∞} and fatigue life, N_f, can be expressed as follows:

$$\Delta W^{\infty} = \Delta W_e^{\infty} + \Delta W_p^{\infty}$$

$$= C_2 N_f^{-1/\beta} + C_1 N_f^{-1/\gamma} \tag{3.1}$$

where ΔW^{∞} is the applied deformation work density which consists of elastic and plastic parts. C_1, C_2, β and γ are constants. ΔW_e^{∞} and ΔW_p^{∞} are related to the applied stress and strain ranges.

J is related to deformation work density, $J = \eta \int \sigma d\varepsilon = \eta W_D$ [6,7,9,18,37]. Dowling and Begley [26] and Dowling [22] correlated fatigue crack growth with ΔJ; and Chen, Zheng, and Tsai [38] have correlated low cycle fatigue lives with the deformation work density.

In this section, the cyclic life will be related to the applied stress and strain ranges, $\Delta\sigma_{\infty}$ and $\Delta\varepsilon_{\infty}$. The relation will be derived from the relation between J and the far field parameters together with the cyclic crack growth relation in Sections I and II.

A fatigue crack is often nucleated on a free surface in the shape of a semi-ellipse, and the nucleated crack is often a shear crack. For a part through shear crack, the shear mode of the crack tip field varies from mode II to mode III along the periphery of the crack. For a part through tensile crack, Fig. 3.1, a plane stress crack tip field exists at A, and a plane strain field exists at B. The variation of the character of the crack tip field is determined by the crack orientation and the applied stresses.

Along the periphery of a semi-elliptical shear crack, the value of J varies. Equations (1.33) and (1.34) have to be modified by a function of θ, $\phi(\theta)$. $\phi(\theta)$ prescribes the θ-variation of J along the crack periphery. In the steady state growth of a small crack, the geometry of the growing crack can be assumed to remain similar. For geometric similar cracks, $\phi(\theta)$ remains unchanged, and only a single crack length parameter is needed to characterize the crack tip field. Therefore, equations in the forms of (1.33) and (1.34) are applicable to the geometrically similar semi-elliptical shear cracks, as well as to the geometrically similar semi-ellipitical tensile cracks.

The relations between J and the far field parameters were developed for monotonic loading. For completely reversed cyclic loading, R = -1 and $\sigma_{mean} = 0$, a crack will close under compression, losing its effectiveness. Therefore, the processes of developing the characteristic crack tip field, crack tip opening, and crack growth occur during the tensile half cycle, i.e. during the part of the loading curve ABC in Fig. 2.10. The effective ΔJ for crack growth corresponds to this part of the loading curve. Hence, the effective stress range, $\Delta\sigma_\infty$, and effective strain range, $\Delta\varepsilon_\infty$, are $\frac{\Delta\sigma}{2}$ and $(\Delta\varepsilon_p + \frac{\Delta\varepsilon_e}{2})$. Therefore, σ_∞ and ε_∞ in Eqns. (1.24) and (1.25) should be replaced by these two quantities, correspondingly. The

quantity σ_Y and ε_Y are used to normalize the expression for J in Figs. 1.17 and 1.18. Hence, $\sigma_Y\varepsilon_Y$ can be changed into $\sigma_{YC}\varepsilon_{YC}$ without major change in the form of the derived relation. A small change in the form of a constant factor can be absorbed into the constant η_2.

In Section II, the J of a mode I through crack has been investigated. For geometrically similar part-through semi-elliptical cracks in infinite solids, with the θ-variation omitted, the J integral can be written in the similar form. For a piecewise power hardening material,

$$\Delta J = (\eta_1 \, DW + \eta_2 \sigma_{YC} \varepsilon_{YC}) a \tag{3.2}$$

where η_1 and η_2 are functions of n and they are constants for a given material. DW is the deformation work parameter. It can be either $\Delta\sigma_\infty \Delta\varepsilon_\infty$ or ΔW_D.

In Section II, the data indicate that a general crack growth relation can be put in the form

$$\frac{da}{dN} = A \frac{\Delta J_{th}}{\sigma_{YC}} \left(\frac{\Delta J}{\Delta J_{th}} - 1\right)^m \tag{3.3}$$

If the growth of semi-ellipitical cracks follows the same relation, and substituting Eqn. (3.2) into Eqn. (3.3) and integrating, we obtain the following expression. During the propagation of a small crack, DW is assumed to be constant.

$$(N_f - N_o) = \frac{\sigma_{YC}}{A(m-1)[\eta_1 \, DW + \eta_2 \sigma_{YC} \varepsilon_{YC}]} \left\{ \frac{1}{\left(\frac{a_o}{a_{th}} - 1\right)^{m-1}} - \frac{1}{\left(\frac{a_f}{a_{th}} - 1\right)^{m-1}} \right\} \tag{3.4}$$

where a_o and a_f are initial and final crack lengths. N_o and N_f are crack initiation life and total fatigue life. a_{th} can be considered as the maximum size of a non-propagating crack at the applied cyclic load.

$$a_{th} = \Delta J_{th}/(\eta_1 \, DW + \eta_2 \sigma_{YC} \epsilon_{YC}) \tag{3.5}$$

At a given value of DW, a_{th} is constant.

If a_f is much larger than a_o, the second term within the bracket of (3.4) is much smaller and can be neglected. After rearrangement, Eqn. (3.4) becomes

$$\left(\frac{[\eta_1 \, DW + \eta_2 \sigma_{YC} \epsilon_{YC}]a_o}{\Delta J_{th}}\right)^{m-1} [\eta_1 \, DW + \eta_2 \sigma_{YC} \epsilon_{YC}](N_f - N_o) = \frac{\sigma_{YC}}{A(m-1)} \tag{3.6}$$

Fatigue life is a function of the deformation work, DW. Thus we have

$$(N_f - N_o) = f(DW) = f_1(\Delta\sigma_\infty \Delta\epsilon_\infty) = f_2(\Delta W_D) \tag{3.7}$$

a_o is related to the microstructural feature of the crack nucleation process. For a given material, a_o is a constant. η_2 is negligible if the value of n is not too large. N_o is negligible if there exist material and fabrication defects or if environmental attact is severe. If a_o is much larger than a_{th}, and if η_2 and N_o are negligible, then we have

$$(DW)^m N_f = \frac{\sigma_{YC}}{A(m-1)\eta_1^m} \left(\frac{\Delta J_{th}}{a_o}\right)^{m-1} = C \tag{3.8}$$

The right hand side of Eqn. (3.8) is a constant. Or

$$(\Delta\sigma_\infty \Delta\epsilon_\infty)^m N_f = C_1 \tag{3.9}$$

and

$$\Delta W_D^{\,m} N_f = C_2 \tag{3.10}$$

The total life consists of fatigue crack initiation and propagation, N_o and $(N_f - N_o)$. The crack initiation period is strongly affected by the size of the material and fabrication defects, a_o. A large a_o will reduce the total fatigue

life. The quantity, a_{th} can be considered as the size of a non-propagating crack, at the applied stress and strain ranges. If a_o is less than a_{th}, the crack will not grow and no fatigue failure will occur. Fatigue life is also affected strongly by the crack growth characteristics A, m and ΔJ_{th}.

Because of the uncertain nature of the cyclic crack tip field due to the lack of the precise cyclic constitutive relation, the lack of the calculated cyclic crack tip field, the lack of the information on shear cracks and the uncertain nature of the frictional shear stress between mating crack surfaces, the relations given by Eqns. (3.4, 3.6, 3.7, 3.8, 3.9 and 3.10) may not be accurate quantitatively. However, these equations give the basic forms of the expressions for fatigue life, and how fatigue life is related to all of these factors. And these equations also help us to develop meaningful correlations of the experimental data and to assess the contributions from various physical and mechanical factors.

Chen, Zheng, and Tsai [38] conducted strain controlled fatigue tests on copper-aluminum wrought alloys. The chemical compositions of the aluminum alloys are shown in Table 3.1. Their mechanical properties are tabulated in Table 3.2. The specimen geometry is shown in Fig. 3.2.

The plots of $(\Delta\sigma_\infty \Delta\varepsilon_\infty)$ vs N_f and $\frac{\Delta\sigma_\infty}{2}(\Delta\varepsilon_p + \frac{\Delta\varepsilon_e}{2})$ vs N_f are shown in Figs. 3.3 and 3.4. Figure 3.4a shows the fatigue lives of both smooth specimens and precracked specimens. The specimens were precracked by electrostatic discharge machining. Both lines in Fig. 3.4a are parallel. The difference in cyclic life can be interpreted as the number of cycles to grow a crack from its "natural" crack nucleus size to the size of the precrack. If we denote a_{o1} and N_{f1} as the precrack size and the fatigue life of a precracked specimen, Eqns. (3.8 and 3.10) give the ratio N_f/N_{f1} = constant. Therefore, the plot of

the fatigue lives of smooth and precracked specimens should be parallel as shown in Fig. 3.4a. But the lines of the precracked specimens are shifted to the left.

The plots of ΔW_D vs N_f are shown in Figs. 3.5 and 3.6. ΔW_D can be defined as

$$\Delta W_D = \int_0^{\Delta\varepsilon_p + \Delta\varepsilon_e/2} \sigma d\varepsilon \qquad (3.11a)$$

ΔW_D is for the part of the loading curve that causes a crack to open and to grow, i.e. ABC in Fig. 2.10. For these specimens, the values of deformation work density were directly measured from stabilized cyclic stress-strain hysteresis loops at approximately half of the fatigue life. The plots of the area under the hysteresis curve vs N_f are shown in Fig. 3.5.

ΔW_D can also be defined as

$$\Delta W_D = \int_0^{\Delta\varepsilon_e/2} \sigma d\varepsilon + \int_0^{\Delta\varepsilon_p} \sigma d\varepsilon \qquad (3.11b)$$

Take the approximation of the cyclic stress and strain ranges in the form $(\Delta\sigma - \sigma_{YC}) = \Delta\varepsilon_p^{n'}$ for $\frac{\Delta\sigma}{2} > \sigma_{YC}$ and integrating Eqn. (3.11b), we obtain

$$\Delta W_D = \frac{\Delta\sigma^2}{8E} + \left[\frac{1}{1+n'}\,\Delta\varepsilon_p^{n'} + \sigma_{YC}\right]\Delta\varepsilon_p$$

$$= \frac{\Delta\sigma^2}{8E} + \left[\frac{1}{1+n'}(\Delta\sigma - \sigma_{YC}) + \sigma_{YC}\right]\Delta\varepsilon_p \qquad (3.12)$$

The first term for the plastic strain is much smaller and can be neglected.

$$\Delta W_D = \frac{\Delta\sigma^2}{8E} + \sigma_{YC}\Delta\varepsilon_p \tag{3.13}$$

Substituting Eqn. (3.13) into Eqn. (3.8), we obtain

$$\left[\frac{\Delta\sigma^2}{8E} + \sigma_{YC}\Delta\varepsilon_p\right]^m N_f = \frac{\sigma_{YC}}{A(m-1)(n_1')^m}\left(\frac{\Delta J_{th}}{a_o}\right)^{m-1} \tag{3.14}$$

where a_o is the initial crack length. The plots of $\Delta W_D = [\frac{\Delta\sigma^2}{8E} + \sigma_{YC}\Delta e_p]$ vs N_f are shown in Fig. 3.6.

Straight lines correlate the data very well in all of these figures, Figs. 3.3 to 3.6, over the fatigue life range from 10 to 10^5 cycles. Therefore Eqns. (3.9) and (3.10) are valid over three to four orders of magnitude of fatigue life. Additionals data are necessary to distinguish these four correlations.

Equations (3.9) and (3.10) can be written in the forms

$$E(\frac{\Delta\varepsilon_e}{2})^2 N_f^{\frac{1}{m}} + \frac{\Delta\sigma}{2}\Delta\varepsilon_p N_f^{\frac{1}{m}} = C' \tag{3.15a}$$

and

$$\frac{E}{2}(\frac{\Delta\varepsilon_e}{2})^2 N_f^{\frac{1}{m}} + \sigma_{YC}\Delta\varepsilon_p N_f^{\frac{1}{m}} = C'' \tag{3.15b}$$

The left hand sides of these two equations consist of the elastic and the plastic parts. Each of these parts is similar to the basic form of the elastic and plastic contributions of strain controlled fatigue, i.e.

$$\Delta\varepsilon_e N_f^{\gamma_1} = C_1$$

and (3.16)

$$\Delta\varepsilon_p N_f^{\gamma_2} = C_2$$

When the elastic part is negligible, the plastic part becomes the original Coffin-Manson low cycle fatigue law.

Table 3.1 Chemical Composition for the Alloys Tested

	Cu	Mn	Si	Fe	Mg	Zn	Ni	Al
LD-10	4.56	0.86	1.01	0.24	0.70	0	0	92.631%
LY-12	3.8∿3.9	0.3∿0.9	0.5	0.50	1.2∿1.8	0.3	0.1	91∿93.31%

Table 3.2 The Material Properties for LD-10 and LY-12 Aluminum Alloys

		σ_Y(MPa)	σ_u(MPa)	E(MPa)	σ_{Yc} (MPa)
Al. Alloy	Heat treatment Condition	Yield Strength	Ultimate Strength	Young's Modulus	Cyclic Yield Strength
LD-10	Cold rolling	281	439	7.10×10^4	323
LY-12	Natural age	416	578	7.35×10^4	465
LY-12	Artificial age	313	411	7.45×10^4	274

CONCLUSIONS

1. A characteristic crack tip field exists for a small through crack in a large plate in both plane strain and plane stress conditions. The crack tip field can be characterized by J.
2. For small cracks, J is linearly proportional to crack length and proportional to the far field parameters: the product $\sigma_\infty \varepsilon_\infty$ and the applied deformation work density.
3. Fatigue crack growth rate in general yielding correlates well with ΔJ.
4. An expression for the general fatigue crack growth behavior is developed in terms of ΔJ.
5. An equation for fatigue life is derived from the general crack growth behavior. This equation relates fatigue life to various physical and mechanical aspects of fatigue damage, such as crack nuclei size, fracture toughness and fatigue crack growth behavior.
6. Low cycle fatigue lives of two aluminum alloys correlate well with deformation work density.
7. The derived equation for fatigue life is reduced to Coffin-Manson low cycle fatigue law in the high strain region.

ACKNOWLEDGEMENT

The work was conducted at the George Sachs Fracture and Fatigue Research Laboratory at Syracuse University. The financial support by NASA, Grant No. NAG 3-348 and the Visiting Scholarship by the People's Republic of China to Mr. Zheng Minzhong are acknowledged. The Computer Center of the Syracuse University for making computer time available to the authors and the Hibbit, Karlsson, and Sorensen, Inc. for the privilege of using the ABAQUS finite element program are also acknowledged. The assistance by Mrs. Helen Turner, Mr. Rolf Zeimer and Mr. Qi Chen in manuscript preparation is very much appreciated.

REFERENCES

[1] L. C. Coffin, Jr., "A Study of the effects of cyclic thermal stresses on a ductile metal," Trans. ASME 76, 1954, p. 931.

[2] R. W. Smith, M. H. Hirschberg, and S. S. Manson, "Fatigue behavior of materials under strain cycling in low and intermediate life range," NASA TN D-1574, Nat. Aero. and Space Adm., 1963.

[3] H. D. Solomon, "Low cycle fatigue crack propagation in 1018 steel," Journal of Materials, JMLSA, Vol. 7, No. 3, September 1972, pp. 299-306.

[4] J. W. Hutchinson, "Singular behavior at the end of a tensile crack in a hardening material," J. of Mech. and Phys. of Solids, Vol. 16, 1968, p. 13.

[5] J. R. Rice and G. F. Rosengren, "Plane strain deformation near a crack top in a power-law hardening material," J. of Mech. and Phys. of Solids, Vol. 16, 1968, p. 1.

[6] N. L. Goldman and J. W. Hutchinson, "Fully plastic crack problems: The center-cracked strip under plane strain," Int. J. Solids Structures 11, 1975, p. 575.

[7] C. F. Shih and J. W. Hutchinson, "Fully plastic solutions and large scale yielding estimations for plane stress crack problems," J. Eng. Mat. and Tech., 1976, pp. 289-295.

[8] J. C. Amazigo, "Fully plastic crack in an infinite body under anti-plane shear," Int. J. Solids Structure 10, 1974, p. 1003.

[9] J. R. Rice, Journal of Applied Mechanics, Transactions, American Society of Mechanical Engineers, Vol. 35, 1968, pp. 379-386.

[10] C. F. Shih, "J-integral estimates for strain hardening materials in anti-plane shear using fully plastic solution," Mechanics of Crack Growth, ASTM STP 590, 1976, pp. 3-26.

[11] A. A. Ilyushin, "The theory of small elastic-plastic deformation," Prikadnaia Matematika Mekhanika, P.M.M. 10, 1946, p. 347.

[12] L. M. Kachanov, "Fundamentals of the theory of plasticity," translated from the Russian by M. Konyaeva, Mir Publishers, Moscow, 1974.

[13] J. W. Hutchinson, "Singular behaviour at the end of a tensile crack in a hardening material, and plastic stress and strain fields at a crack tip," J. Mech. Phy. Solids 16, 13, 1968, 337.

[14] R. M. McMeeking and D. M. Parks, "On criteria for J-dominance of crack tip fields in large scale yielding," Elastic-Plastic Fracture, ASTM, STP 668, Am. Soc. for Testing and Materials, 1979, pp. 175-194.

[15] C. F. Shih and M. D. German, "Requirements for a one parameter characterization of crack tip fields by the HRR Singularity," Int. J. of Fracture 17, No. 1, Feb. 1981, pp. 27-43.

[16] W. L. Hu, "A finite element study on crack tip deformation," Ph.D. Dissertation, Solid State Science and Technology, Syracuse University, 1976.

[17] W. L. Hu and H. W. Liu, "Characterization of crack tip stresses and strains -- small scale yielding and general yielding," Proceedings of the Second Intl. Conf. on Mechanical Behavior, Aug. 16-20, 1976, Boston, Mass.

[18] H. Tada, P. Paris, and G. Irwin, "The Stress Analysis of Cracks Handbook," published by the Del Research Corporation, 1973.

[19] A. S. Kobayashi, "Numerical analysis in fracture mechanics," The Office of Naval Research under Contract N00014-76-C-0060 NR 064-478. Technical Report No. UWA/DME/TR-83/45.

[20] Zhaung Tao, Ph.D. Dissertation, Dept. of Chemical Eng. and Mat. Sci., Syracuse University, 1984. To be published.

[21] L. R. Kaisand and D. F. Mowbray, "Relationships between low-cycle fatigue and fatigue crack growth rate properties," Journal of Testing and Evaluation, JTEVA, Vol. 7, No. 5, Sept. 1979, pp. 270-280.

[22] N. W. Dowling, "Crack growth during low-cycle fatigue of smooth axial specimens," Cyclic Stress-Strain and Plastic Deformation Aspects of Fatigue Crack Growth, ASTM STP 637, 1977, pp. 97-121.

[23] R. P. Skelton, "Growth of short cracks during high strain fatigue and thermal cycling," Low-Cycle Fatigue and Life Prediction, ASTM STP 770, 1982, pp. 337-381 .

[24] V. M. Radhakrishnam, "Damage accumulation and fracture life in high-temperature low-cycle fatigue," Low-Cycle Fatigue and Life Prediction, ASTM STP 770, 1982, pp. 135-151.

[25] V. Kumar, M. D. German, and C. F. Shih, "An engineering approach for elastic-plastic fracture analysis," Electric Power Research Institute, NP-1931 Research Project 1237-1, Topical Report, July 1981.

[26] N. E. Dowling and J. A. Begley, "Fatigue crack growth during gross plasticity and the J-integral," Mechanics of Crack Growth, ASTM STP 590, 1976, pp. 80-103.

[27] M. H. El Haddad and B. Mukherjee, "Elastic-plastic fracture mechanics analysis of fatigue crack growth," Elastic-Plastic Fracture: Second Symposium, Vol. II - Fracture Resistance Curves and Engineering Applications, ASTM STP 803, 1983, pp. II-689-II-707.

[28] K. Tanaka, T. Hoshide, and M. Nakata, "Elastic-plastic crack propagation under high cyclic stresses," Elastic-Plastic Fracture: Second Symposium, Vol. II - Fracture Resistance Curves and Engineering Applications, ASTM STP 803, 1983, pp. II-689-707.

[29] B. Tomkins, J. of Engineering Materials and Technology, Transactions of ASME, Series H., Vol. 97, 1975, pp. 289-297.

[30] B. Tomkins, G. Sumner, and J. Wareing, in Inter. Symposium on Low Cycle Fatigue Strength and Elasto-Plastic Behaviour of Materials, Deutscher Verband für Material Prüfung, Berlin, 1979, pp. 495-507.

[31] J. R. Haigh and R. P. Skelton, Materials Science and Engineering 36, 1978, pp. 17-25.

[32] M. W. Brown, H. W. Liu, A. P. Kfouri, and K. J. Miller, "An analysis of fatigue crack growth under yielding conditions," Advances in Fracture Research edited by D. Francois et al., Pergamon Press, Oxford and New York, 1980.

[33] H. W. Liu and Dai Liu, "A quantitative analysis of structure sensitive fatigue crack growth in steels," Scripta Metallurgica 18, 1984, pp. 7-12.

[34] G. R. Yoder, L. A. Cooley, and T. W. Crooker, Naval Research Laboratory Memorandum Report 4576, July 1981.

[35] A. S. Kuo, and H. W. Liu, "An Analysis of Unzipping Model for Fatigue Crack Growth," Scripta Met. 10, p. 723, 1976.

[36] C. Y. Yang and H. W. Liu, "The application of the unzipping model of fatigue crack growth to micro-cracks," Scripta Metallurgica 14, July 1980, pp. 785-790.

[37] C. K. Tsai, "J-integral analysis," J. of Acta Metallurgica 12, 1(1976), p. 45.

[38] X. X. Chen, M. Z. Zheng, and C. K. Tsai, "Study of strain fatigue in LD-10 alloy," J. of Acta Mechanica Sinica, China 5, 1981.

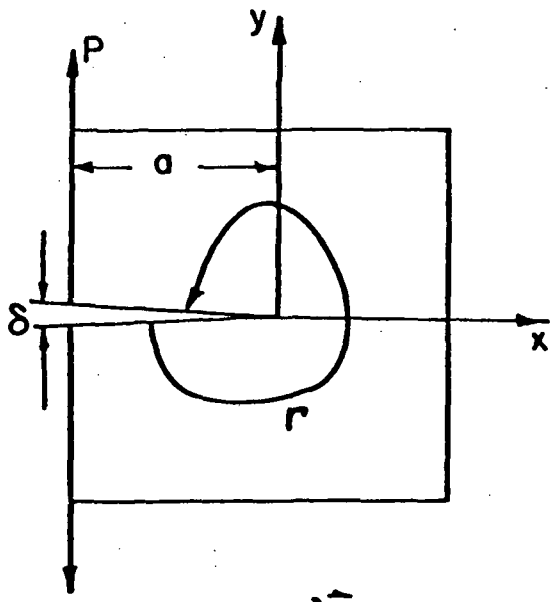

$$J = \int_{\Gamma} W dy - \vec{T} \cdot \frac{\partial \vec{u}}{\partial x} ds$$

$$W = \int_{o}^{\epsilon_{mn}} \sigma_{ij} \, d\epsilon_{ij}$$

(a) Line integral contour.

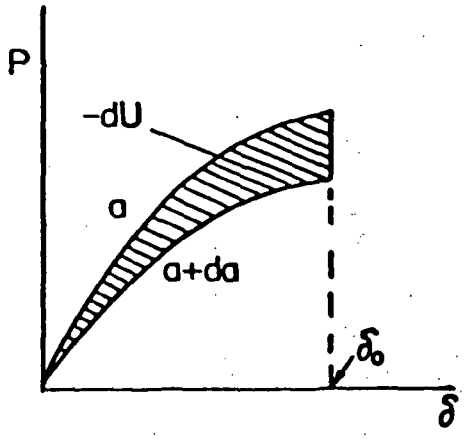

$$J = -\frac{1}{B}\left(\frac{dU}{da}\right)$$

B= Thickness

(b) Deformation work difference

Fig. (1.1) J-Integral of Rice.

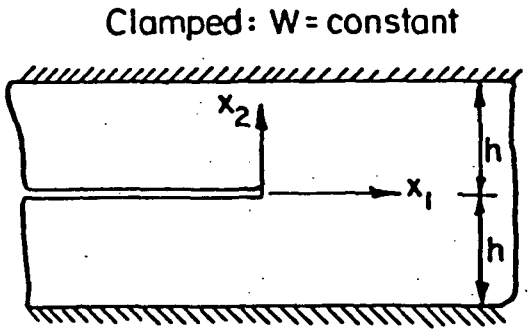

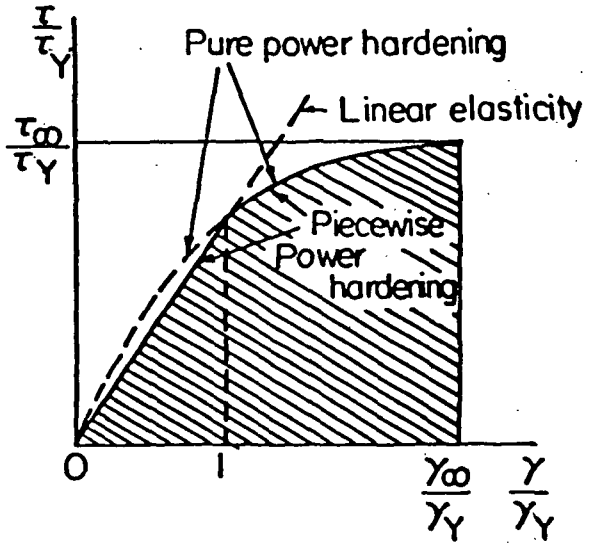

Fig. (1.2) (a) Infinitely wide slab with semi-infinite slit.

(b) Stress-strain relations for pure shear.

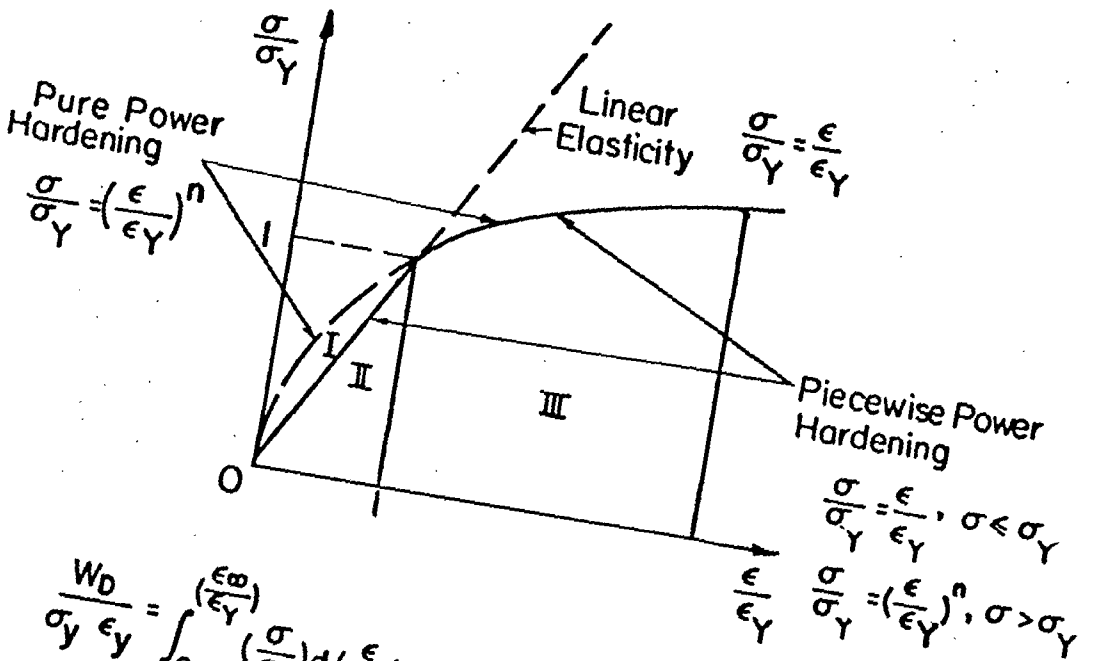

$$\frac{W_D}{\sigma_y\,\epsilon_y}=\int_0^{(\frac{\epsilon_\infty}{\epsilon_Y})}(\frac{\sigma}{\sigma_Y})\,d(\frac{\epsilon}{\epsilon_Y})=\text{II}+\text{III}=(\text{I}+\text{II}+\text{III})-(\text{I}+\text{II})+(\text{IV})$$

$$=\frac{1}{1+n}(\frac{\sigma_\infty\epsilon_\infty}{\sigma_Y\epsilon_Y})-\frac{1}{1+n}(\frac{\sigma_Y\epsilon_Y}{\sigma_Y\epsilon_Y})+\frac{1}{2}(\frac{\sigma_Y\epsilon_Y}{\sigma_Y\epsilon_Y})$$

$$=\frac{1}{2}+\frac{1}{1+n}(\frac{\sigma_\infty\epsilon_\infty}{\sigma_Y\epsilon_Y}-1)$$

Fig. (1.3) The deformation work density for piecewise PH Materials, $\int_{\sigma d\epsilon/\sigma_Y\epsilon_Y}$.

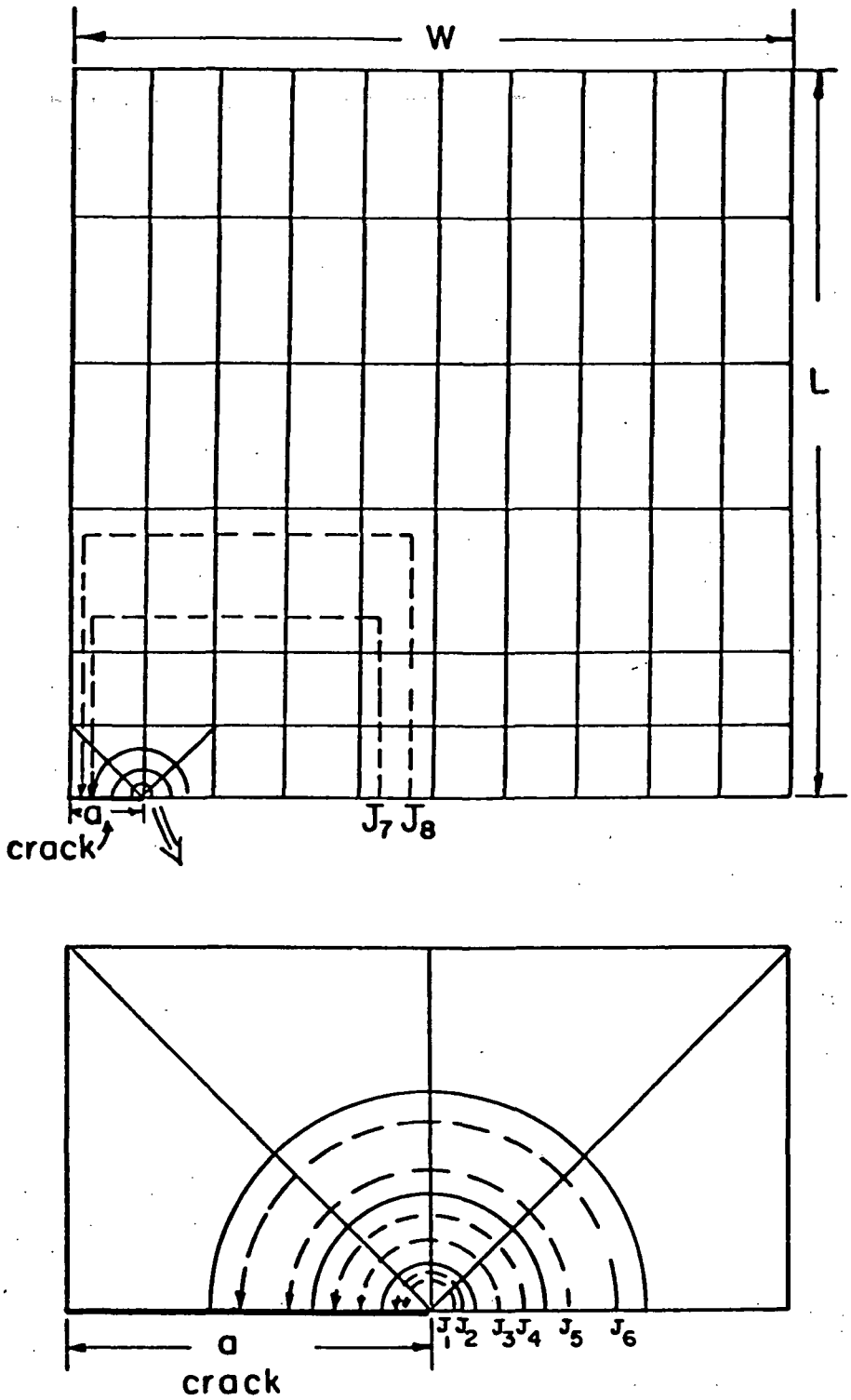

Fig. (1.4) Finite element mesh and J-integral paths for single edge cracked panel in tension. $\frac{a}{w} = 0.1$.

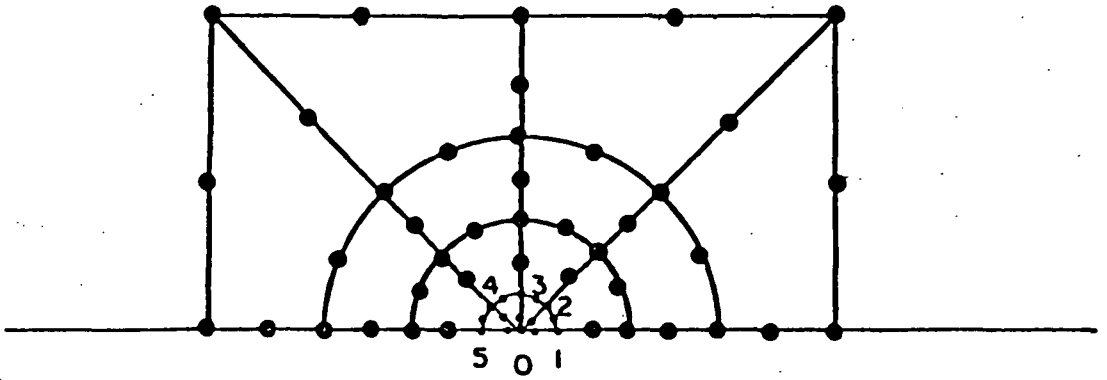

(a) Initial mesh

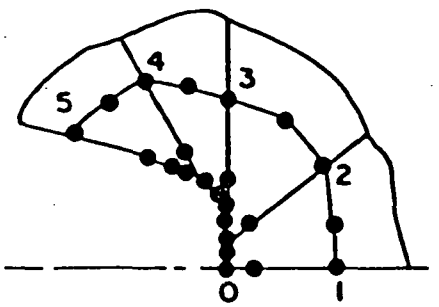

(b) Mesh after crack blunting

Fig. (1.5) Crack tip blunting.

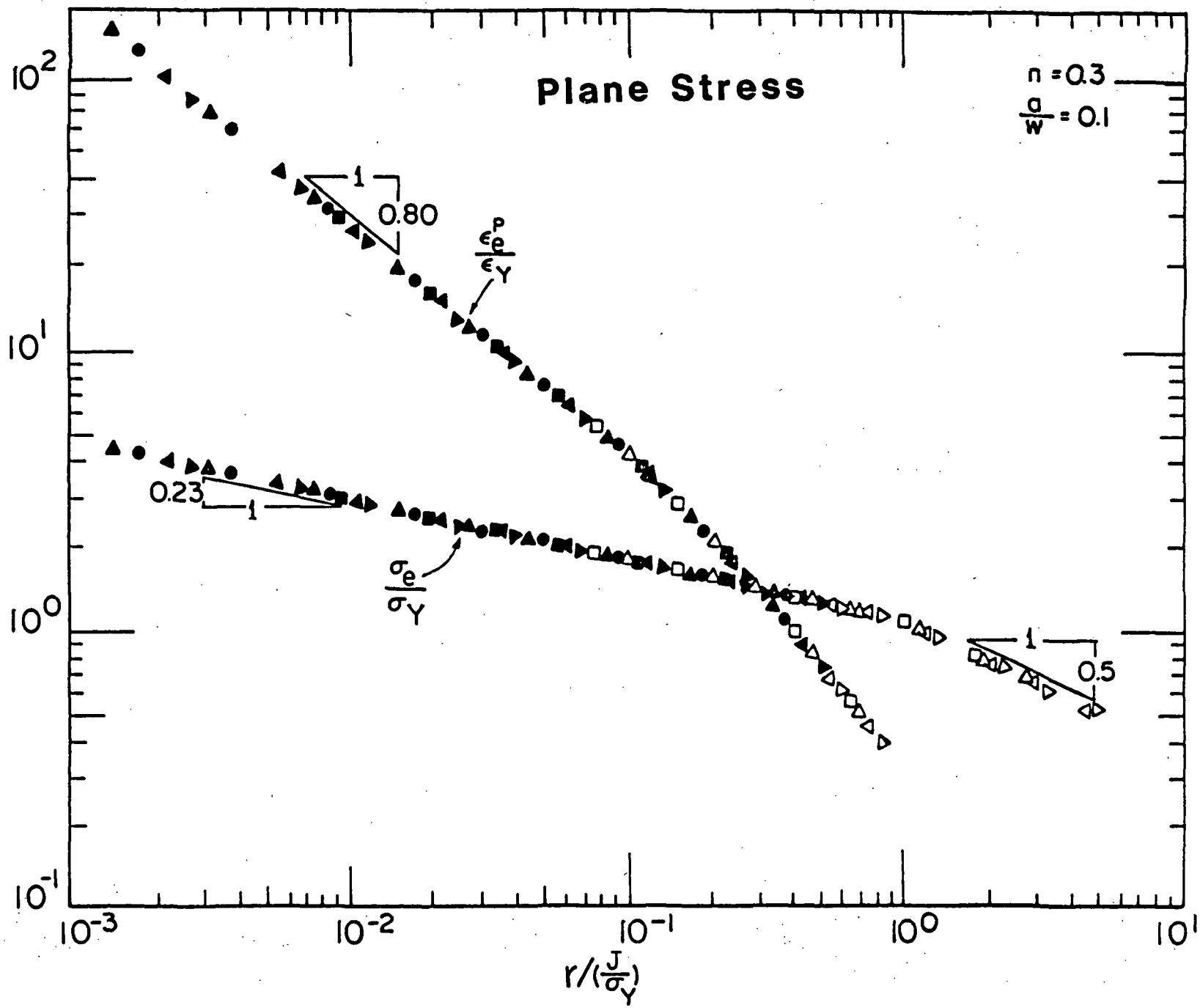

Fig. (1.6) Normalized effective stress and effective strain distribution near the crack tip, n = 0.3, p - σ.

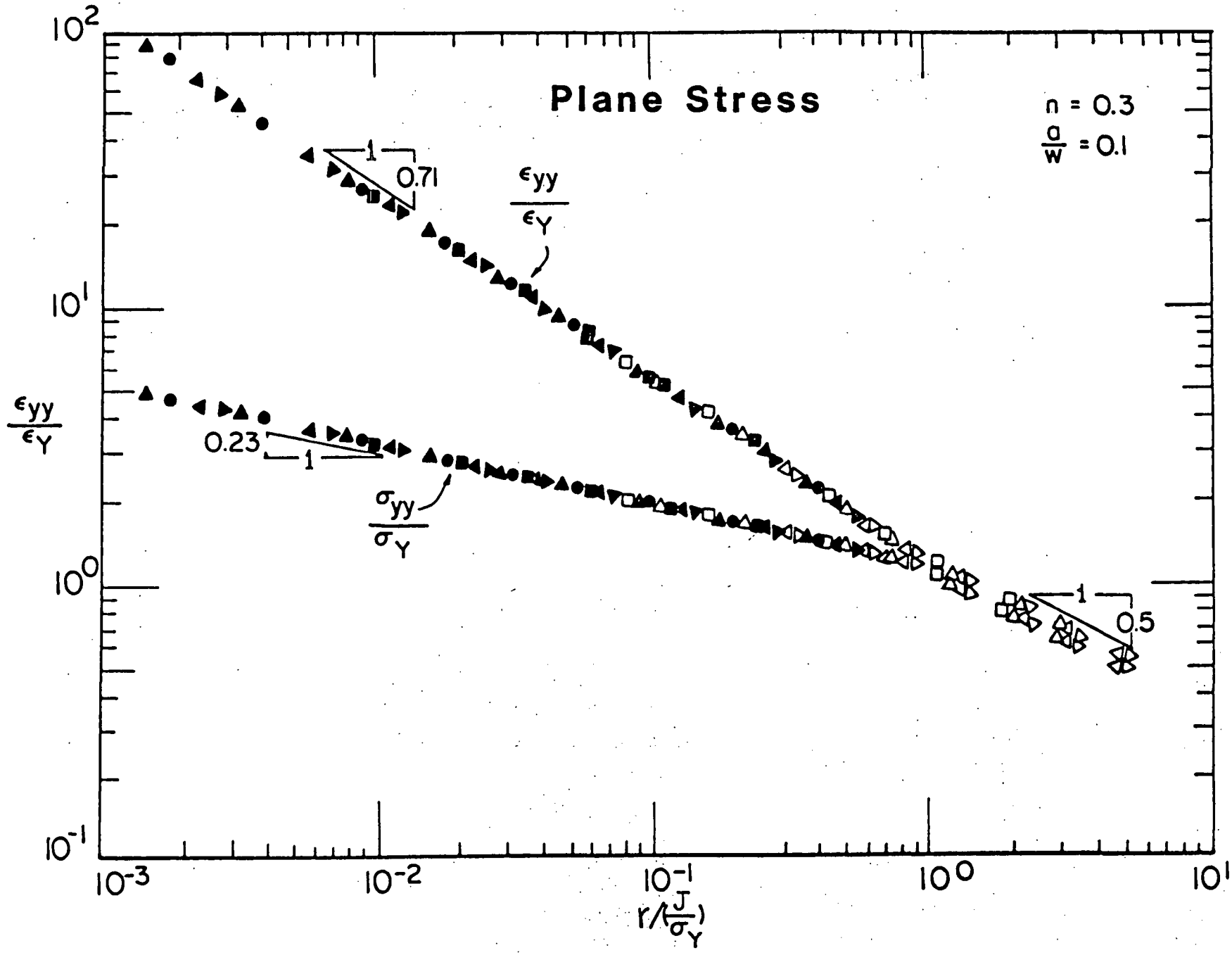

Fig. (1.7) Normalized stress and strain distribution near the crack tip, n = 0.3, p - σ.

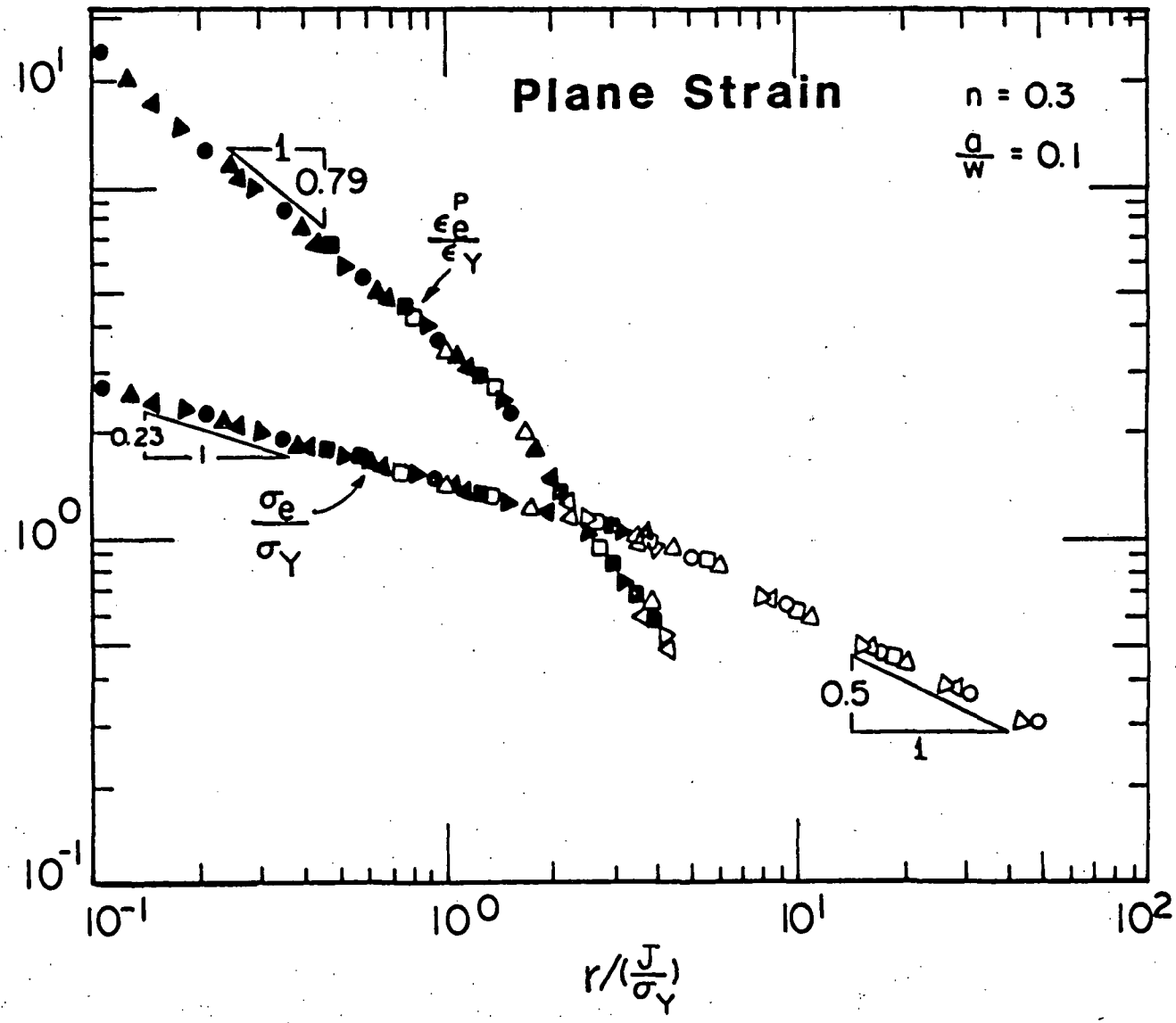

Fig. (1.8) Normalized effective stress and effective strain distribution near the crack tip, $n = 0.2$, p - ε.

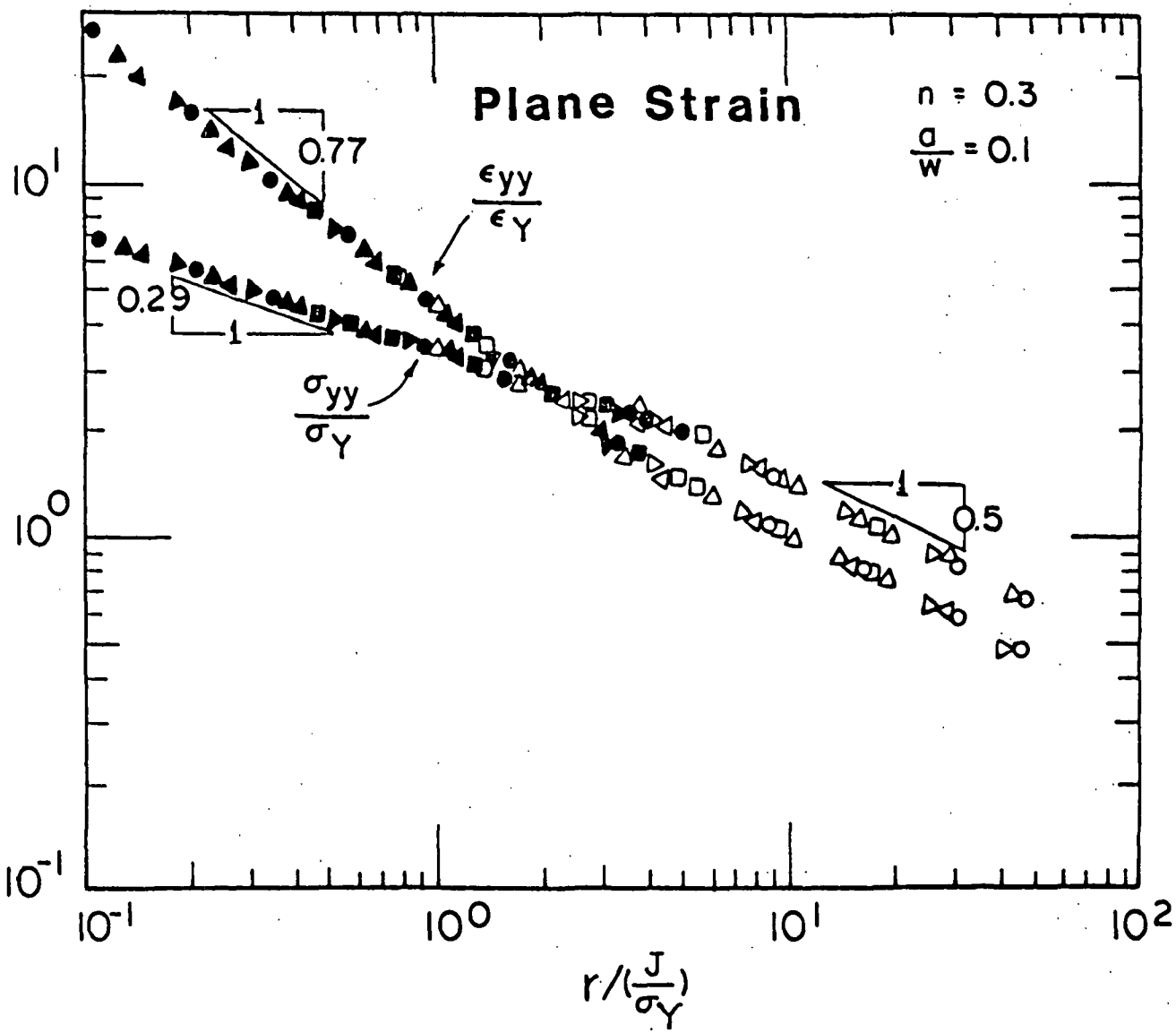

Fig. (1.9) Normalized stress and strain distribution near the crack tip, n = 0.3, p - ε.

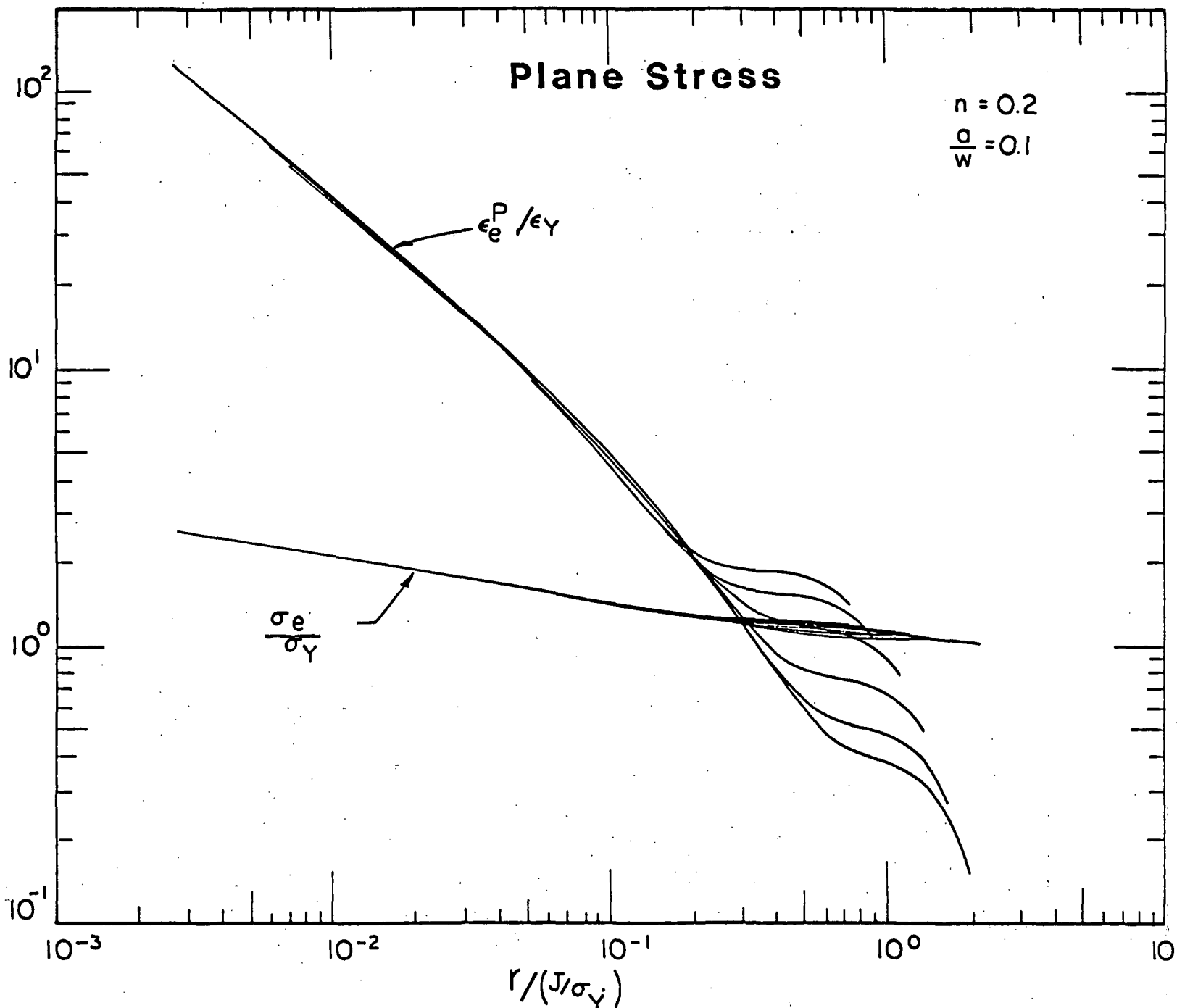

Fig. (1.10) Normalized effective stress and effective strain distribution ahead of the crack tip, n = 0.2, p - σ

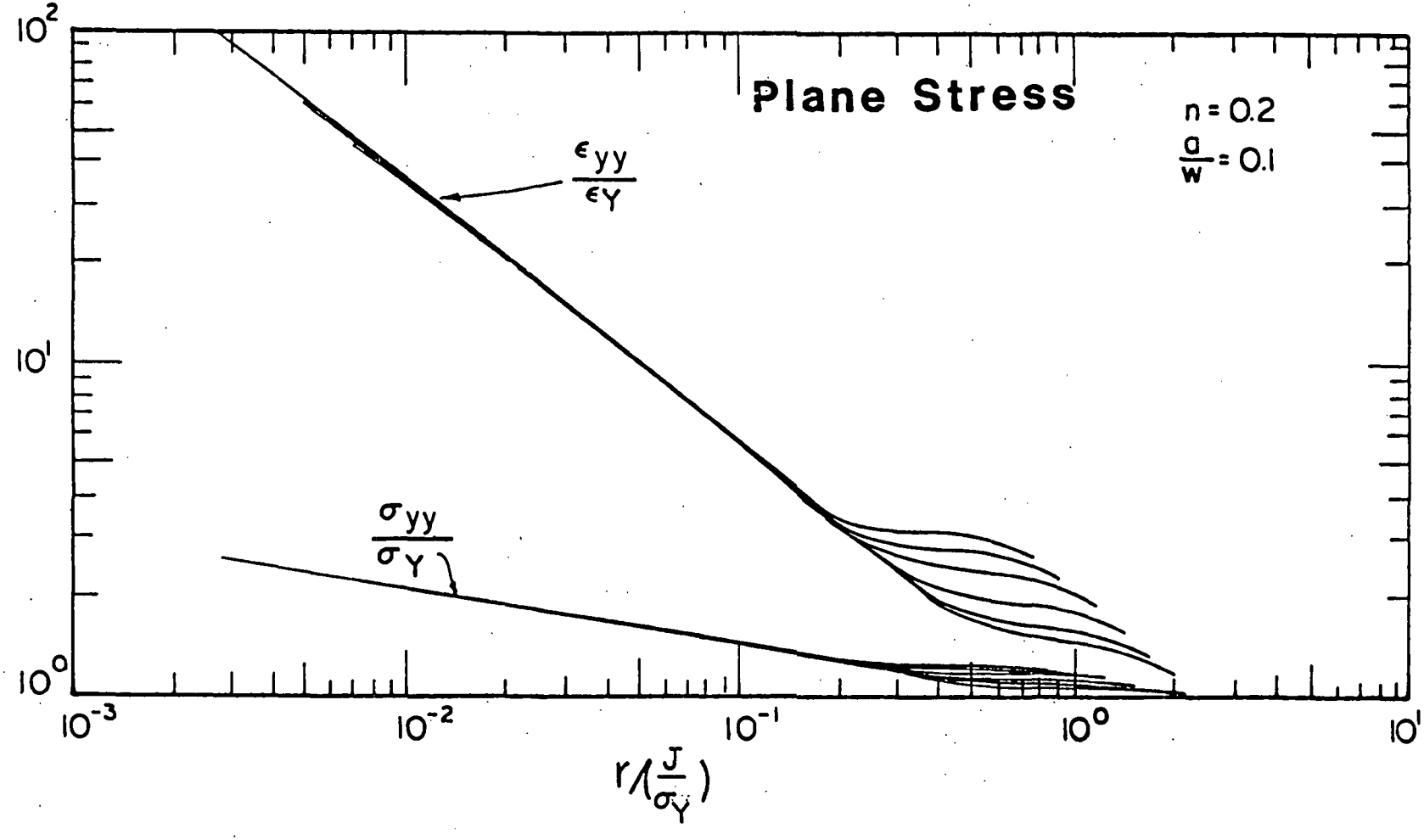

Fig. (1.11) Normalized stress and strain distribution ahead of the crack tip, n = 0.2, p - σ.

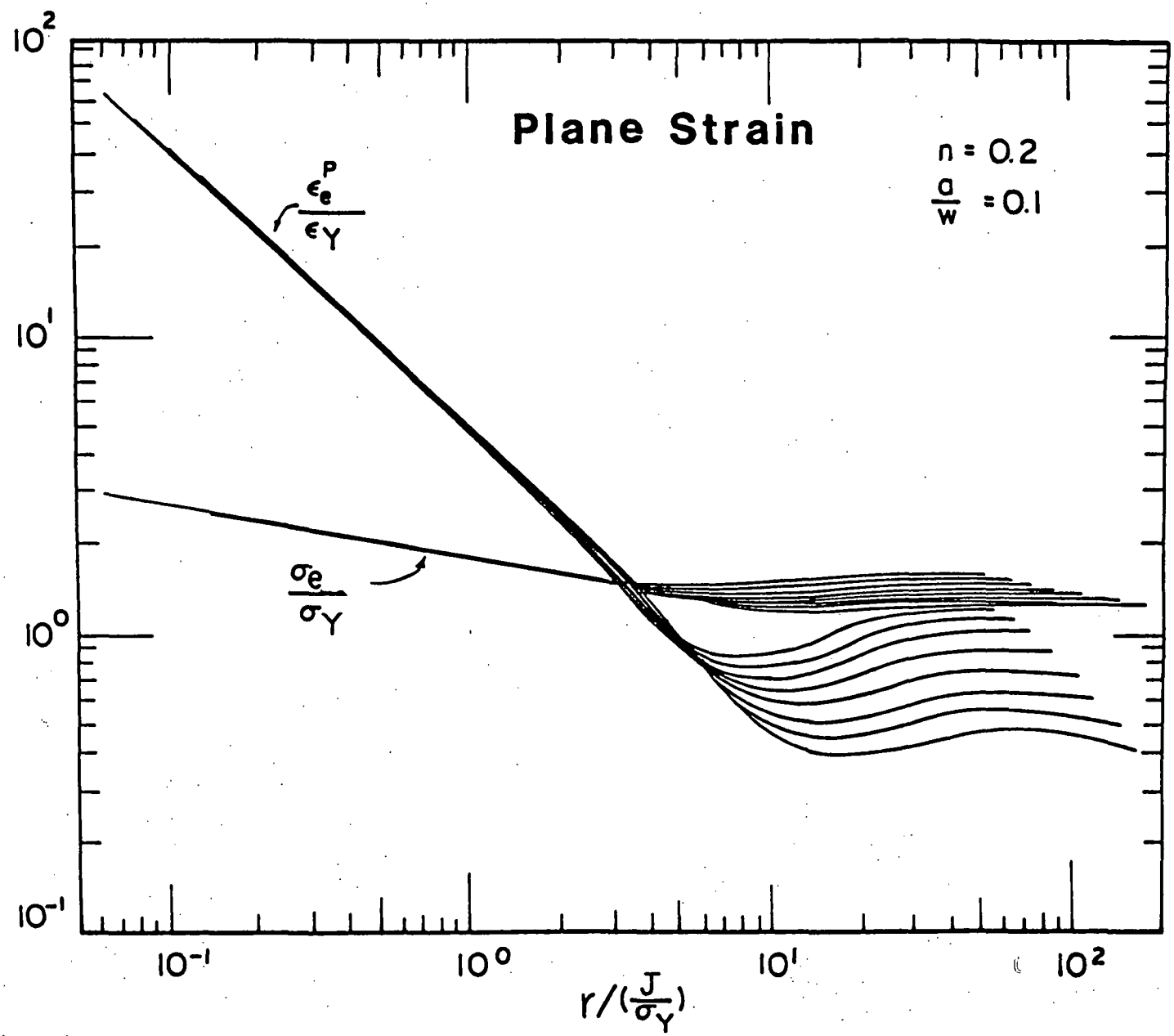

Fig. (1.12) Normalized effective stress and effective strain distribution ahead of the crack tip, $n = 0.2$, $p - \epsilon$.

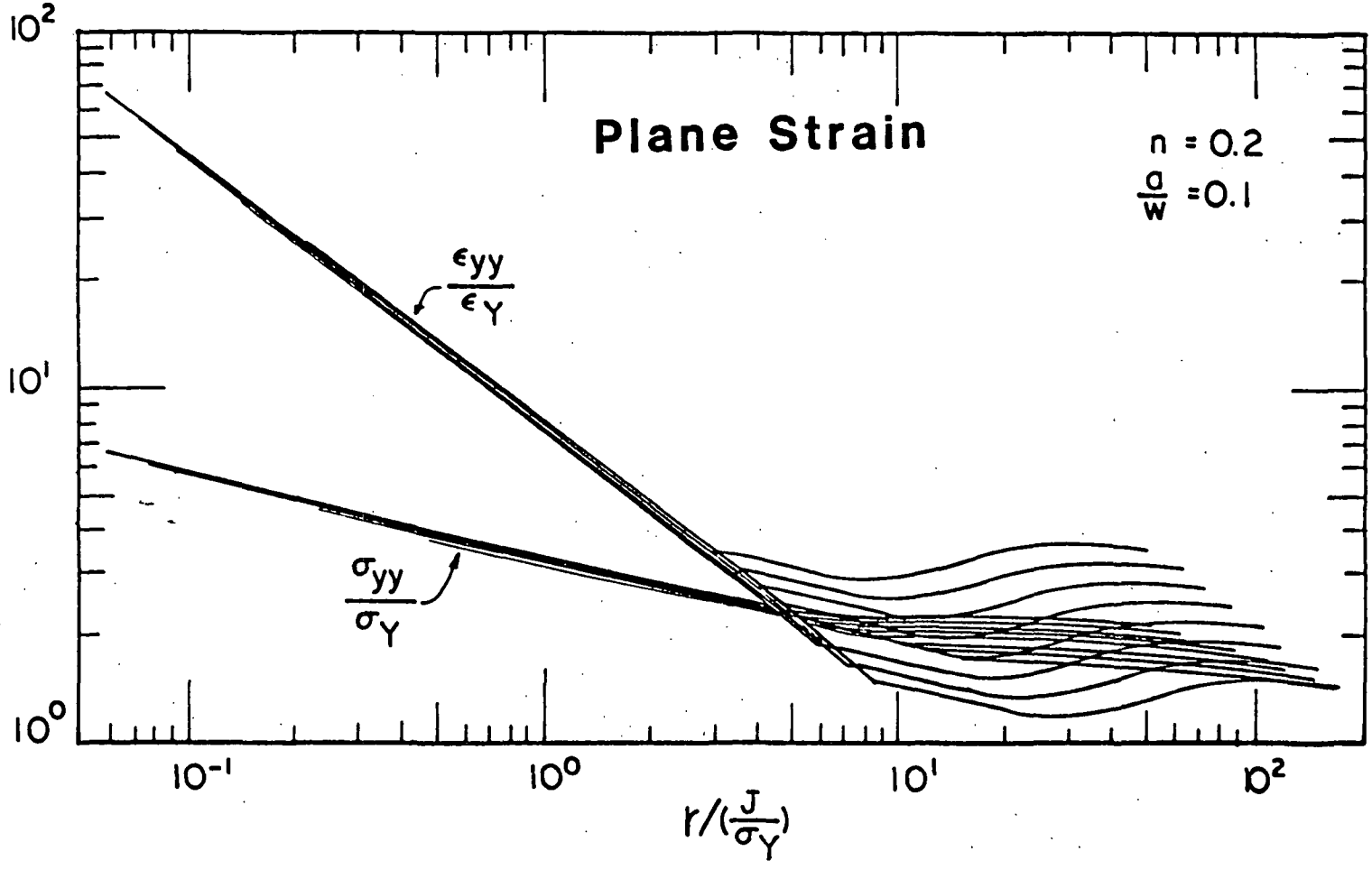

Fig. (1.13) Normalized stress and strain distribution ahead of the crack tip, n = 0.2, p - ε.

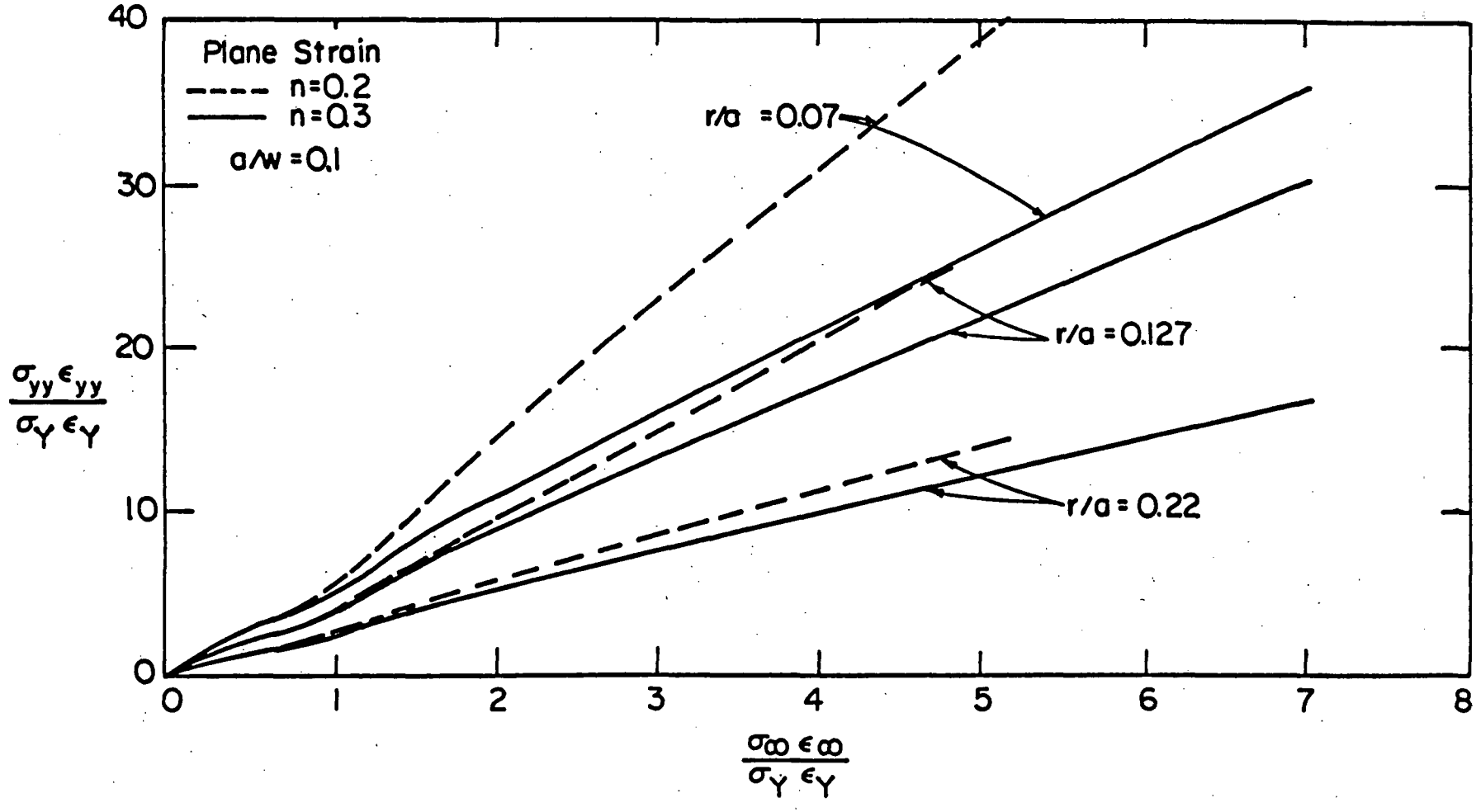

Fig. (1.14) Near field parameter $\sigma_{yy}\varepsilon_{yy}/\sigma_Y\varepsilon_Y$ versus far field parameter $\sigma_\infty\varepsilon_\infty/\sigma_Y\varepsilon_Y$, p - ε.

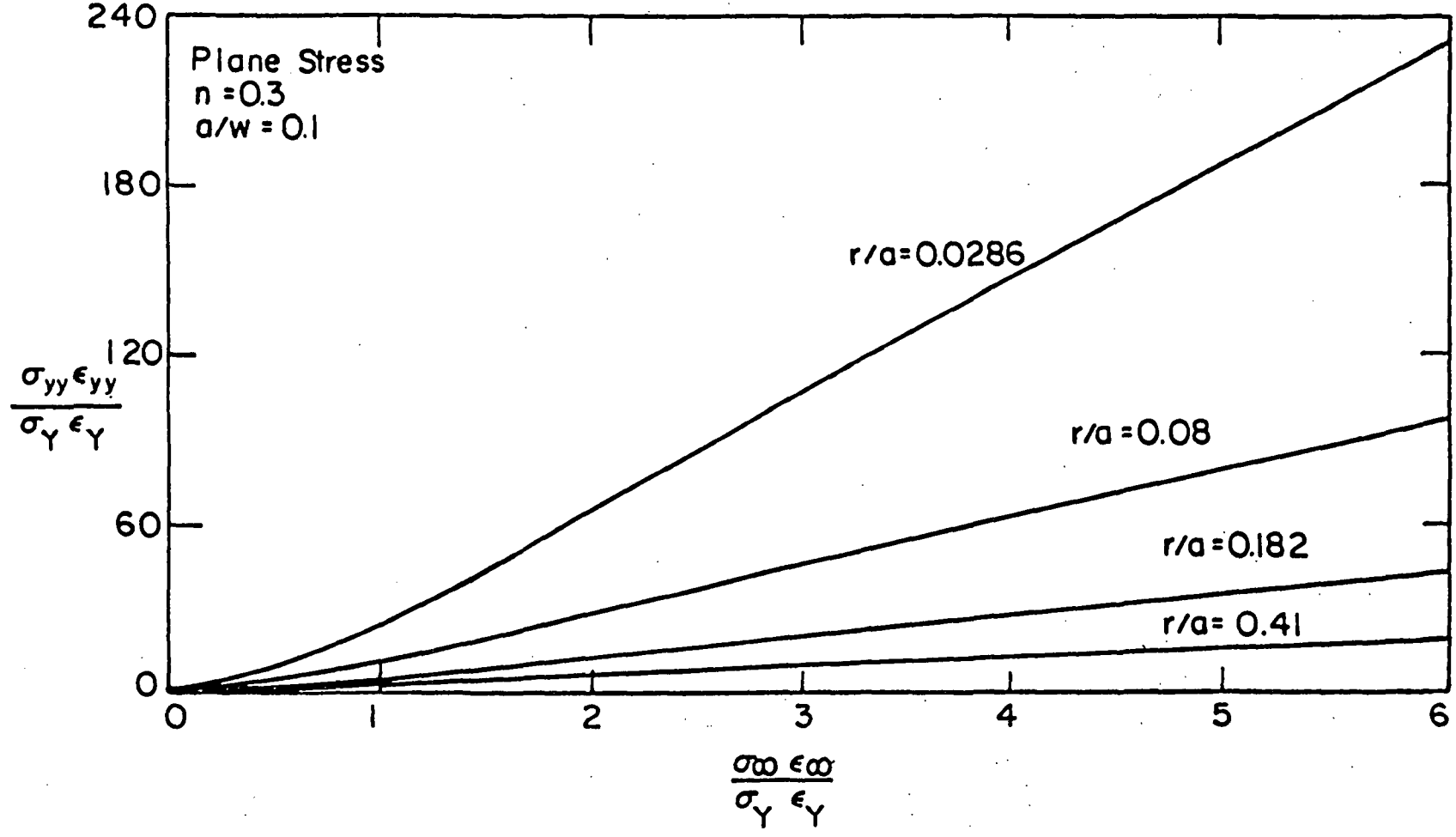

Fig. (1.15) Near field parameter $\sigma_{yy}\varepsilon_{yy}/\sigma_Y\varepsilon_Y$ versus far field parameter $\sigma_\infty\varepsilon_\infty/\sigma\ \varepsilon$, p - σ, n = 0.2.

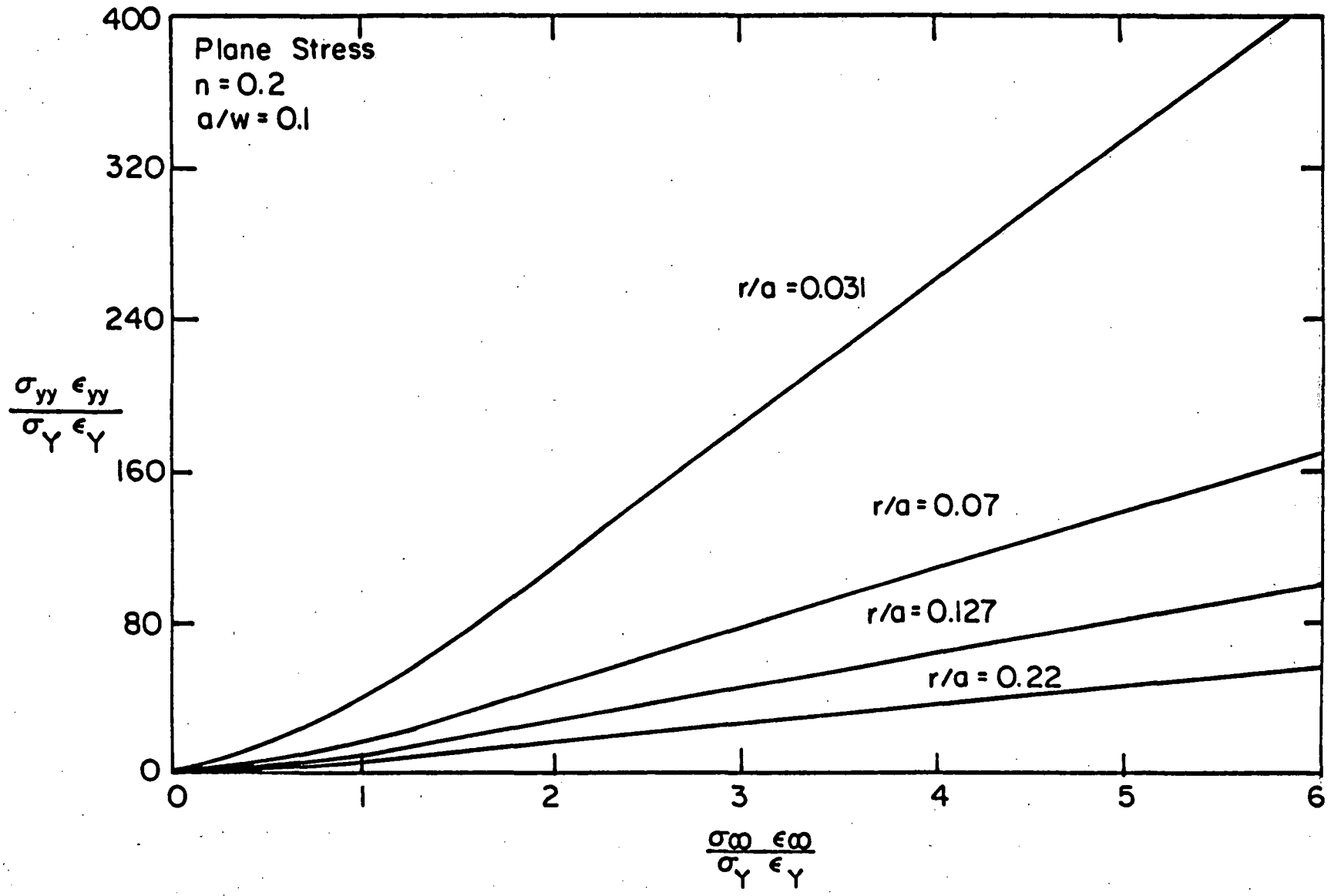

Fig. (1.16) Near field parameter $\sigma_{yy}\varepsilon_{yy}/\sigma_Y\varepsilon_Y$ versus far field parameter $\sigma_\infty\varepsilon_\infty/\sigma_Y\varepsilon_Y$.

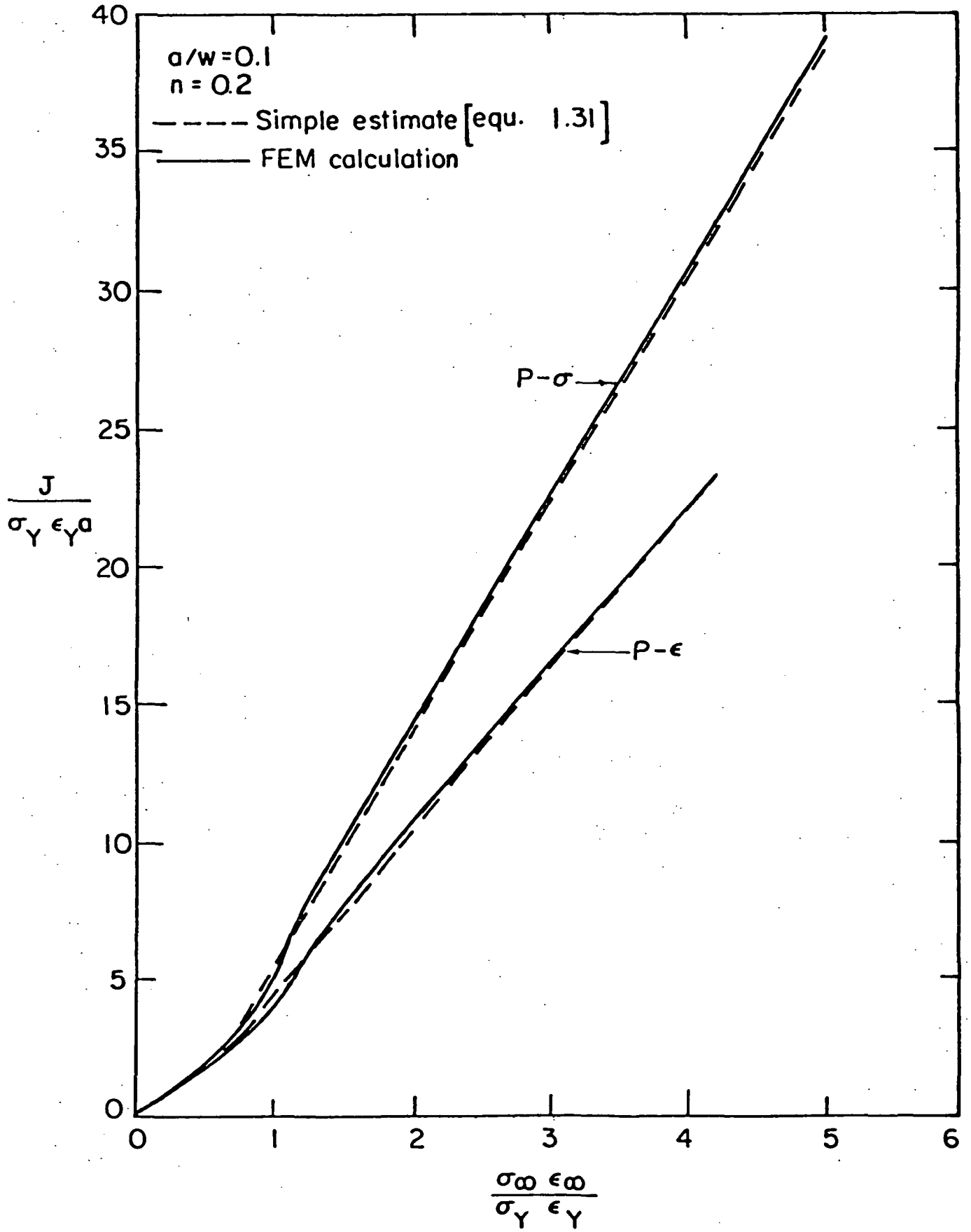

Fig. (1.17) Comparison of simple estimates of Eqn. (1.31) and full FEM calculations for single edge cracked panel in tension with n = 0.2 and a/w = 0.1.

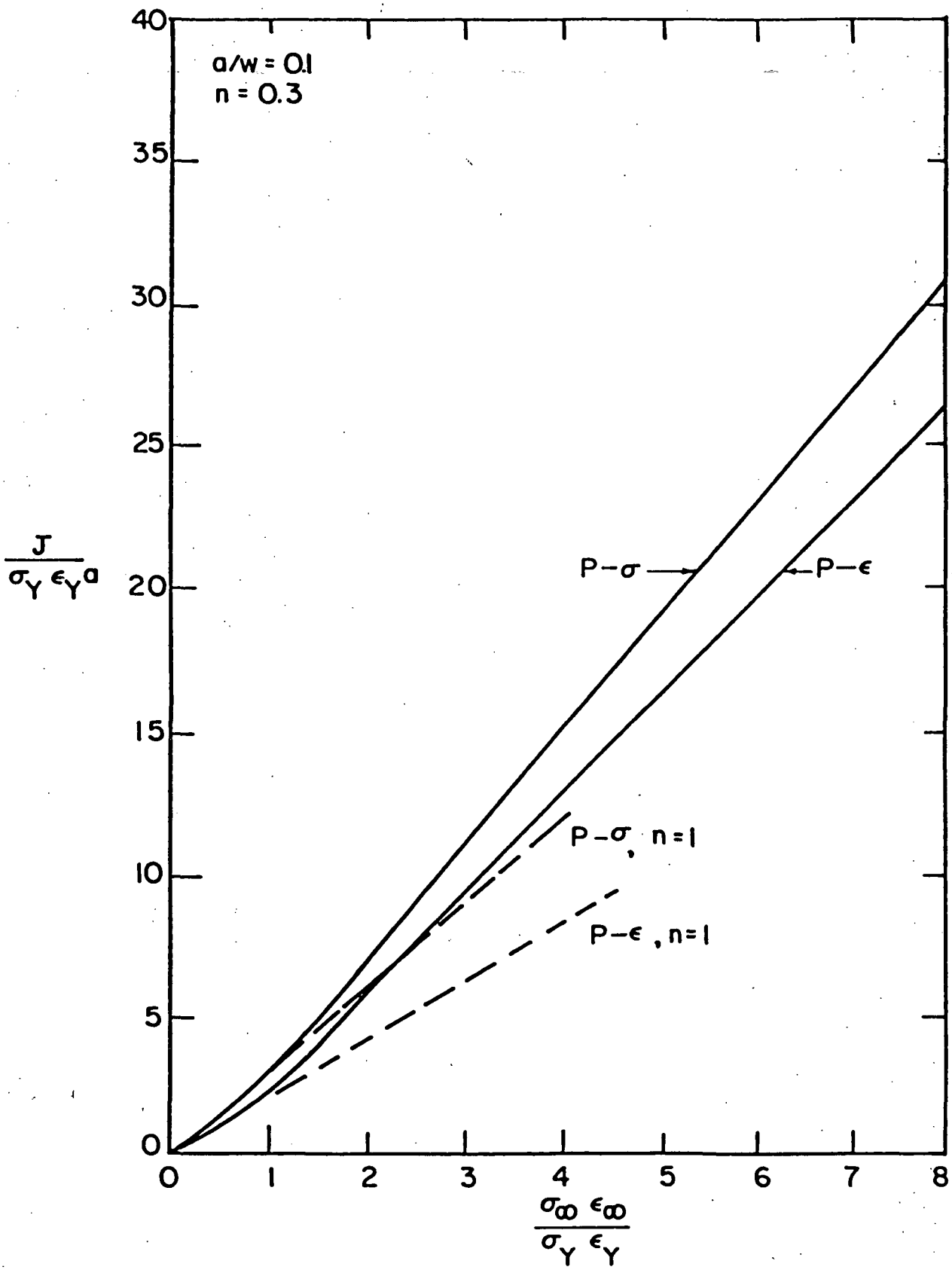

Fig. (1.18) Correlation of dimensionless J versus $\sigma_\infty \varepsilon_\infty / \sigma_Y \varepsilon_Y$ for single edge cracked panel in tension with n = 0.3 and a/w = 0.1.

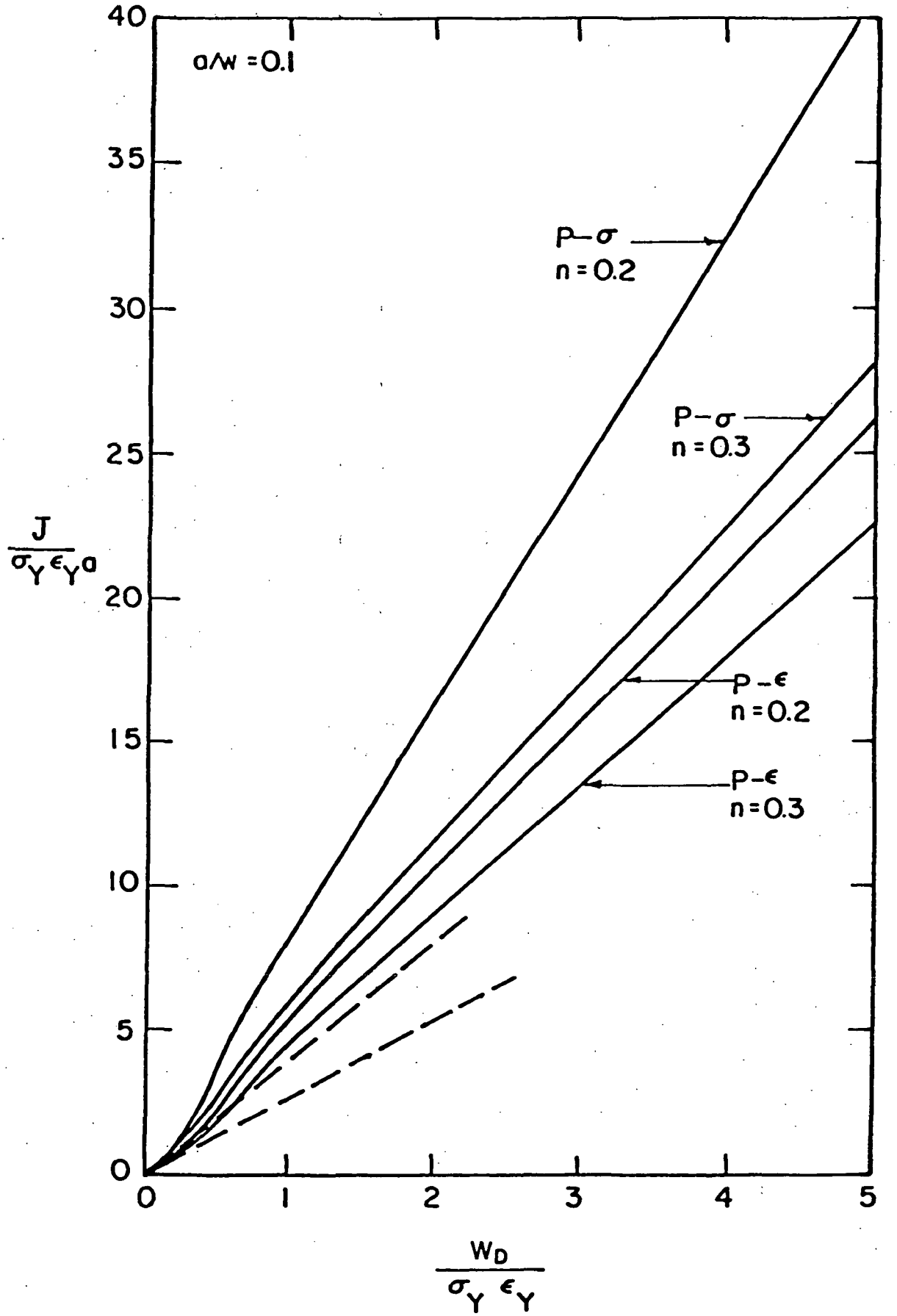

Fig. (1.19) Correlation of dimensionless J. versus $W_D/\sigma_Y\epsilon_Y$ for single edge cracked panel in tension.

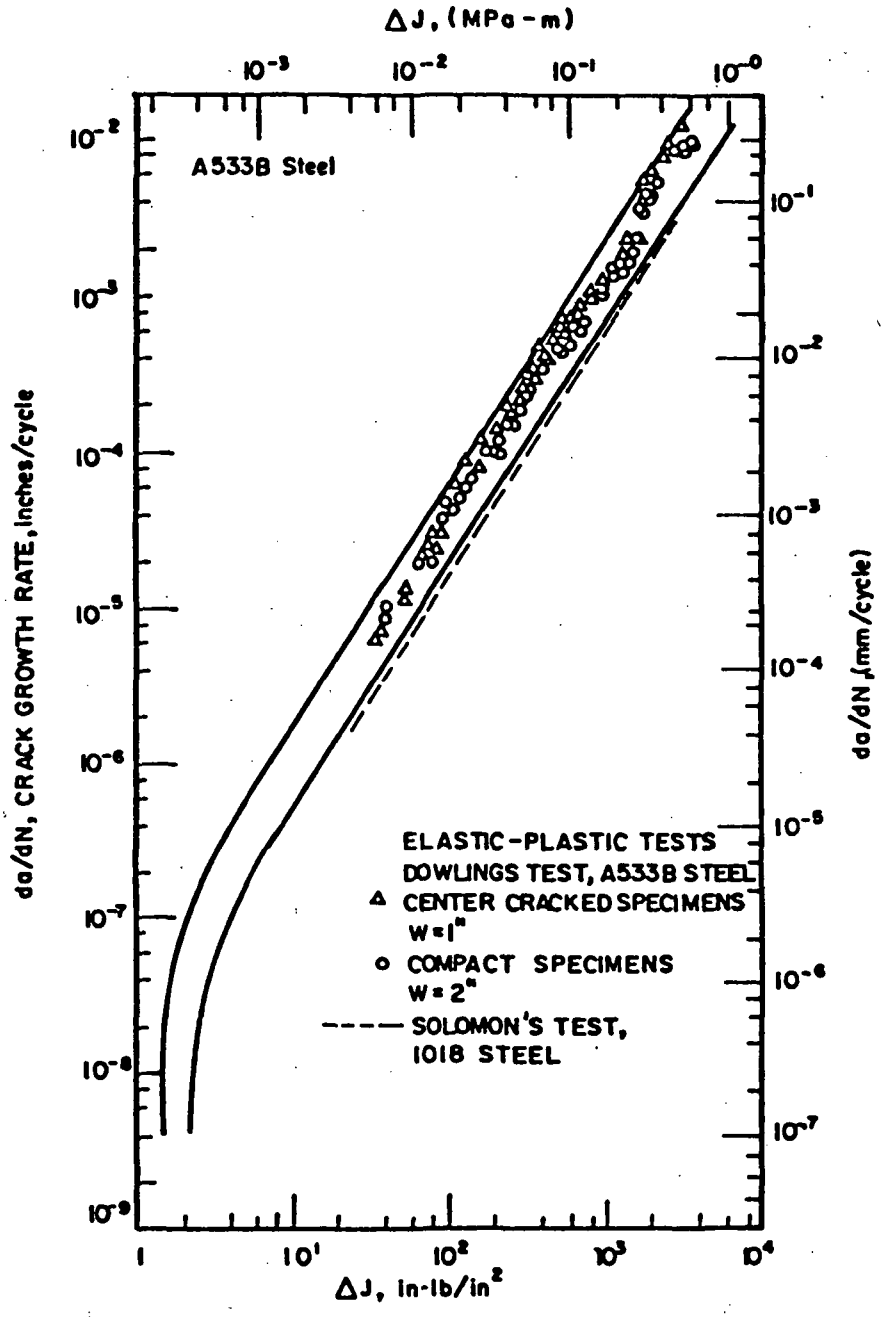

Fig. (2.1) Fatigue Crack Growth Rate versus ΔJ.

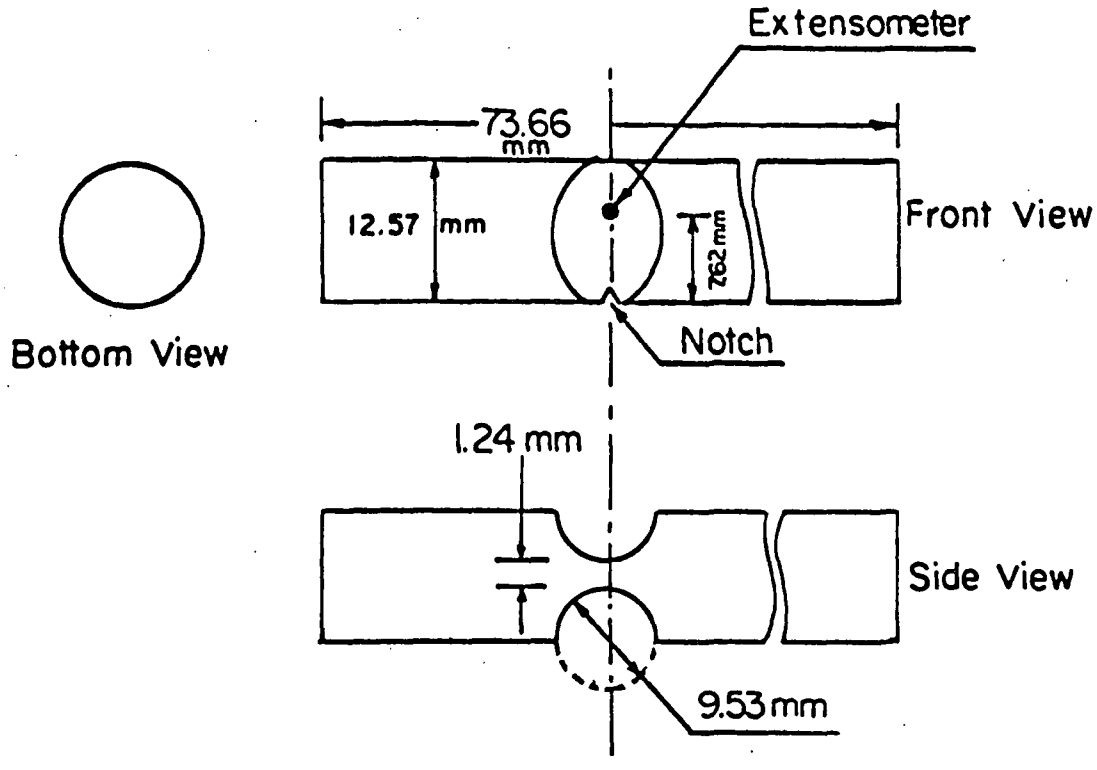

Fig. (2.2) Dimensions of Solomon's specimen.

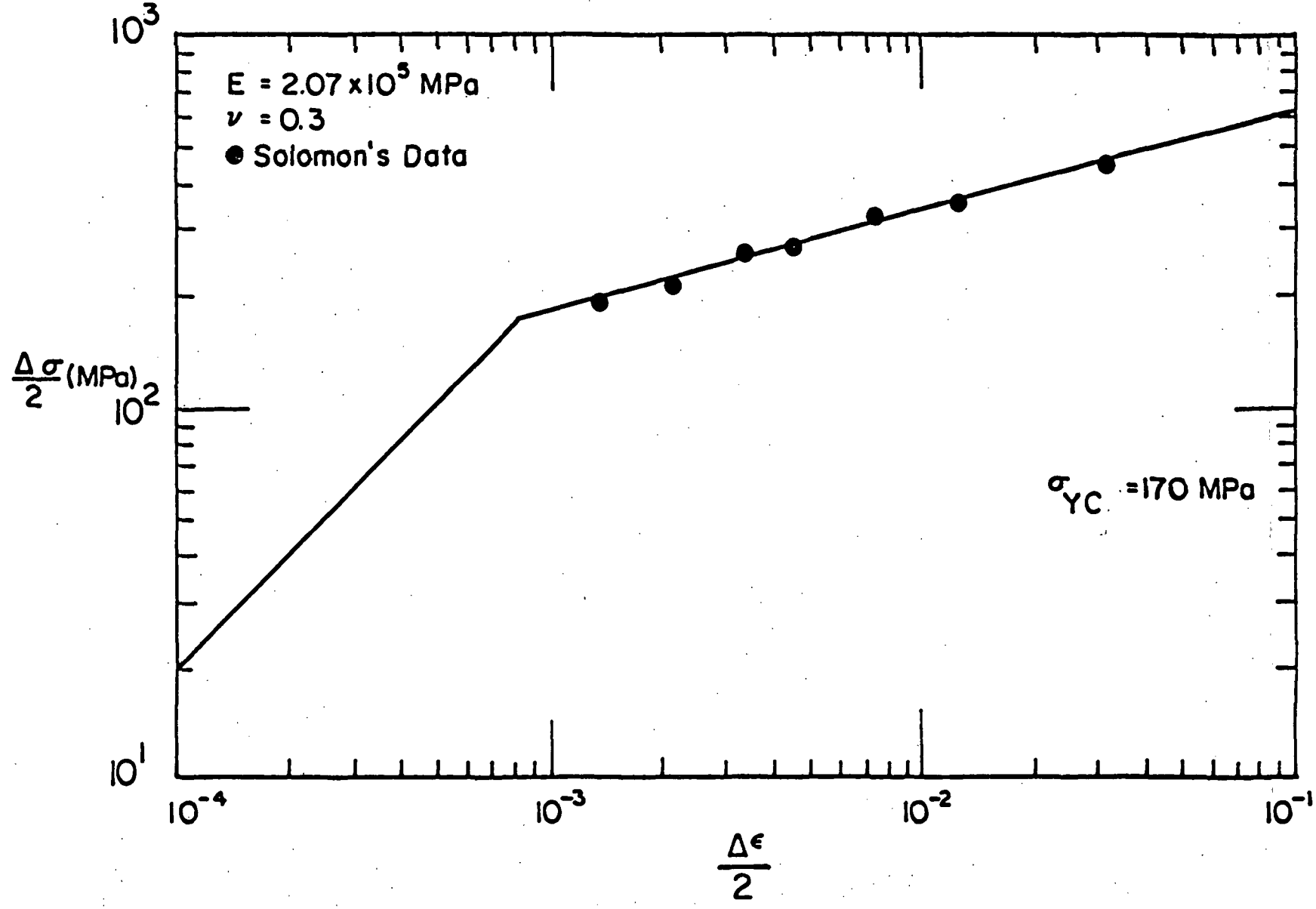

Fig. (2.3) Stress-strain curve of Solomon's specimen.

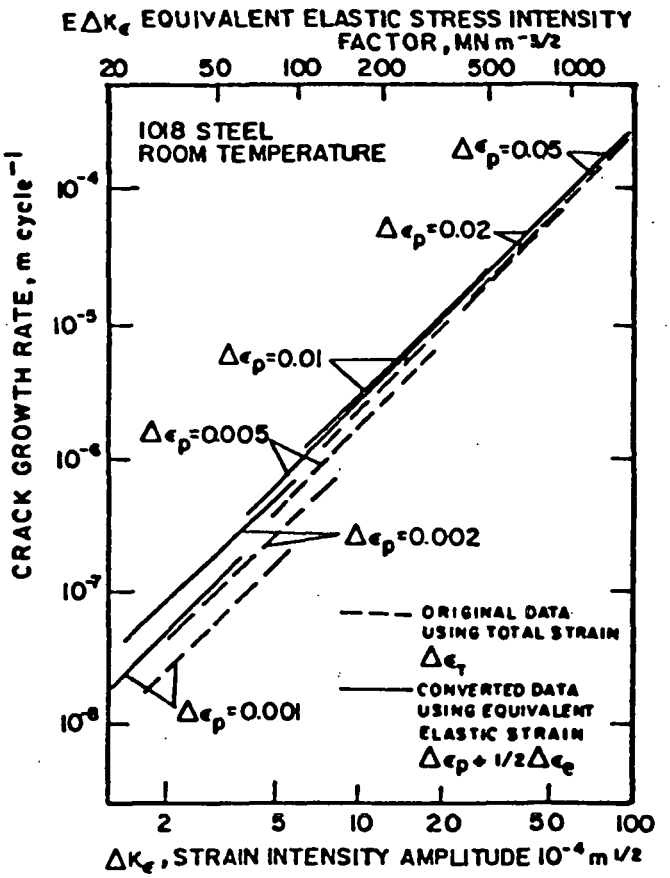

Fig. (2.4) Comparison of Egns. (2.7) and (2.8) using Solomon's data.

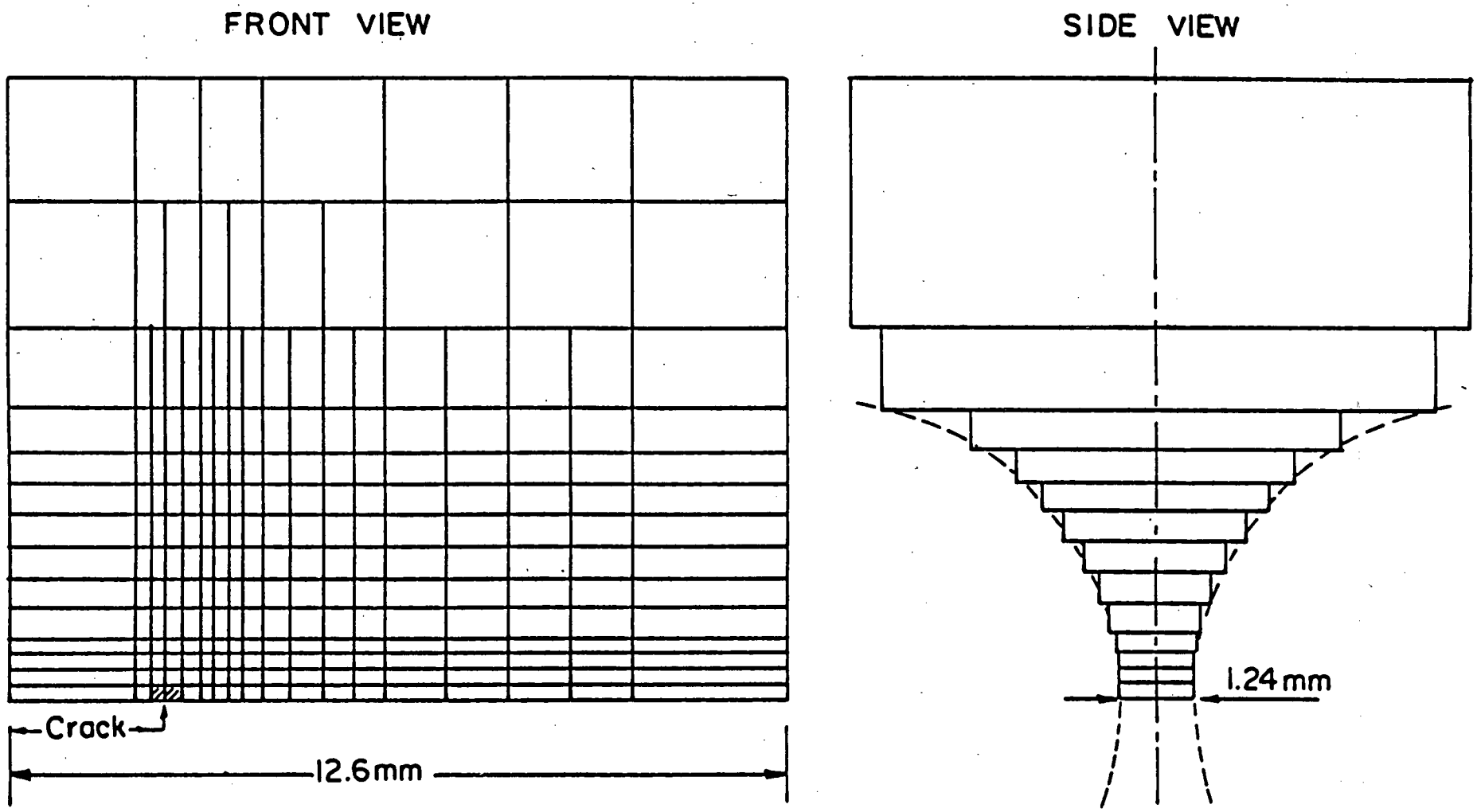

(a) Front view.

(b) Side view.

Fig. (2.5) Finite element idealization for Solomon's specimen, showing top half of the specimen, and cross section.

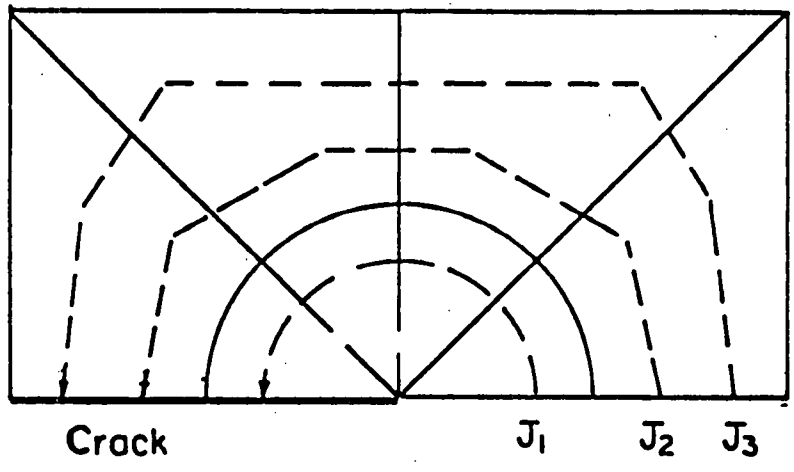

Fig. (2.5) (c) Crack tip mesh and J-integral paths.

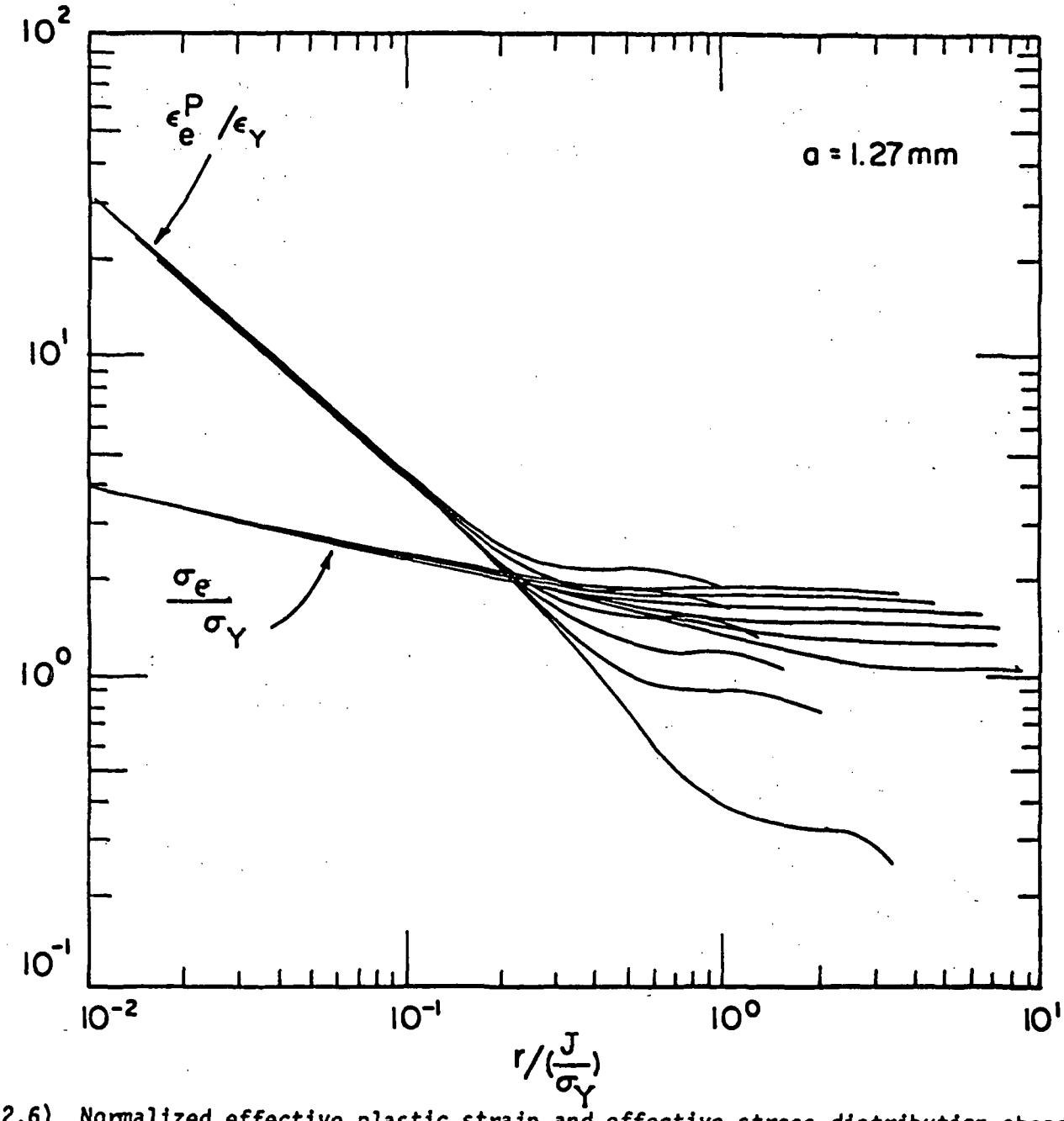

Fig. (2.6) Normalized effective plastic strain and effective stress distribution ahead of the crack tip for Solomon's specimen.

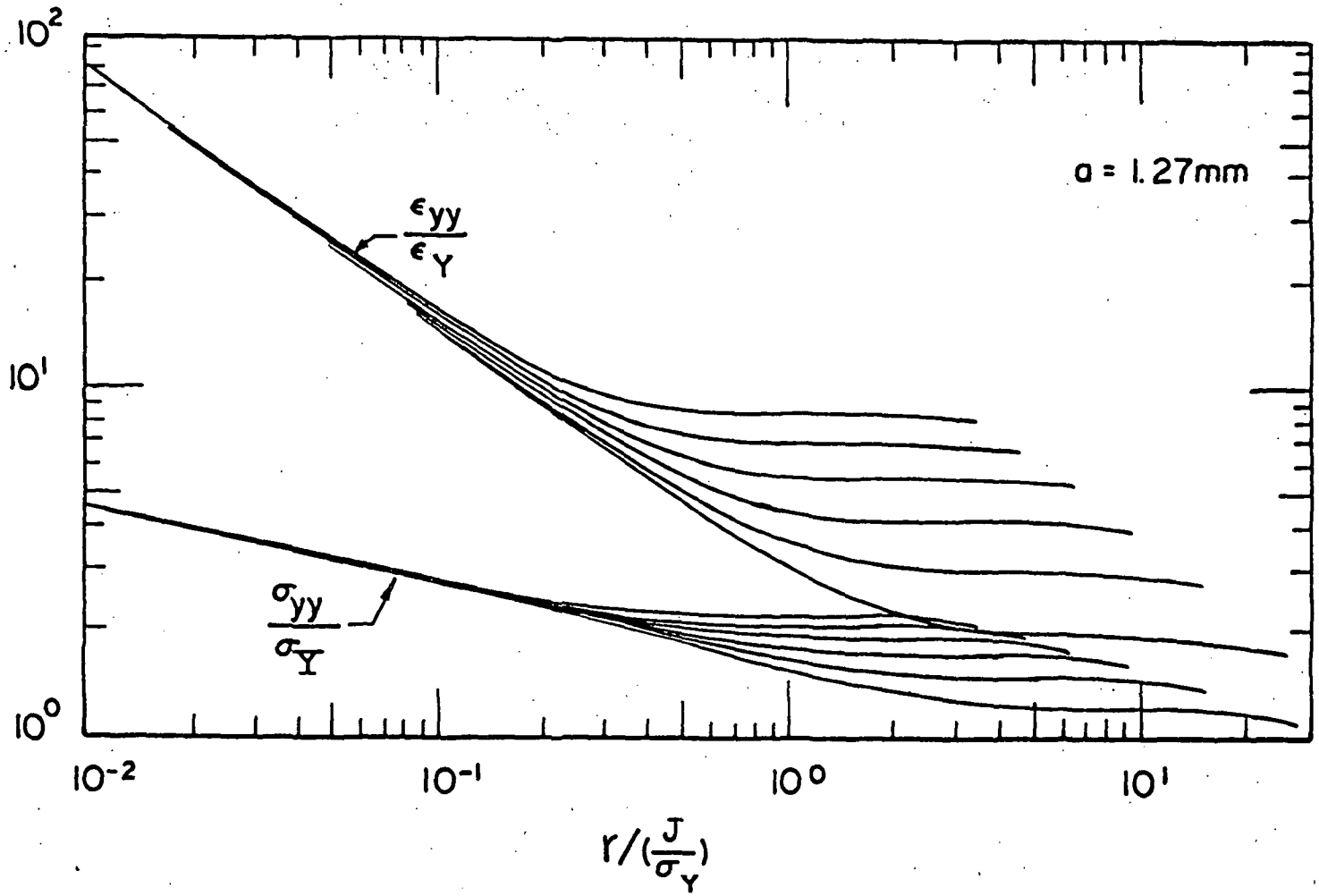

Fig. (2.7) Normalized stress and strain distribution ahead of the crack tip for Solomon's specimen.

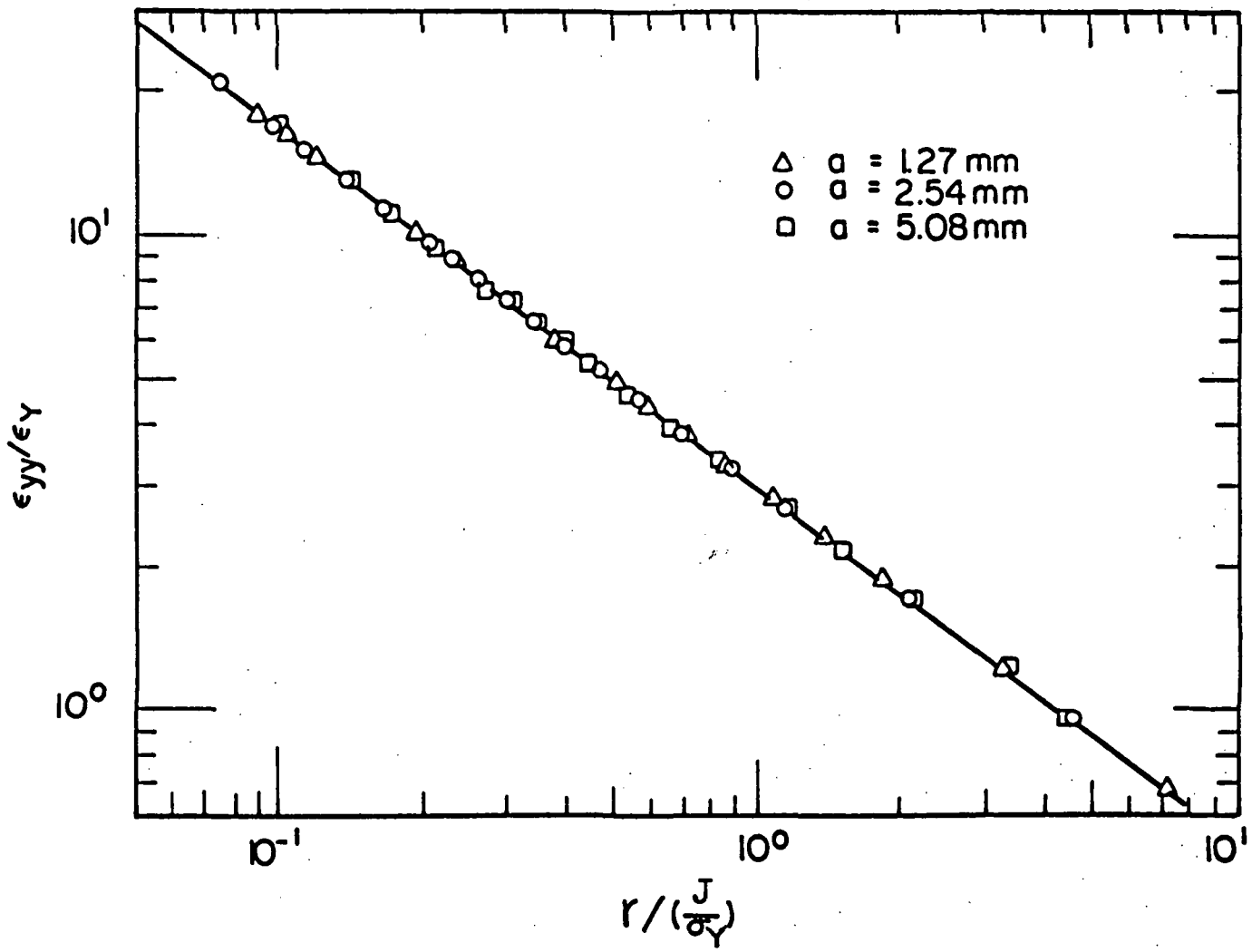

Fig. (2.8) Normalized strain distribution near the crack tip for three different crack lengths.

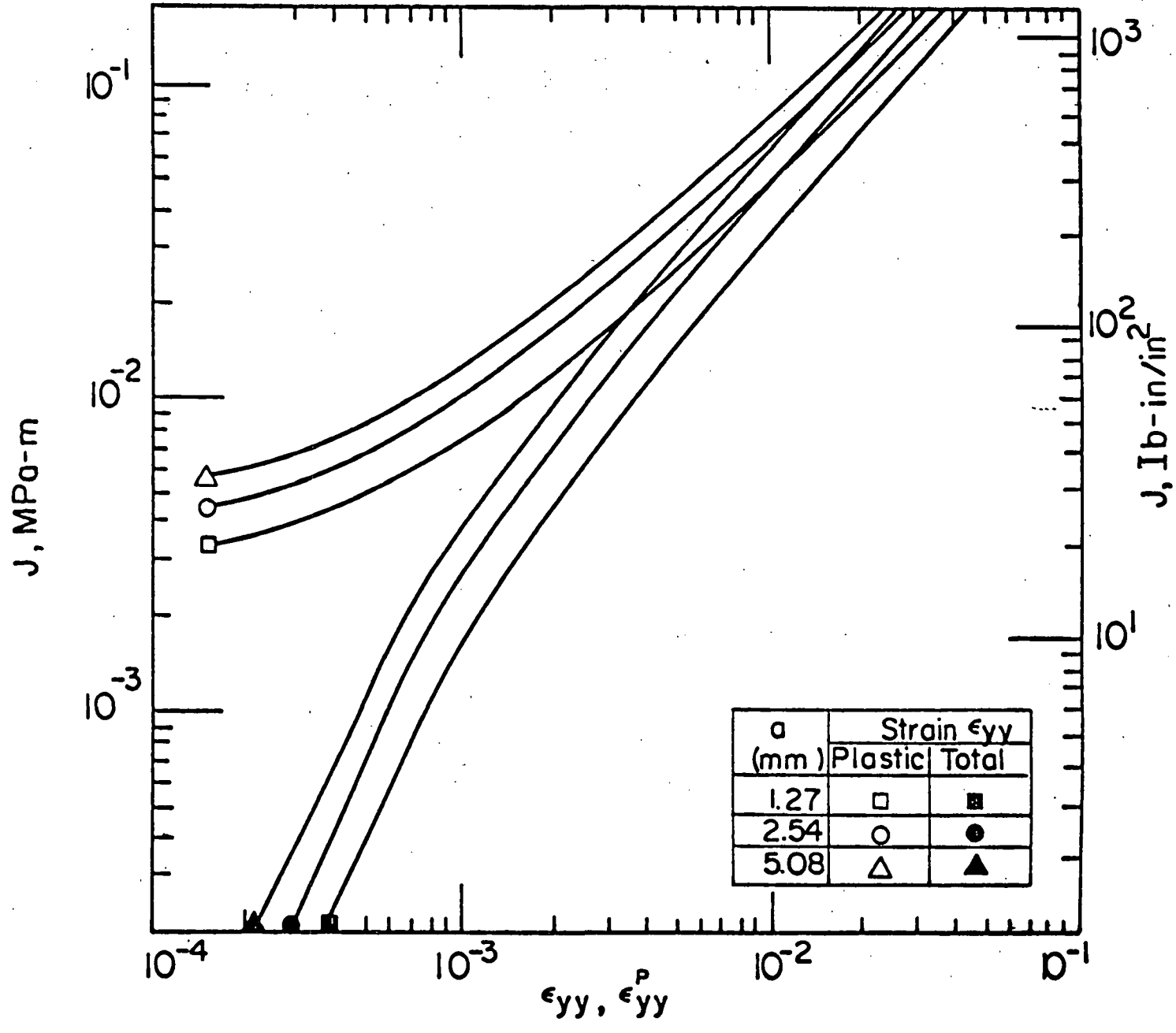

Fig. (2.9) J-integral dependence on applied strain.

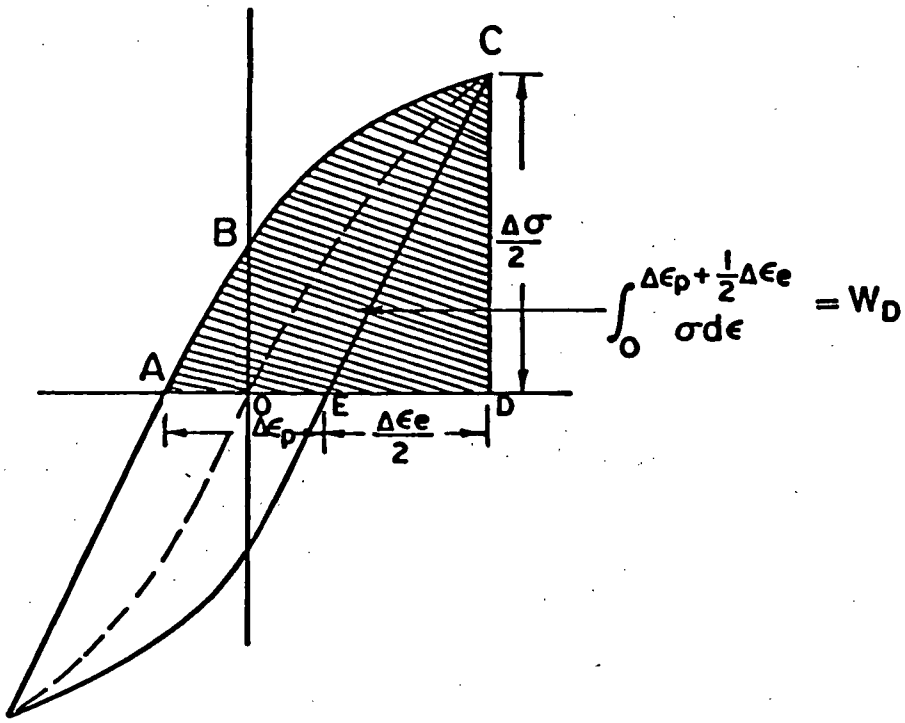

Fig. (2.10) Cyclic stress-starin loop and the deformation work density.

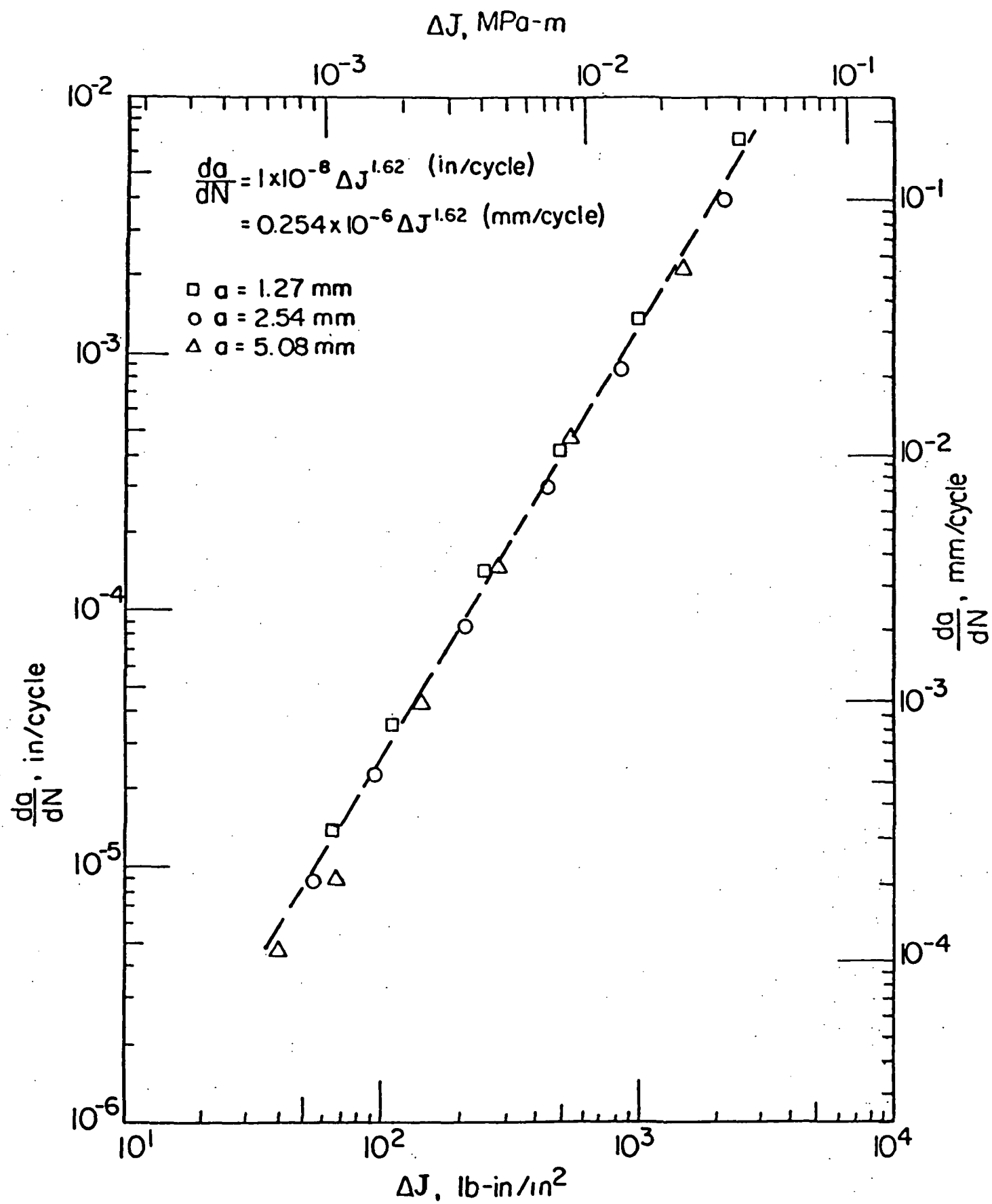

Fig. (2.11) Correlation of da/dN versus ΔJ for Solomon's tests.

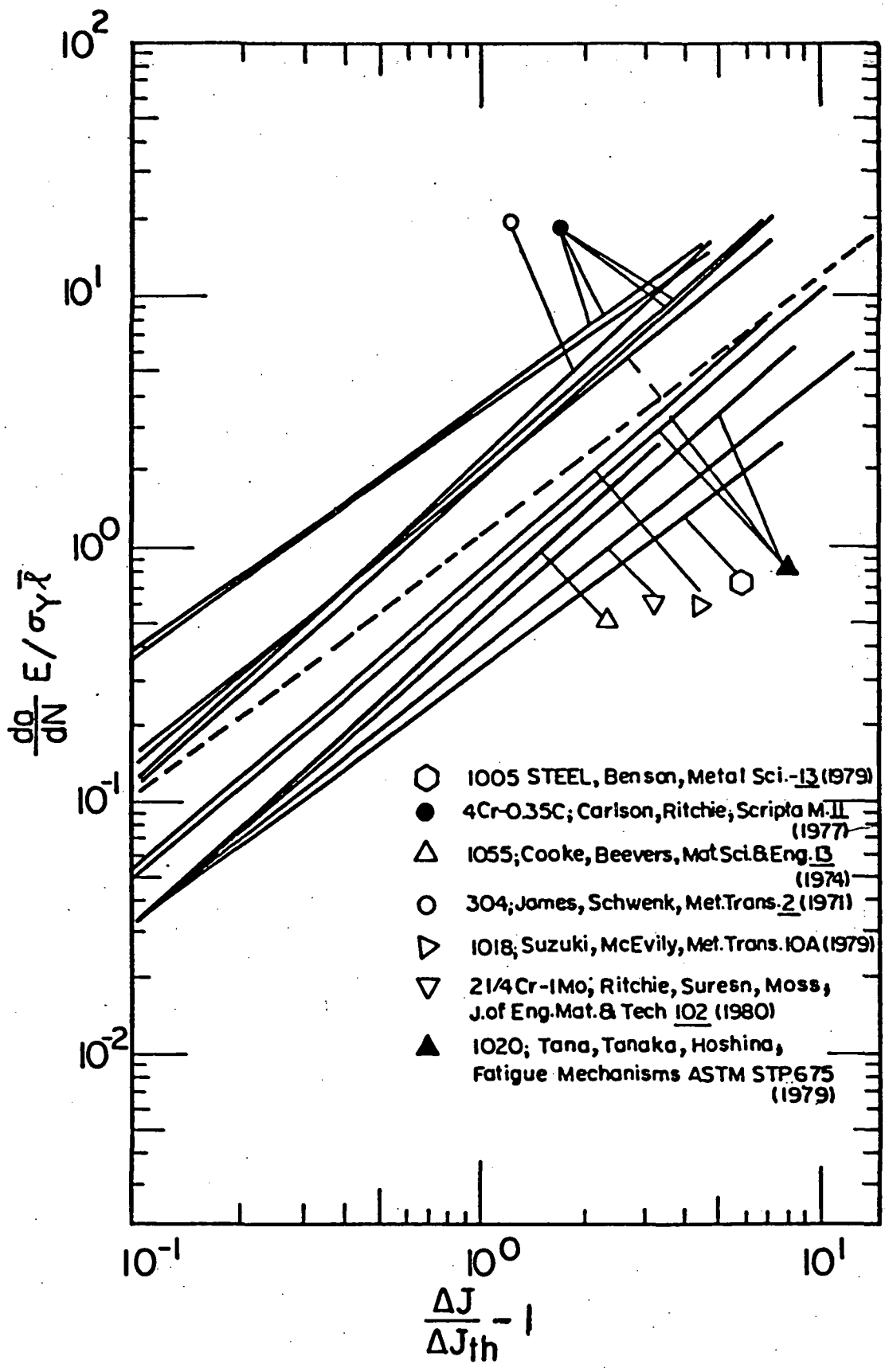

Fig. (2.12) Fatigue crack growth data for steels.

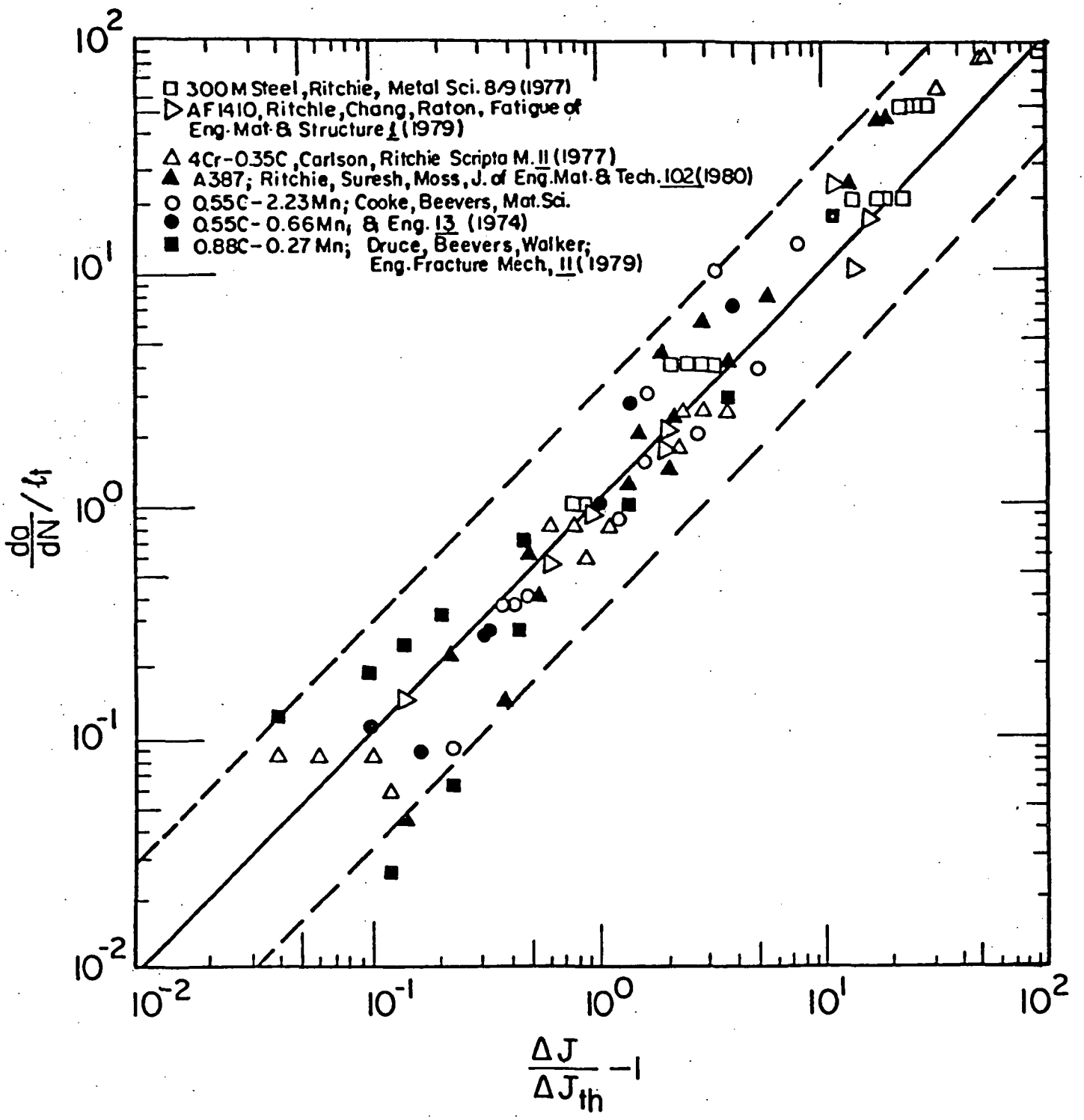

Fig. (2.13) Fatigue crack growth data for steels.

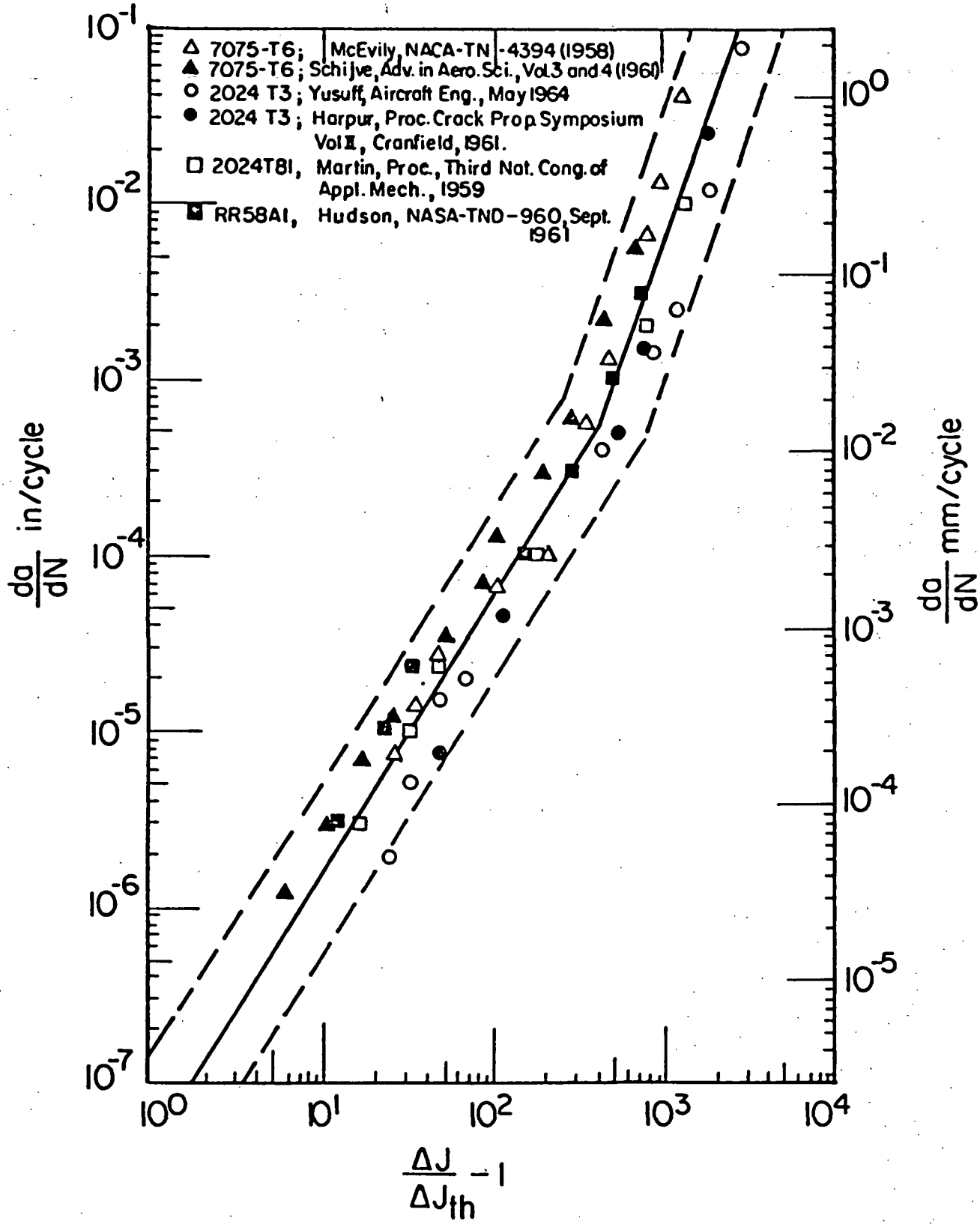

Fig. (2.14) Fatigue crack growth data for aluminum alloys.

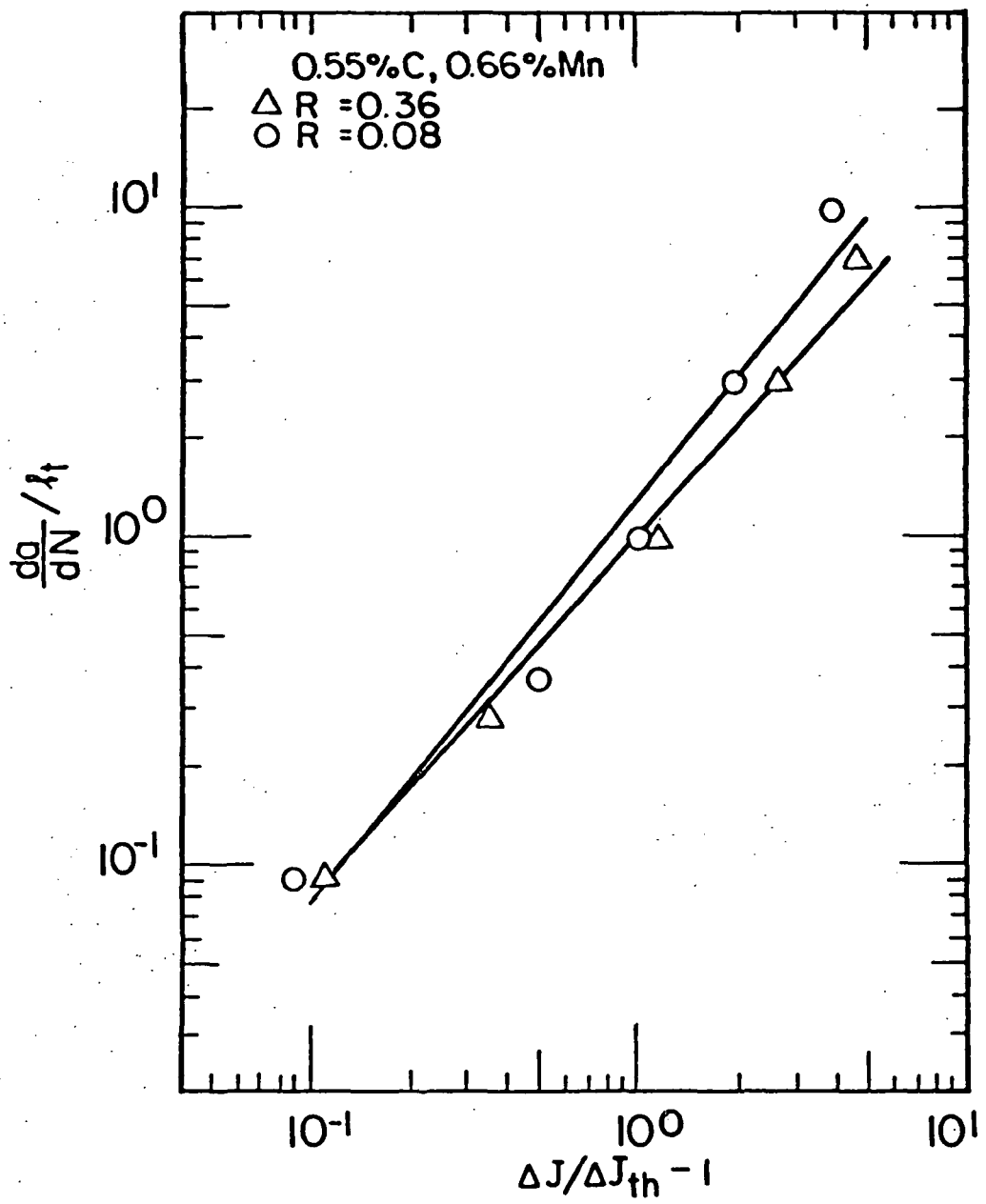

Fig. (2.15) Fatigue crack growth data.

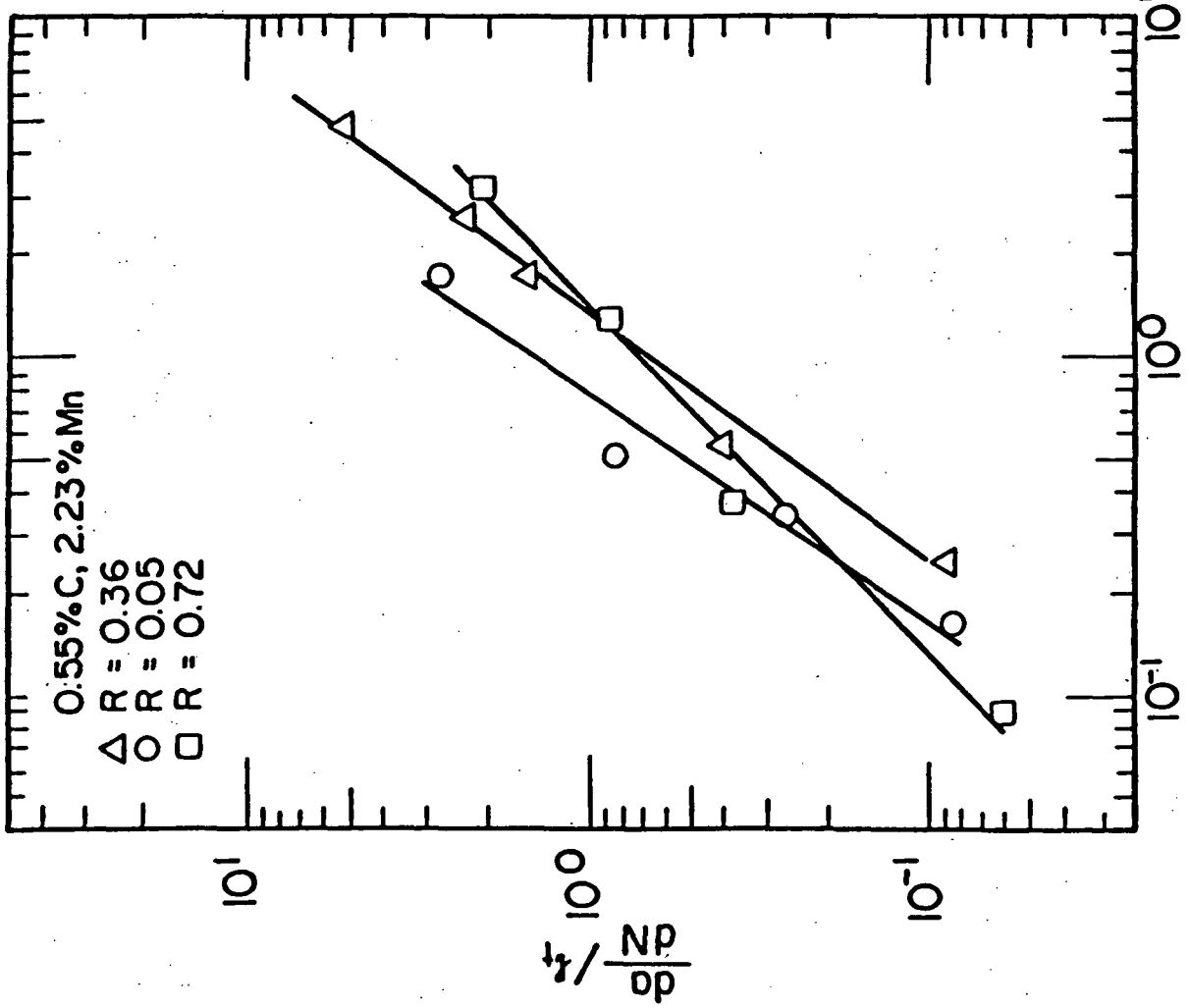

Fig. (2.16) Fatigue crack growth data.

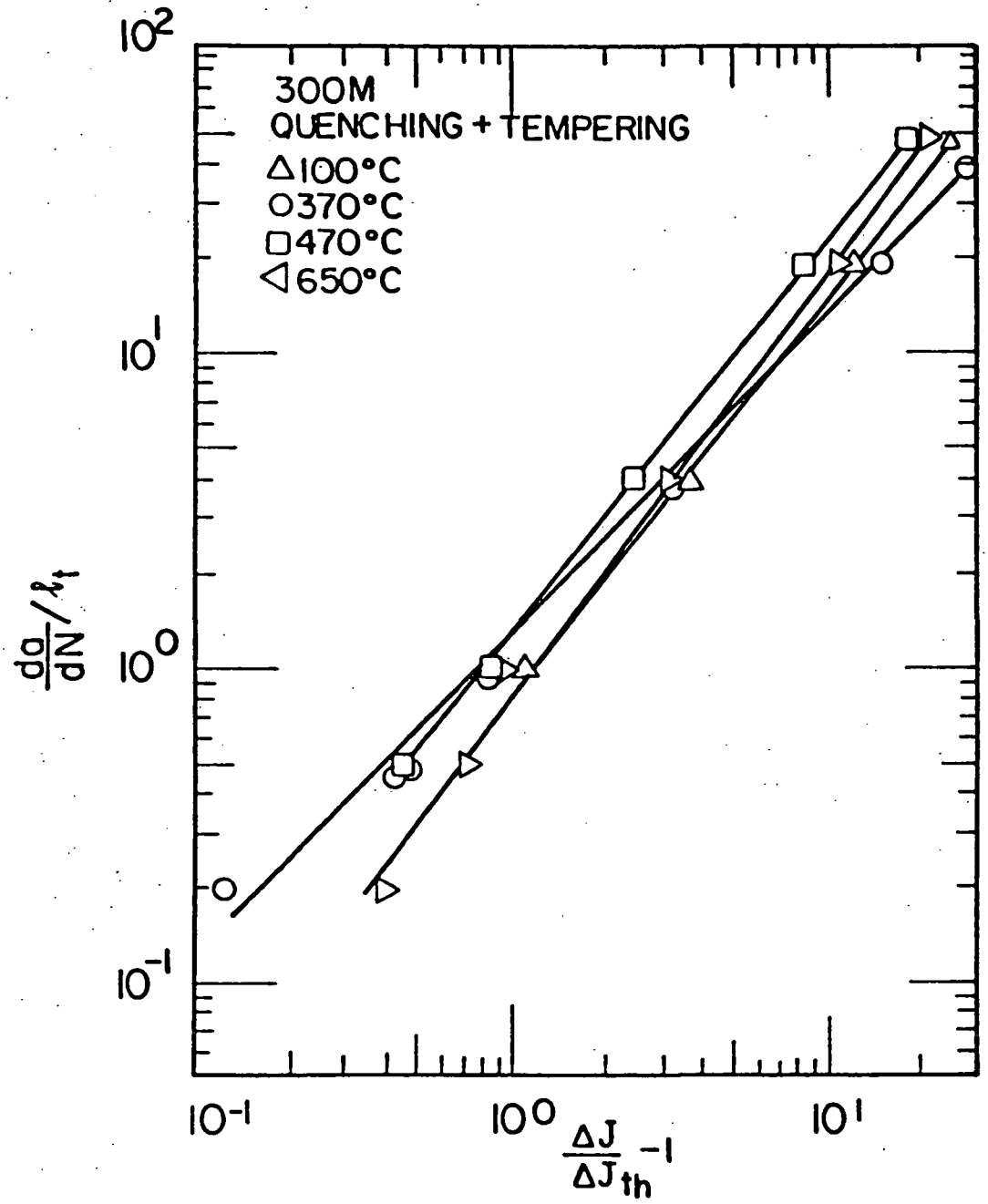

Fig. (2.17) Fatigue crack growth data.

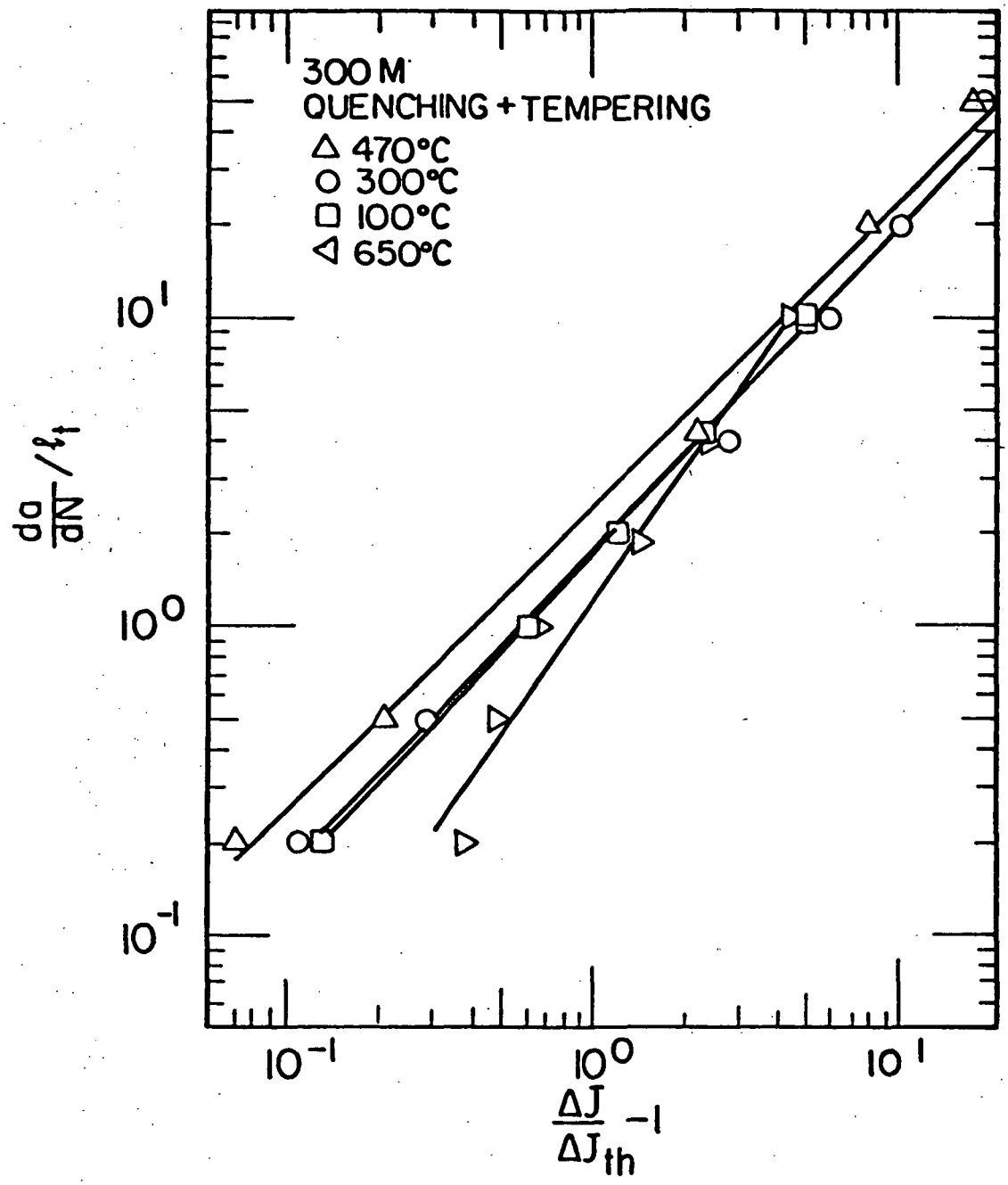

Fig. (2.18) Fatigue crack growth data.

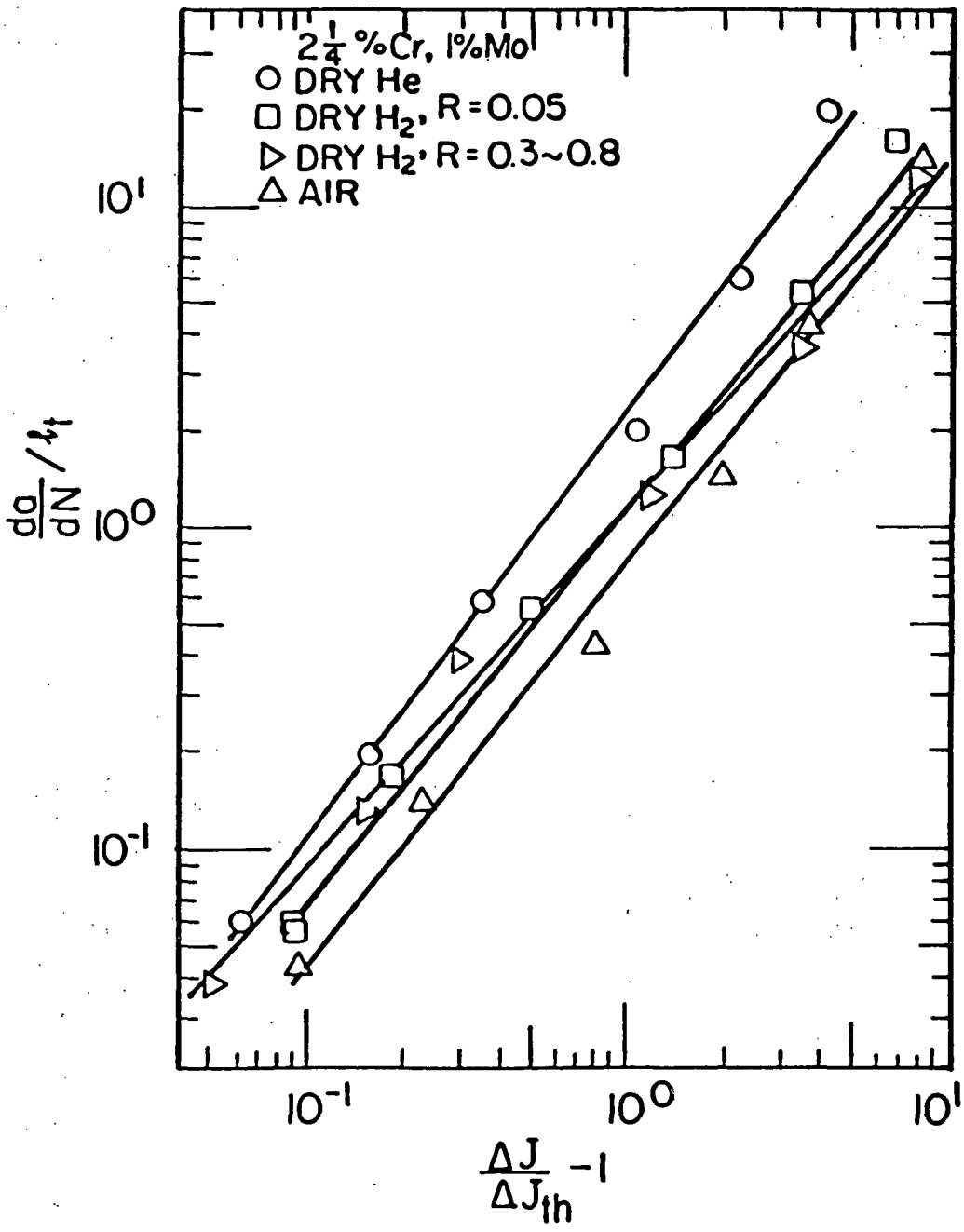

Fig. (2.19) Fatigue crack growth data.

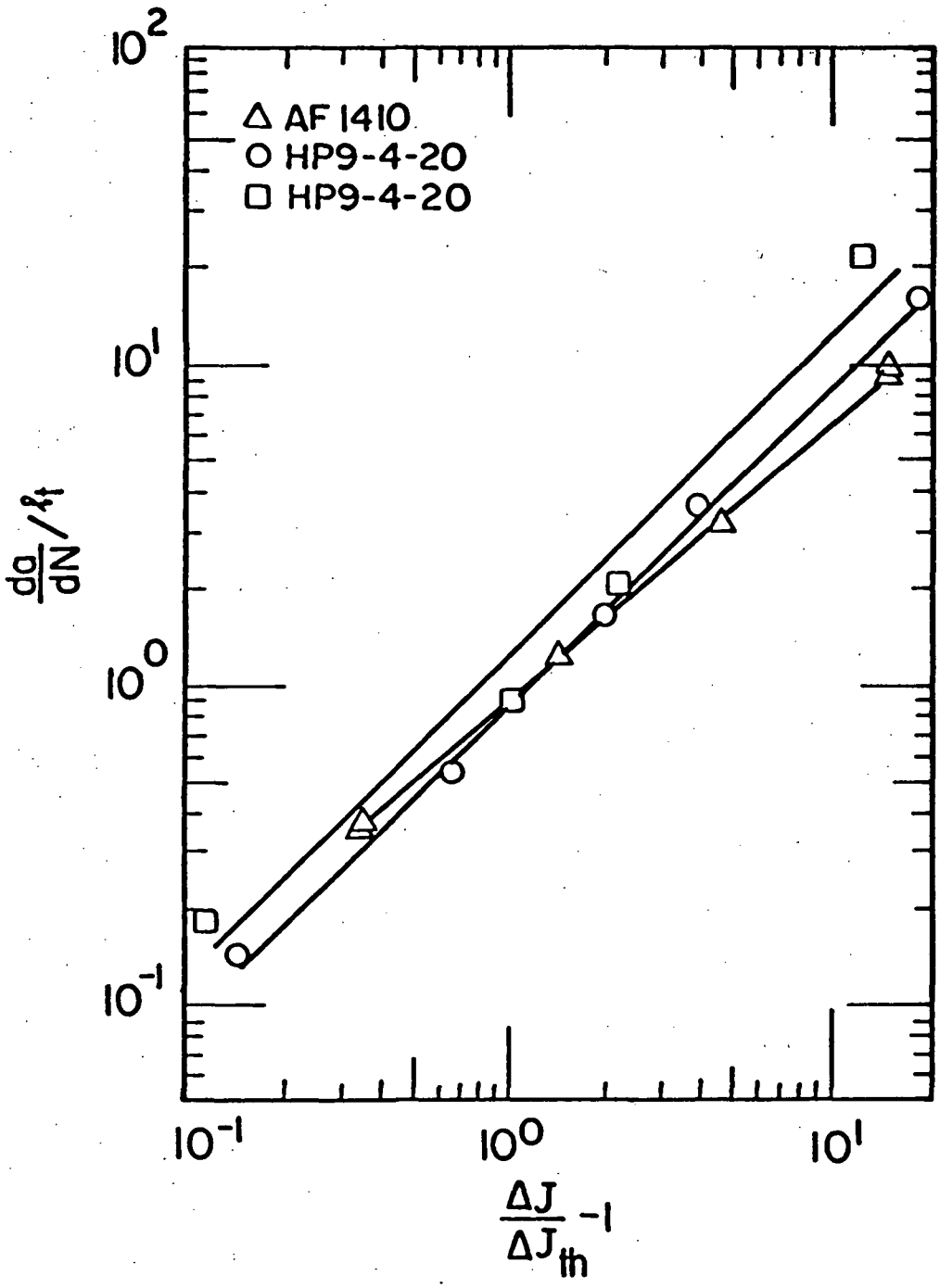

Fig. (2.20) Fatigue crack growth data.

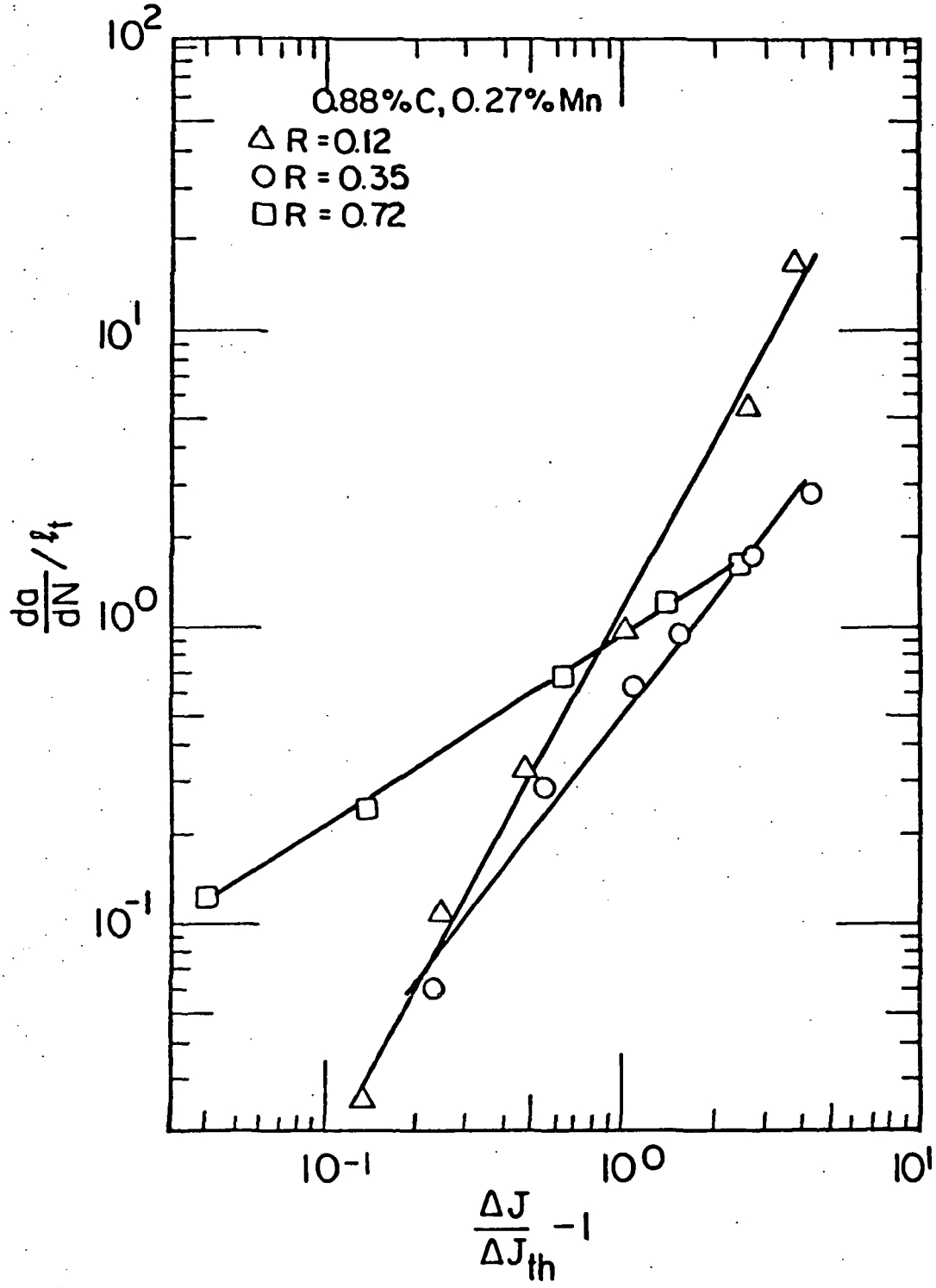

Fig. (2.21) Fatigue crack growth data.

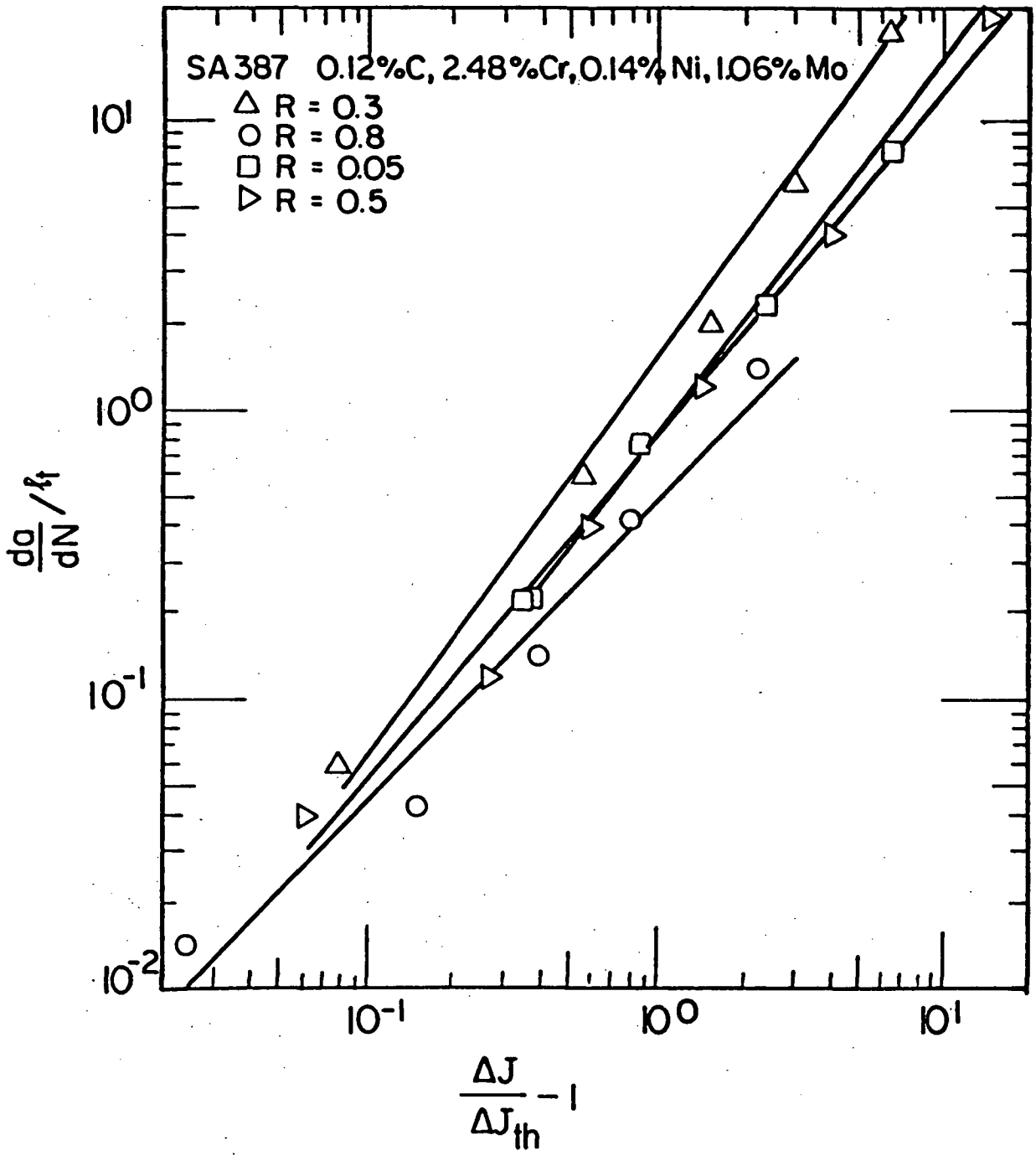

Fig. (2.22) Fatigue crack growth data.

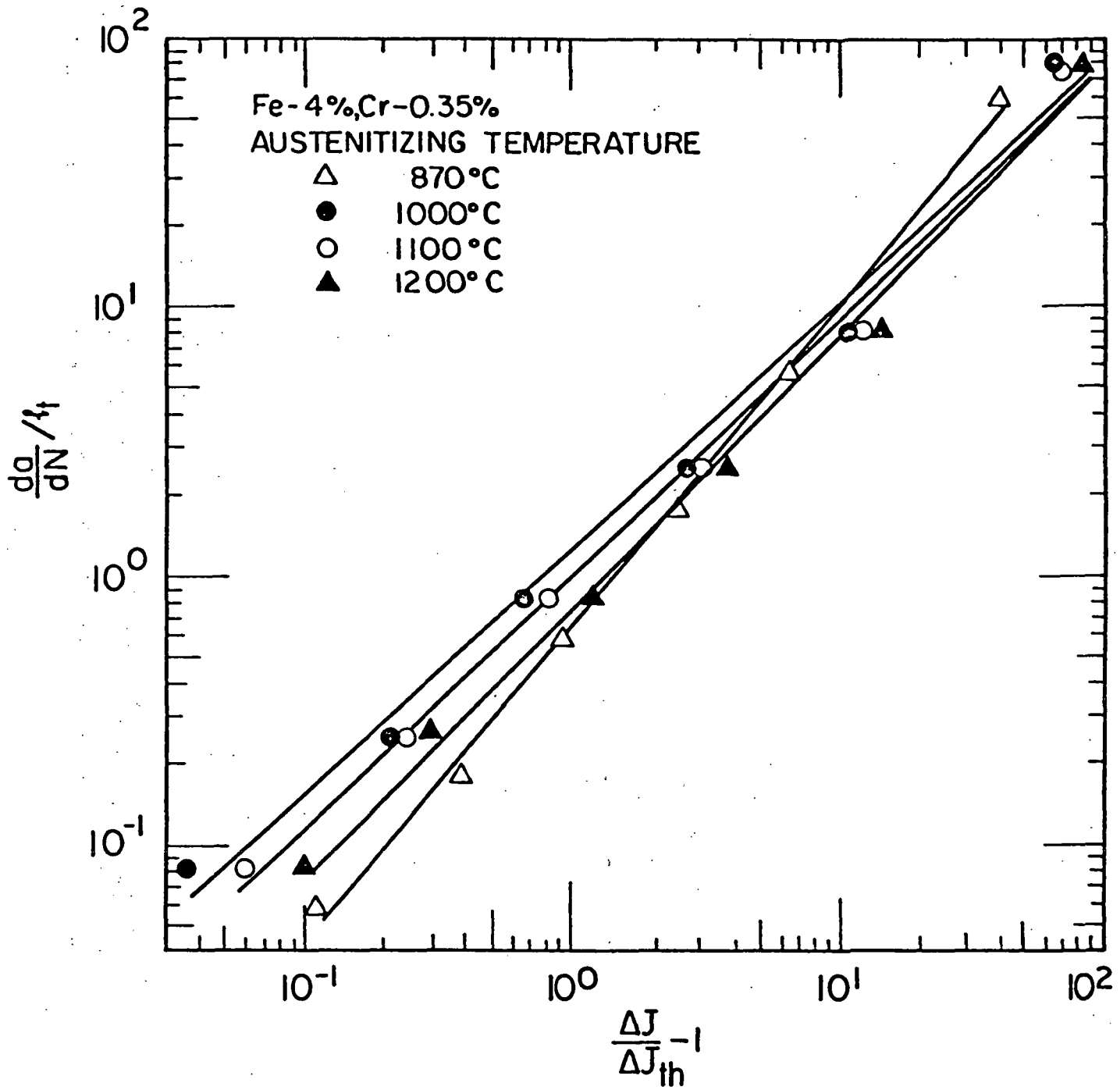

Fig. (2.23) Fatigue crack growth data.

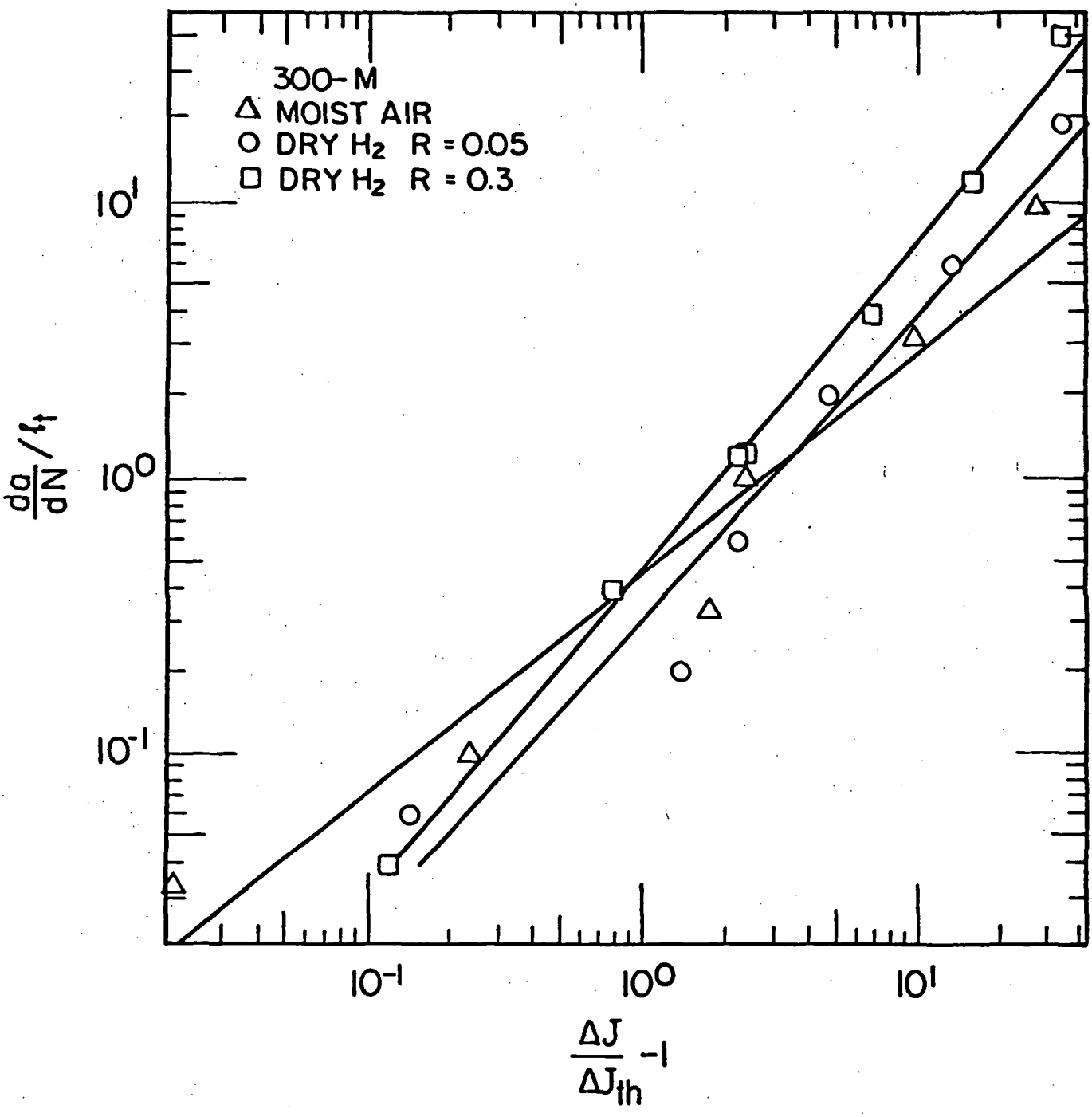

Fig. (2.24) Fatigue crack growth data.

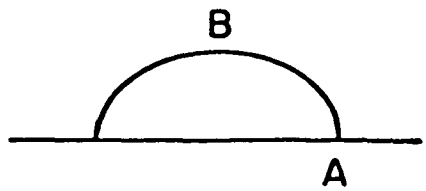

Fig. (3.1) Semi-elliptical surface crack.

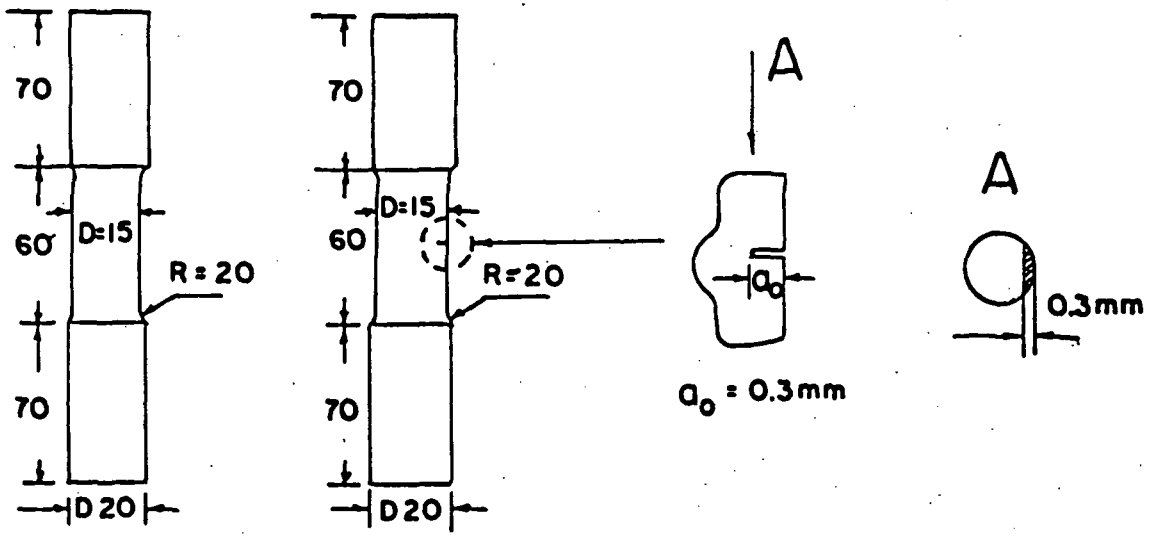

Fig. (3.2) Test specimen dimensions (mm) for LD-10 and LY-12 aluminum alloys. (PRC) Designation).

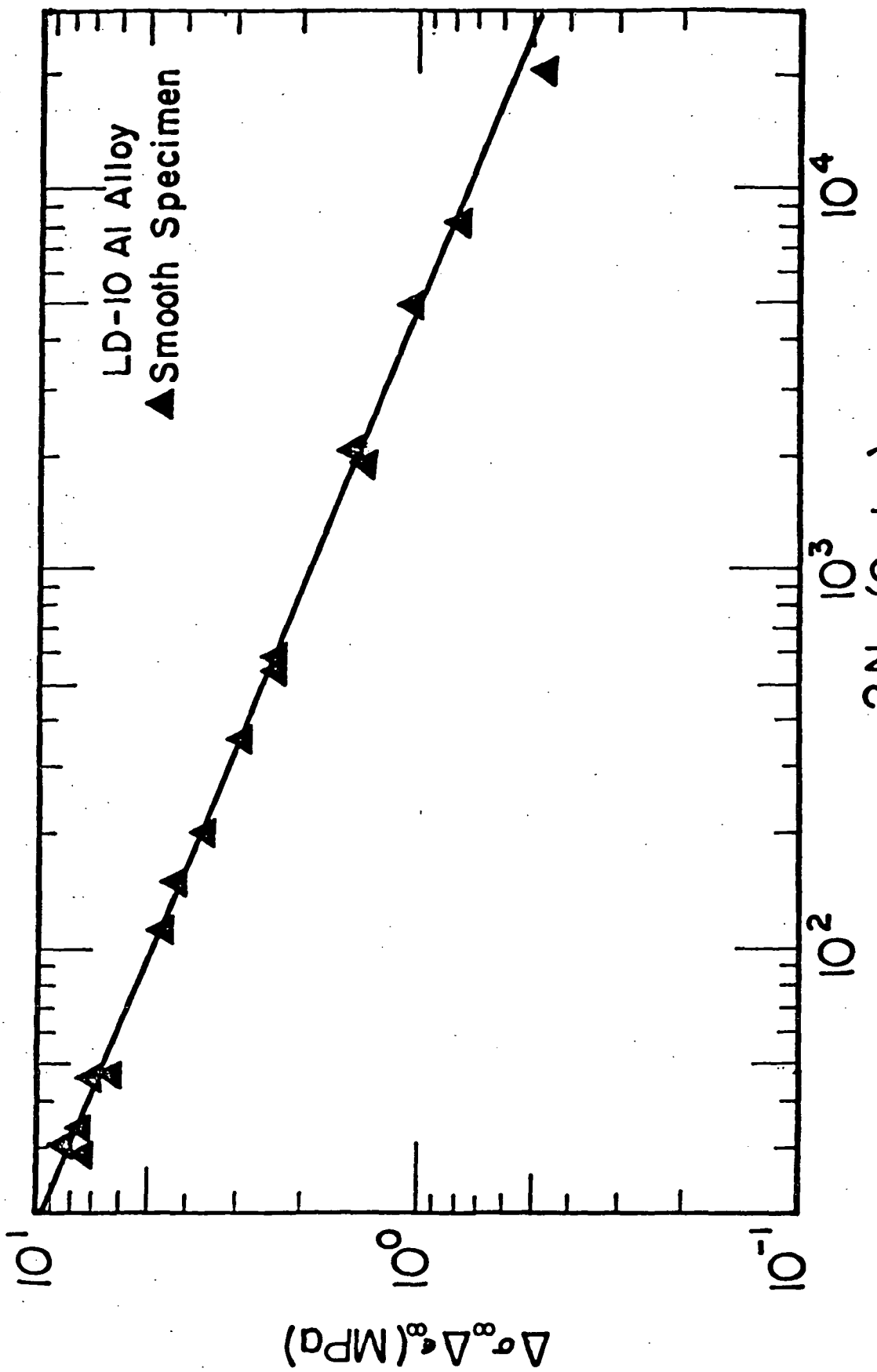

Fig. (3.3a) Correlation of ($\Delta\sigma_\infty\Delta\varepsilon_\infty$) versus ($2N_f$) for LD-10 aluminum alloy.

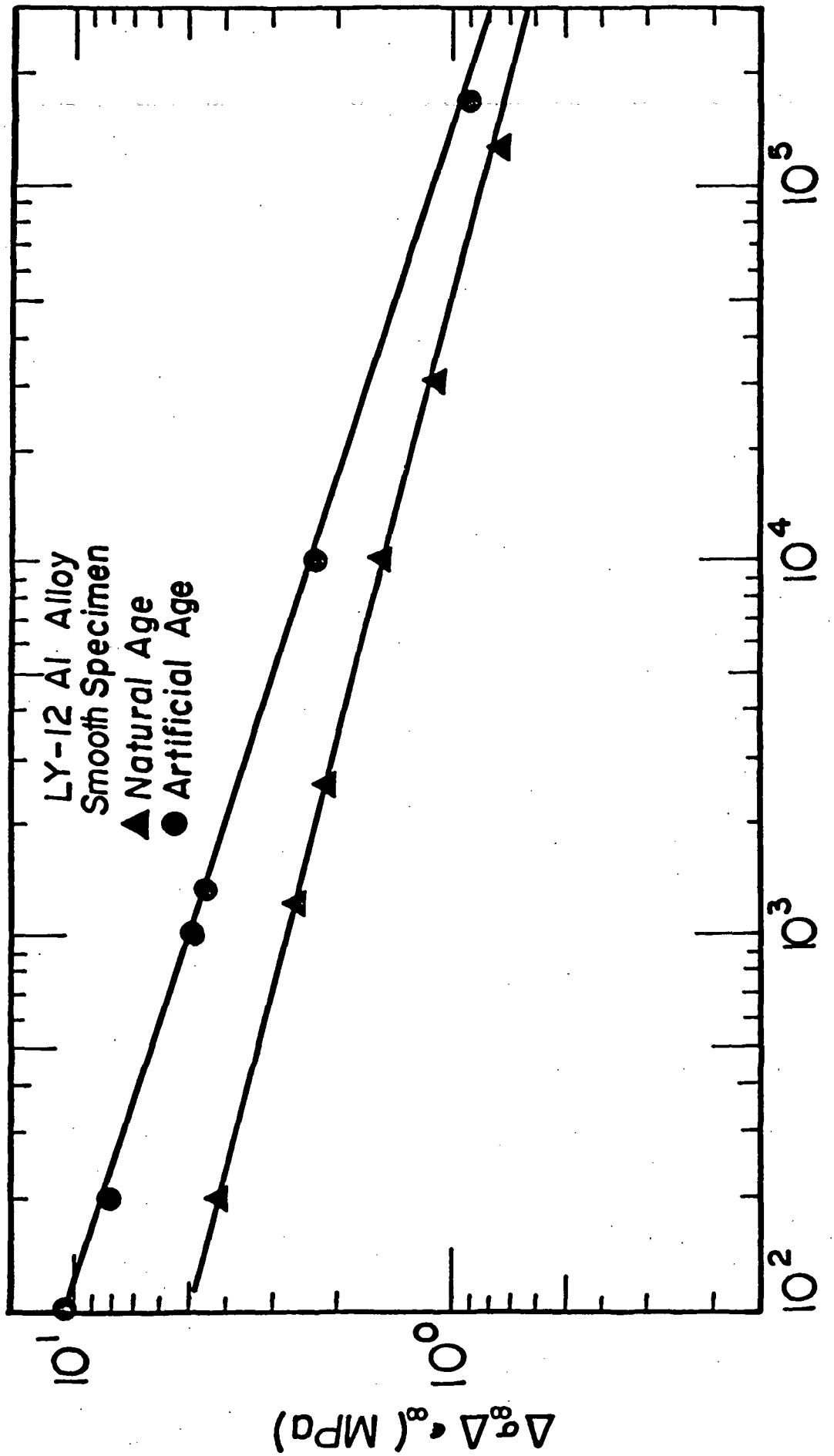

Fig. (3.3b) Correlation of ($\Delta\sigma_a\Delta\varepsilon_a$) versus ($2N_f$) for LY-12 aluminum alloy.

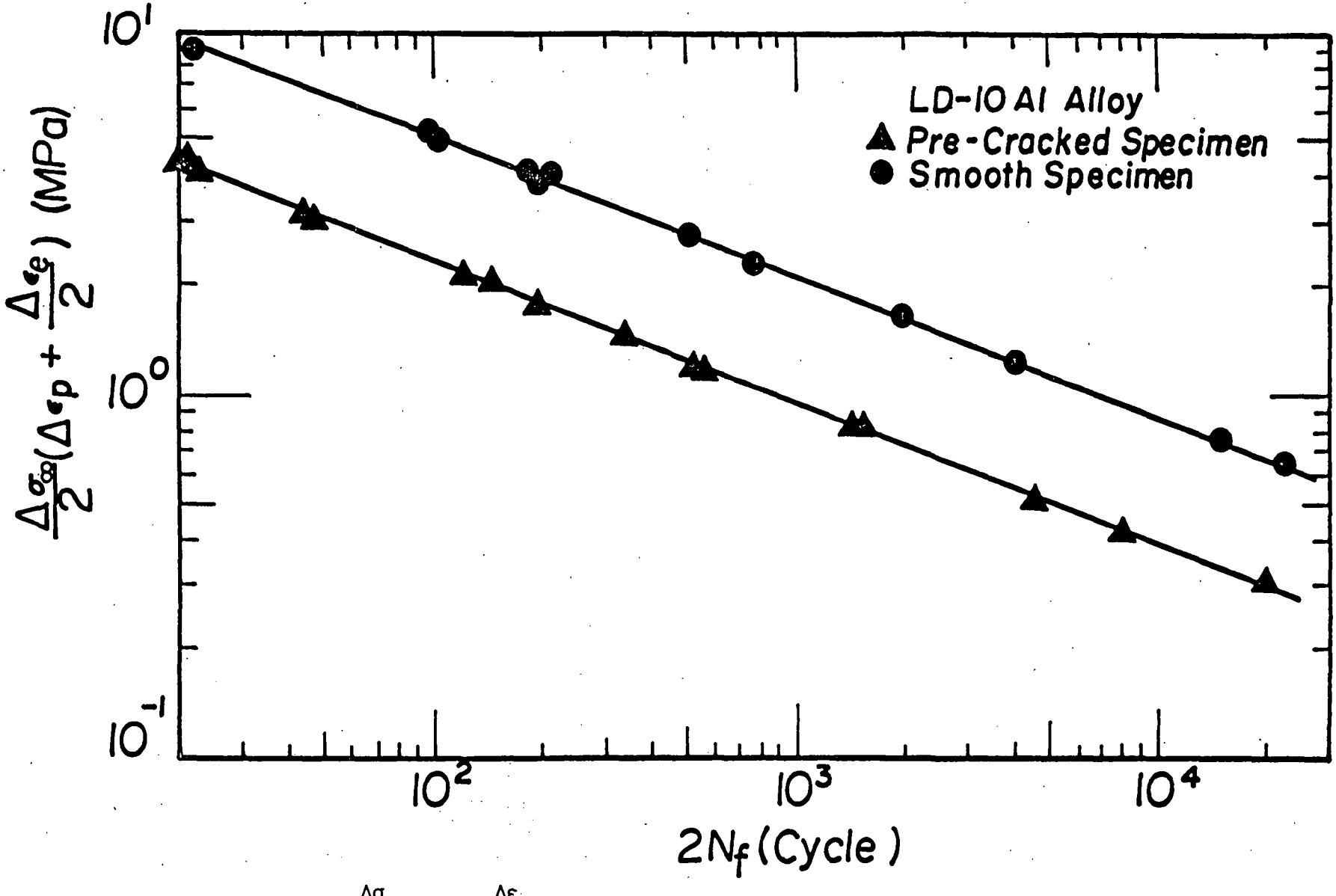

Fig. (3.4a) Correlation of $[\frac{\Delta\sigma_\infty}{2}(\Delta\epsilon_p + \frac{\Delta\epsilon_e}{2})]$ versus $(2N_f)$ for LD-10 aluminum alloy.

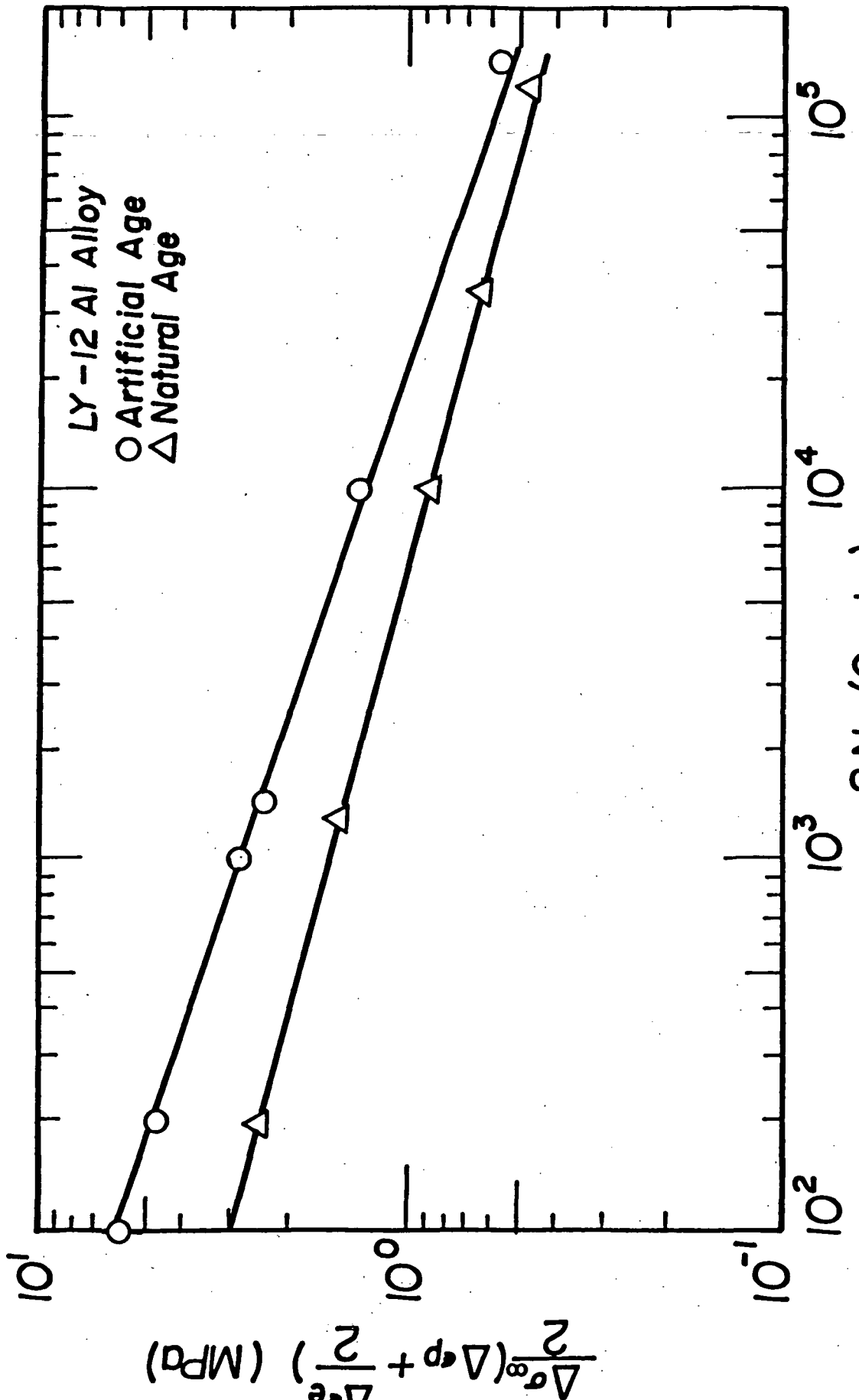

Fig. (3.4b) Correlation of $[\frac{\Delta\sigma_\infty}{2}(\Delta\varepsilon_p + \frac{\Delta\varepsilon_e}{2})]$ versus $(2N_f)$ for LY-12 aluminum alloy.

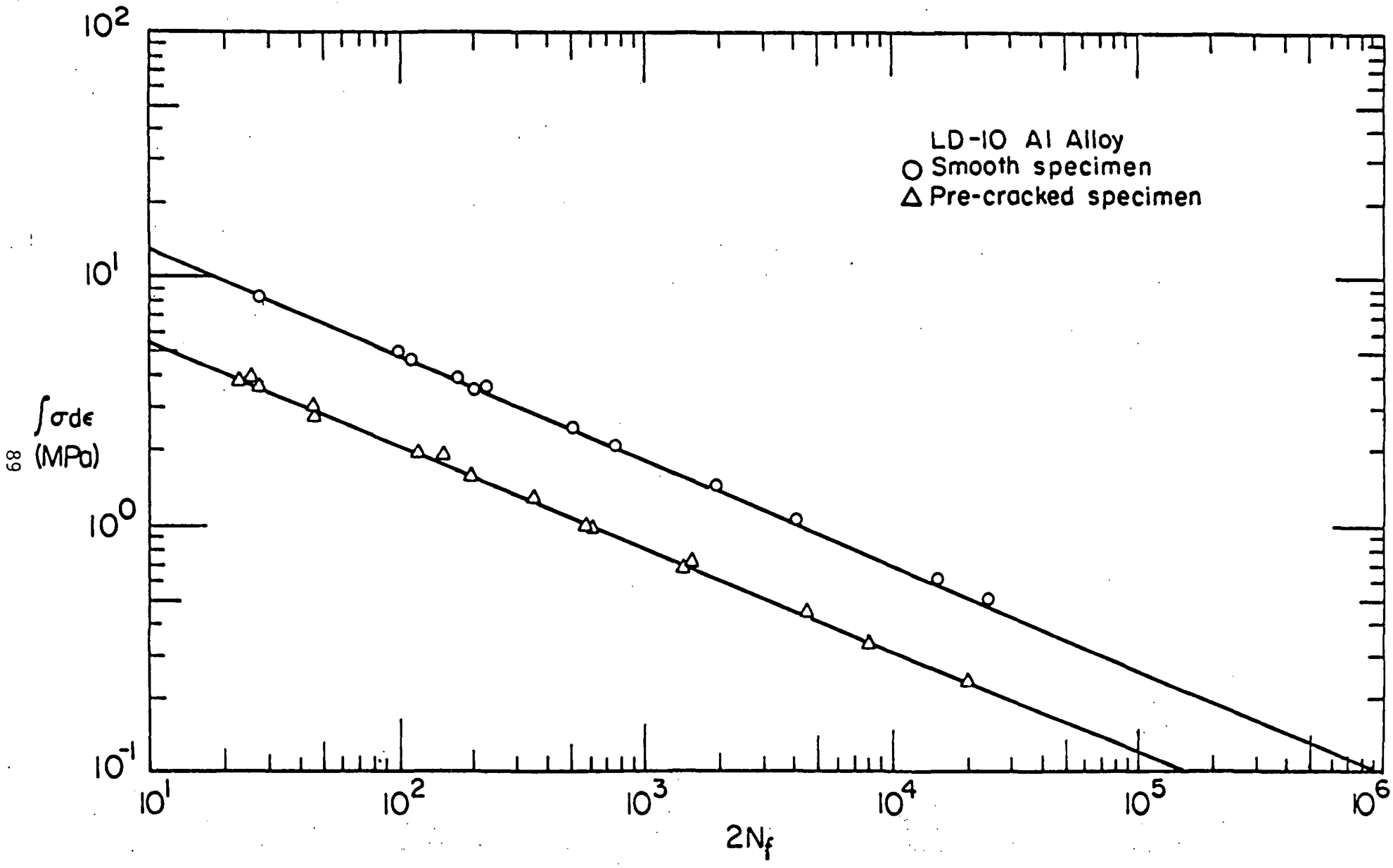

Fig. (3.5a) Correlation of ($\int \sigma d\epsilon$) versus ($2N_f$) for LD-10 aluminum alloy.

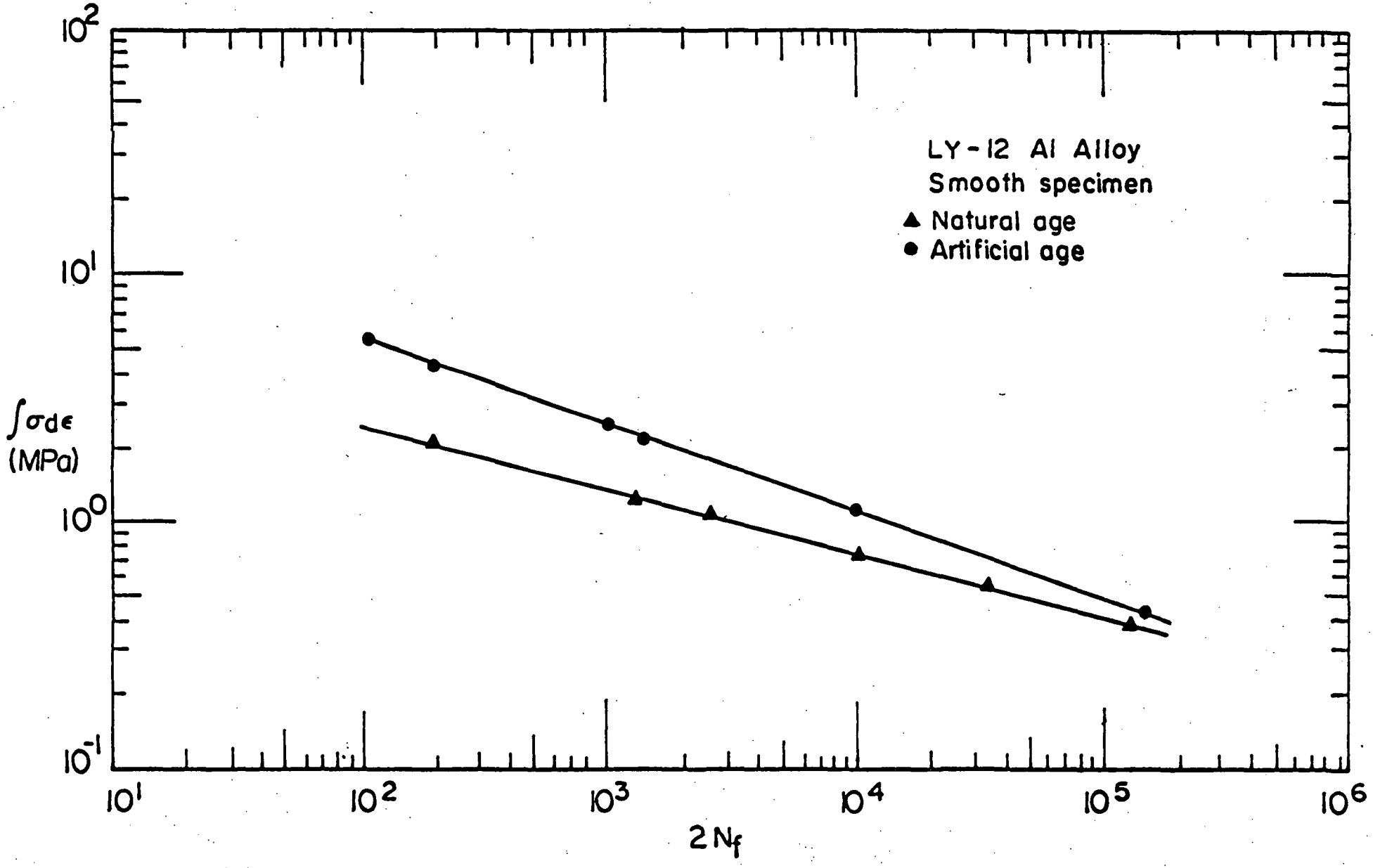

Fig. (3.5b) Correlation of ($\int \sigma d\epsilon$) versus ($2N_f$) for LY-12 aluminum alloy.

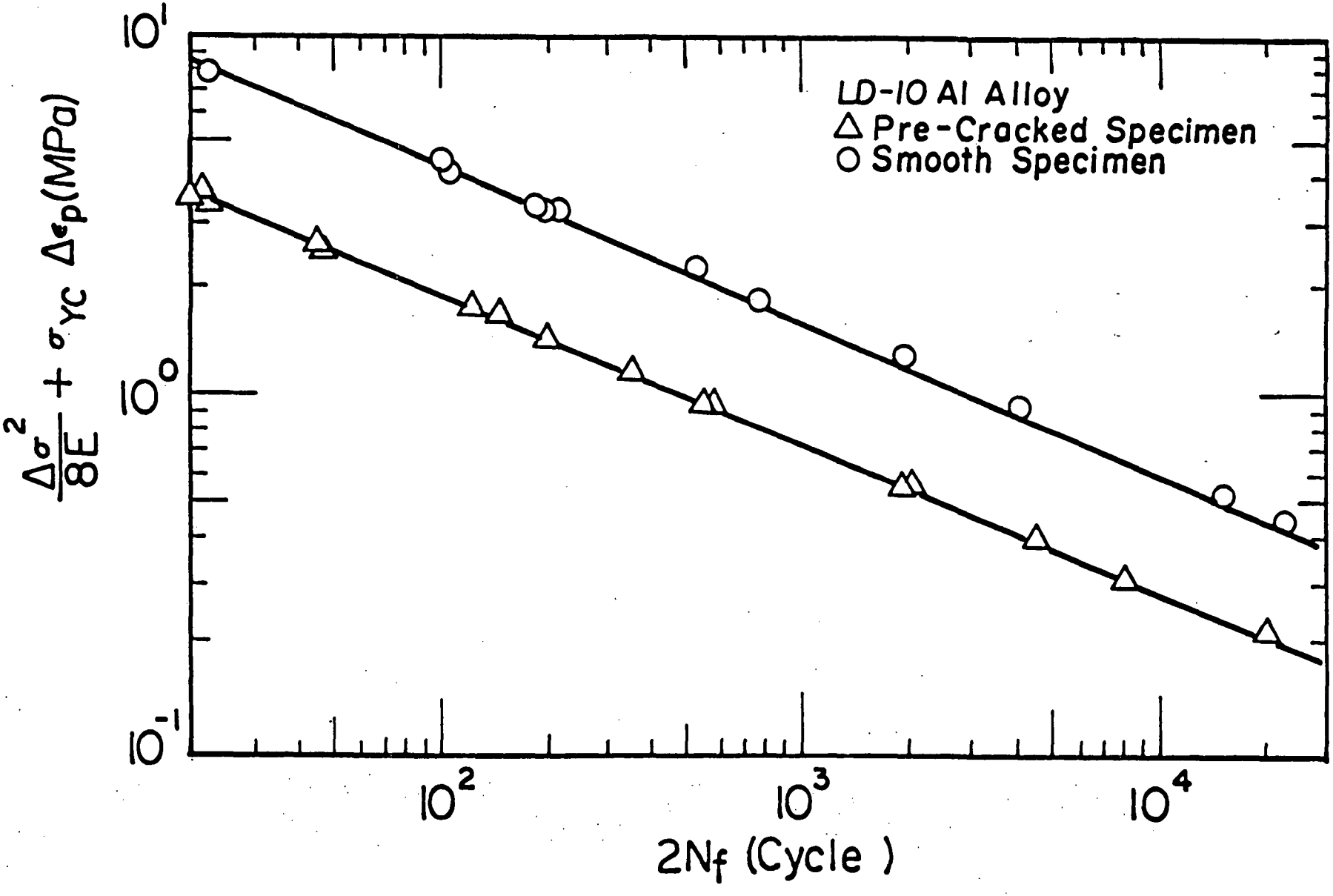

Fig. (3.6a) Correlation of $(\frac{\Delta\sigma^2}{8E} + \sigma_{YC}\Delta\varepsilon_p)$ versus $(2N_f)$ for LD-10 aluminum alloy.

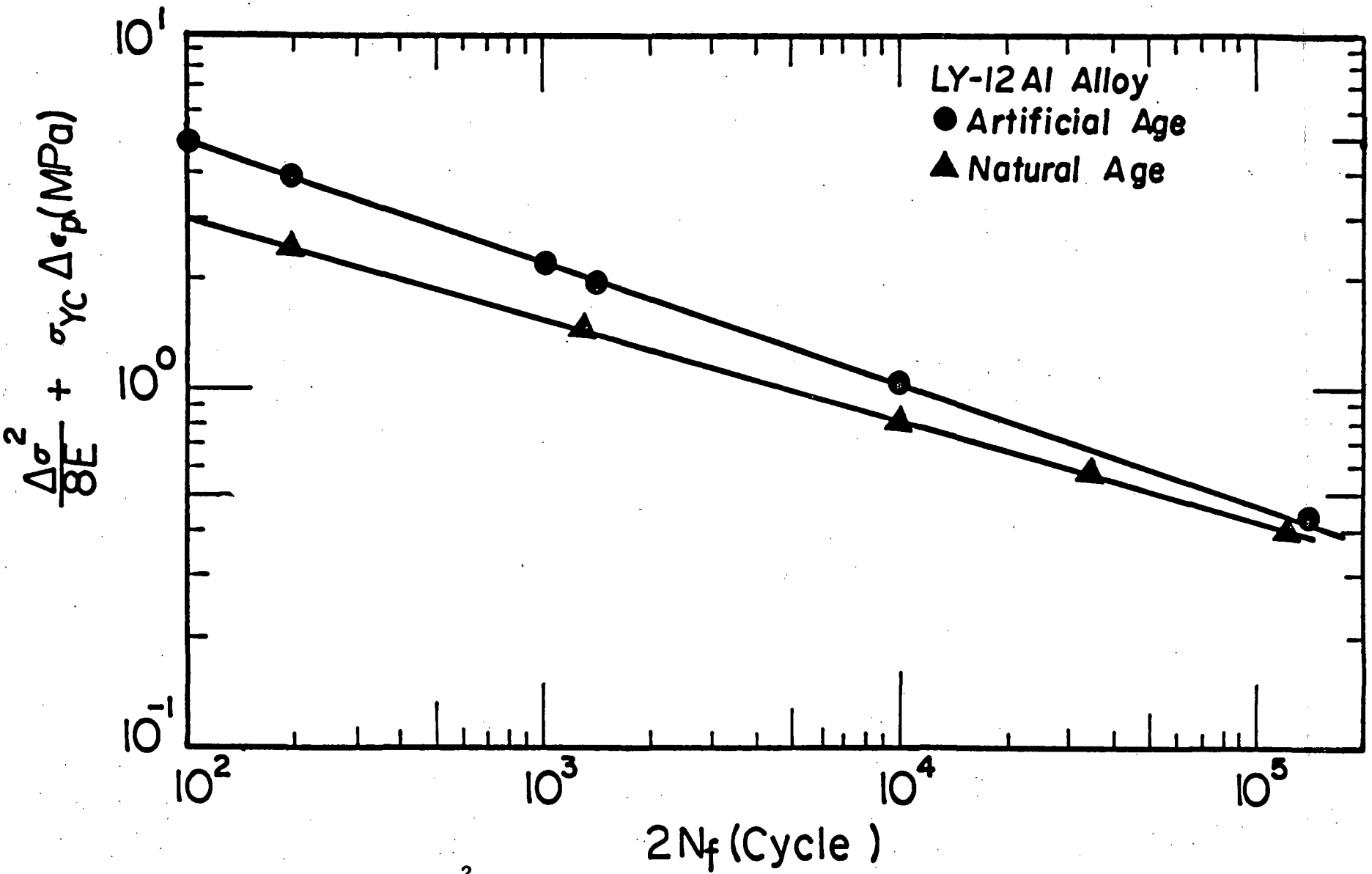

Fig. (3.6b) Correlation of $(\frac{\Delta\sigma^2}{8E} + \sigma_{YC}\Delta\epsilon_p)$ versus $(2N_f)$ for LY-12 aluminum alloy.

1. Report No.	2. Government Accession No.	3. Recipient's Catalog No.
NASA CR-174686		

4. Title and Subtitle	5. Report Date
Crack Tip Field and Fatigue Crack Growth in General Yielding and Low Cycle Fatigue	September 1984
	6. Performing Organization Code
7. Author(s)	8. Performing Organization Report No.
Zheng Minzhong and H. W. Liu	None
	10. Work Unit No.
9. Performing Organization Name and Address	11. Contract or Grant No.
Syracuse University Syracuse, New York 13210	NAG 3-348
	13. Type of Report and Period Covered
12. Sponsoring Agency Name and Address	Contractor Report
National Aeronautics and Space Administration Washington, D.C. 20546	14. Sponsoring Agency Code
	533-04-1A

15. Supplementary Notes

Final report. Project Manager, Jack Telesman, Structures and Mechanical Technologies Division, NASA Lewis Research Center, Cleveland, Ohio 44135. Zheng Minzhong, Visiting Scholar from Aircraft Strength Research Institute, Xian, People's Republic of China.

16. Abstract

Fatigue life consists of crack nucleation and crack propagation periods. Fatigue crack nucleation period is shorter relative to the propagation period at higher stresses. Crack nucleation period of low cycle fatigue might even be shortened by material and fabrication defects and by environmental attack. In these cases, fatigue life is largely crack propagation period. The characteristic crack tip field was studied by the finite element method, and the crack tip field is related to the far field parameters: the deformation work density, and the product of applied stress and applied strain. The cyclic crack growth rates in specimens in general yielding as measured by Solomon are analyzed in terms of J-integral. A generalized crack growth behavior in terms of ΔJ is developed. The relations between J and the far field parameters and the relation for the general cyclic crack growth behavior are used to analyze fatigue lives of specimens under general-yielding cyclic-load. Fatigue life is related to the applied stress and strain ranges, the deformation work density, crack nucleus size, fracture toughness, fatigue crack growth threshold, Young's modulus, and the cyclic yield stress and strain. The fatigue lives of two aluminum alloys correlate well with the deformation work density as depicted by the derived theory. The general relation is reduced to Coffin-Manson low cycle fatigue law in the high strain region.

17. Key Words (Suggested by Author(s))	18. Distribution Statement
Fatigue crack growth Low cycle fatigue J-integral	Unclassified - unlimited STAR Category 26

19. Security Classif. (of this report)	20. Security Classif. (of this page)	21. No. of pages	22. Price*
Unclassified	Unclassified		

*For sale by the National Technical Information Service, Springfield, Virginia 22161

National Aeronautics and
Space Administration

Washington, D.C.
20546

Official Business
Penalty for Private Use, $300

SPECIAL FOURTH CLASS MAIL
BOOK

Postage and Fees Paid
National Aeronautics and
Space Administration
NASA-451

NASA

POSTMASTER: If Undeliverable (Section 158
Postal Manual) Do Not Return